Connexin-43 Mediated Communication in Cancer Gene Therapy

A Thesis

Submitted in Partial Fulfillment of the

Requirements for the award of the degree of

DOCTOR OF PHILOSOPHY

By

Md Asif Raza

Department of Biosciences and Bioengineering

Indian Institute of Technology Guwahati

Assam, India

August 2017

Connexin-43 Mediated Communication in Cancer Gene Therapy

A thesis by Md Asif Raza

Thesis Supervisor,
Prof. Siddhartha Sankar Ghosh

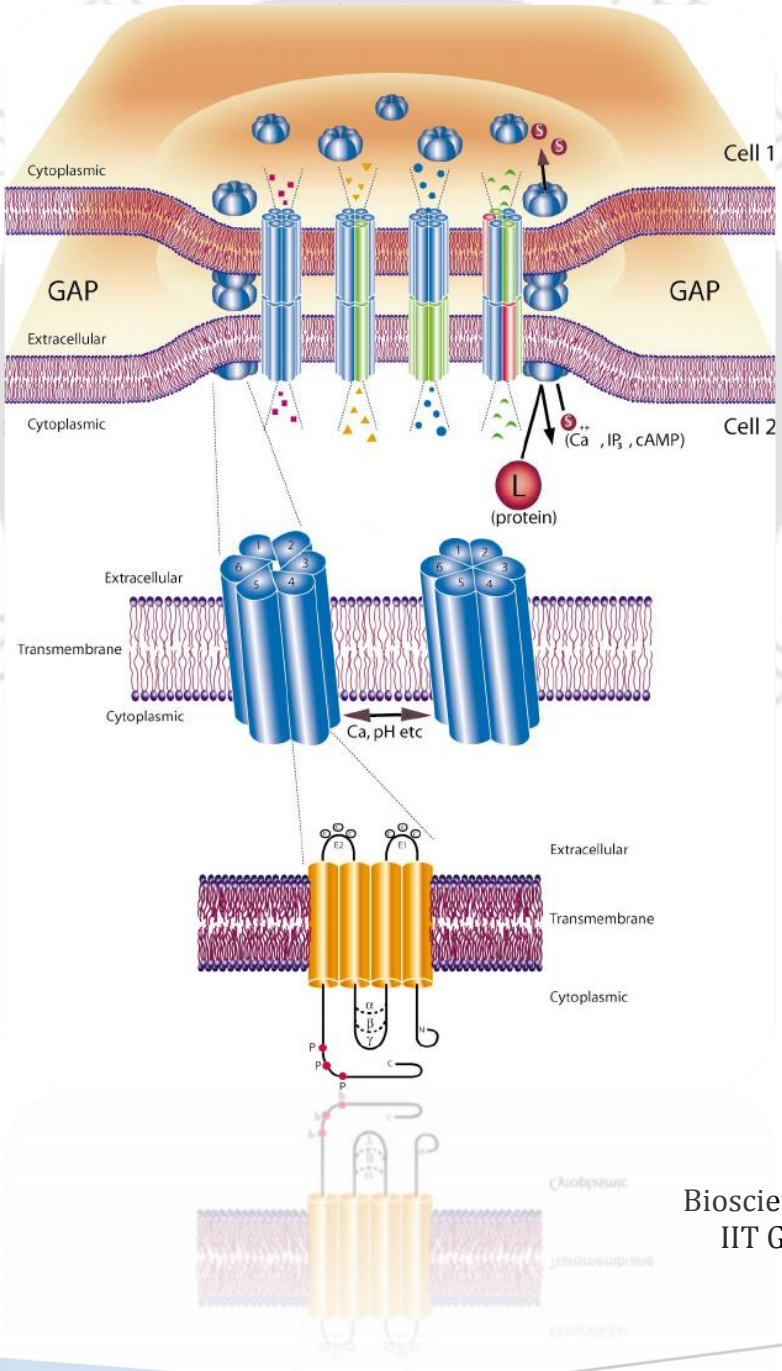

Department of
Biosciences and Bioengineering,
IIT Guwahati, Assam, India

TH-1646_126106007

Dedicated to

My Family for Their

Unconditional Love and Support

भारतीय प्रौद्योगिकी संस्थान गुवाहाटी

Indian Institute of Technology Guwahati
Guwahati 781039, Assam, India

2017

DECLARATION

I, hereby, declare that the matter embodied in this thesis titled "**Connexin-43 Mediated Communication in Cancer Gene Therapy**" is the result of investigations carried out by me under the supervision of **Prof. Siddhartha Sankar Ghosh**, Department of Biosciences and Bioengineering, Indian Institute of Technology Guwahati, India for the award of the degree of **Doctor of Philosophy**. This work has not been submitted elsewhere for any degree, diploma, associateship or membership etc. of any institute or university to the best of my knowledge and belief.

Date: **Md Asif Raza**

Place: Roll no. 126106007

भारतीय प्रौद्योगिकी संस्थान गुवाहाटी

Indian Institute of Technology Guwahati
Guwahati 781039, Assam, India

2017

CERTIFICATE

It is certified that the thesis entitled "**Connexin-43 Mediated Communication in Cancer Gene Therapy**" being submitted to the Indian Institute of Technology Guwahati by **Md Asif Raza** (Roll. No. 126106007) for the award of the degree of **Doctor of Philosophy** in Department of Biosciences and Bioengineering, is a bonafide record of research work carried out by him. The information and data reported by him are solely the results of his original findings. He has meticulously carried out the investigations and followed the guidelines of the laboratory. This work has not been submitted elsewhere for any degree or diploma.

August, 2017

Prof. Siddhartha Sankar Ghosh
(Thesis Supervisior)

Acknowledgements

Creating a PhD thesis is not an individual experience; rather it takes place in a social context and includes several persons who were instrumental in completion of my PhD research and whom I would like to thank sincerely.

When I joined IIT Guwahati, I was eager to do my contribution to the scientific community but the success and final outcome required a lot of guidance and assistance. I am extremely fortunate to get the same throughout my PhD work tenure. I have been nurtured here mentally, personally and professionally. Thus I would like to express my gratitude to my guide and mentor; Prof. Siddhartha Sankar Ghosh who provided me with this golden opportunity to work in such a wonderful milieu. Here I could not only freely execute my ideas but also realize my dreams and thus do research in an amicable way. Thank you Sir, for your guidance which allowed me to stay focused and also motivated all throughout. Your words of encouragement and faith, always helped me to keep my moral high. I am indeed fortunate to have a teacher like you. I will never forget all those times when he has provided endless moral support, especially at times when research failed me and positive results refused to come. With due respect to all my teachers, I believe that one can hardly hope to be inducted under the guidance of such a human being as I was fortunate enough to be. Thank you Sir, for all your motivation, encouragement and support. I could not find a better words to explain the help and support you gave me since the beginning of my PhD tenure.

I am also enormously grateful to my doctoral committee members- Prof. K. Pakshirajan, Dr. Biplab Bose, and Dr. L. M. Kundu, for their valuable suggestions and critical inputs throughout the course of these five years. I am also highly obliged to Dr. Biplab Bose, who has always readily agreed to give his critical suggestions, whenever I have approached him.

I am heavily indebted to my senior lab members- Kohila di, Chocks bhaiya, Subhamoy da and Nidhi di for painstakingly, yet lovingly, imparting to me all their gathered knowledge. I will always remember the affection bestowed upon me by my beloved seniors. I am also thankful to my seniors- Amaresh da, Mitun da, Amit da, Shilpa di, Pallab da, Pojul da, Ashok da, Mohitosh da, Rumi, and Rama for all their help and advice and also providing healthy and cheerful work environment. When I joined PhD, it was my seniors who make me feel like home.

I sincerely appreciate the help of all my labmates and colleagues - Archita, Sharmila, Upashi, Neha, Anil, Srirupa, Rajib, Bandhan, Deepanjalee, Anita, Vanita, Gargi, Gavya, Sandipan, Vimal, Poulomi senior and others. I was fortunate to have a collaborative work with Upashi. She helped me a lot during my final days of PhD.

I specially thank Archita for giving me suggestions and comments when I was writing my papers or thesis or taking any important decisions throughout my PhD tenure.

I am blessed to have friends like Archita, Srirupa, Anil, Poulomi, Mahesh, Satendra, and Zia. They have readily helped me whenever I approached them.

I am grateful to the Department of Biosciences and Bioengineering, Centre for Nanotechnology, DBT support facility and Central Instrumentation Facility, IIT Guwahati, for providing me with all the support required for carrying out my thesis work. I would like to thank all the staff members as well.

Finally, my parents, brother and sister deserve a special mention here. I would not have reached the position that I am in now, if not their love, care and encouragement. Even in the most difficult situations, they have always supported me to choose the career I wished. Whatever I have achieved today is only because of them. I would also like to acknowledge my wife, Shazia for supporting me during the most hectic and tedious final days of my PhD work.

In the last five years, I have realized that Ph.D. is not only about doing research. It is also a training to face failures in life. And I am always indebted to the supreme power, the God Almighty for giving me the strength and mental toughness to face failures and success alike.

Md Asif Raza

Abstract

Connexin-43 Mediated Communication in Cancer Gene Therapy

By

Md Asif Raza

Submitted to the Indian Institute of Technology Guwahati in August, 2017 in Partial Fulfillment of the Requirements for the Degree of Doctor of Philosophy in Biosciences and Bioengineering

Abstract:

Cancer cells are known to lack regulation of cell proliferation due to the aberrant behavior of a myriad of signaling pathways. It is a disease of "abnormal homeostasis" mediated by defects in intra-, extra-, and intercellular forms of communications. Intercellular communication between cells is achieved with the help of gap junctional intercellular communication (GJIC). GJIC plays a crucial role in maintaining cell-cell homeostasis by keeping growth control signals at equilibrium among GJIC connected cells. The majority of neoplastic cells have less number of gap junctions, smaller in size, express less connexin (Cx), and have reduced GJIC as compared to normal cells. A Gap junction (GJ) channel consists of two juxtaposed Cx hexamers. Connexin-43 (Cx43), a tumor-suppressor gene, is one of the most abundant Cx proteins and ubiquitous in many tissues. A plethora of studies demonstrates the role of Cx43 in regulating tissue homeostasis through channel dependent as well as independent manner.

The present thesis aims to exploit the gap junction-dependent as well as independent anti-tumour property of Cx43 in combination with the plant based, semi-synthetic, anti-malarial drug called artesunate (ART). The GJIC deficient cell line was selected and the forced expression of Cx43 was performed by two different means – using gene therapy and by the inducible expression of Cx43 using drugs. In **Chapter 1** (review of literature), the burgeoning field of cancer gene therapy has been delved into. Essentially, the role of GJIC in cancer cells, their potential clinical usage as well as the advantages they hold over current modes of cancer therapy, have been encompassed in this chapter. Specifically, the GJ forming protein named Cx43 was discussed and the effect of Cx43 re-expression in Cx43 deficient cancer cells was evaluated. The GJ-dependent as well as independent mode of anti-tumour property mediated by Cx43 and the role of GJIC in mediating 'bystander effect' in combination with chemotherapeutic drugs was also discussed in this chapter. Gene therapy as well as histone deacetylase inhibitor (HDACi), more specifically 4-phenylbutyrate (4-PB) was used to established GJIC in cancer cells and combination therapy with the ART has also been discussed in this chapter.

In **Chapter 2,** the establishment of functional GJIC by cloning and expression of Cx43 has been reported. Further, the therapeutic implications of Cx43 in enhancing

the tumor suppressing activity of artesunate via gap junction-dependent as well as independent pathways in human breast cancer cells were discussed. The pathway by which Cx43 showed the GJ independent anti-tumour activity has been deciphered. GJIC mediated bystander cell death after treatment with ART and the transfer of ROS between the neighbouring cancer cells not exposed to ART was demonstrated by performing co-culture experiment.

In **Chapter 3,** the use of 4-PB in forceful expression of Cx43 and its synergistic interaction with ART both in MCF-7 cells as well as in DLA bearing mice was demonstrated. Re-expression of Cx43 in MCF-7 cells leads to the regulation of anti-tumour proteins, which further enhanced the dose dependent cytotoxicity of ART. Moreover, 4-PB attenuated the mRNA and proteins expression of the crucial DNA damage response (DDR) elements of nonhomologous end-joining (NHEJ) pathway and the central DDR transducer proteins, consequently enhancing the DNA damaging effect of ART. Combination therapy showed improvement in the life expectancy of the treated mice and a prominent reduction in the tumour volume without interfering with the normal biochemical, haematological and histological parameters of the mice. Overall, in chapter 3, a novel potential combination therapy in which 4-PB potentiated the cytotoxicity of ART synergistically and provided a promising combination drug for an effective cancer therapy was explained.

Chapter 4 reported the sub-cloning of *E. coli* cytosine deaminase (CD) and its mutants in mammalian expression vector. The mutants have been previously designed in our lab using *in silico* mutagenesis. Out of several mutants, F186W mutant was selected based on *in vitro* experimental data. F186W mutant has previously showed enhanced binding affinity towards prodrug 5-FC as compared to the natural substrate cytosine, *in vitro.* The chapter 4 dealt with the expression and functional analysis of CD and F186W mutant in A549 cells after transfection. Experimental results of *E. coli* cytosine deaminase mutant in A549 cells had validated *in silico* and *in vitro* predicted data. Further, the potency of the mutant was improved by co-transfecting it in the MCF-7 cells expressing Cx43. The F186W-Cx43 mutant required a much lower dose of 5-FC to reach its IC50, thus minimizing the systemic side effects of large doses of 5-FC as required for wtCD and F186W alone. The overall improvement in the cytotoxic activity of the F186W mutant in conjunction with the Cx43 has been reported in this chapter.

In **Chapter 5,** the fabrication of a versatile novel 4-PB bound composite nanoparticles has been demonstrated. In this approach, silver nanoclusters (AgNCs) embedded chitosan nanocarrier were utilized for analysis of binding, tracking, and sustained release of 4-PB from the nanocarrier. Inferences were drawn based on luminescence detection using fluorescence spectrometry, flow cytometry, and high-end confocal microscopy. The stability imparted by the nanocarrier to the 4-PB resulted in enhanced anti-tumor efficacy. Most importantly, this method implied improved cancer therapy without dose-dependent side effects of the drug, as the AgNCs ensured the stability of the 4-PB in cancer cells. The efficacy of the 4-PB bound nanocarrier was also evaluated in spheroids based model. Time-dependent uptake of

luminescent silver clusters was demonstrated by confocal microscopy and flow cytometry.

In the final section on **Conclusions and Future Prospects**, the anti-tumour mechanism of Cx43 has been delineated and its application with the other therapies have been highlighted. In brief, the functional GJIC has been established in GJ devoid cells using 4-PB drug or Cx43 gene cloning. The GJ-dependent as well as independent anti-tumour activity of the Cx43 gene has been investigated extensively in conjunction with the drug ART. The Cx43 also enhanced the CD/5-FC suicide gene therapy system and showed an effective gene therapy module. Binding with noble metal nanocarrier enhanced the efficacy of the 4-PB and enabled luminescence based binding, imaging, and uptake studies. The current therapeutic approach holds immense promise in the field of *in vivo* cancer therapeutics.

Table of Contents

List of Figures

Figure Captions:

List of Tables

Table Headings: **Page No.**

Glossary of Acronyms

5-FC	**5-**fluorocytosine
5-FU	5-fluorouracil
4-PB	4-phenylbutyrate
AgNCs	Silver Nanoclusters
ANOVA	Analysis of Variance
AO	Acridine Orange
ART	Artesunate
BSA	Bovine Serum Albimin
CD	Cytosine Deaminase
cDNA	Complimentary DNA
CFDA-SE	Carboxyfluorescein diacetate succinimidyl ester
Chi	Chitosan
Cxs	Connexins
Cx43	Connexin-43
DCFDA	Dichlorofluorescin diacetate
DEPC	Diethyl pyrocarbonate
DLS	Dynamic light scattering
DMEM	Dulbecco's Modified Eagle's Medium
DMSO	Dimethyl Sulfoxide
DNA	Deoxyribose Nucleic Acid
Dox	Doxorubicin
DDR	DNA Damage Repair
EtBr	Ethidium Bromide
FACS	Fluorescence Activated Cell Sorting
FBS	Fetal Bovine Serum
FDA	Food and Drug Administration
FESEM	Field Emission Scanning Electron Microscopy
FITC	Fluorescein isothiocyanate
GFP	Green Fluorescence Protein
GJ	Gap Junction
GJIC	Gap Junction Intercellular Communication
HDACs	Histone deacetylases
HDACi	Histone deacetylases Inhibitor
HRP	Horse Radish Peroxidase
Lip	Lipoic Acid
MTT	MTT 3-(4,5-dimethylthiazol-2-yl)-2,5-diphenyltetrazolium Bromide
NCs	Nanocarriers
PBS	Phosphate Buffered Saline
PBST	PBS with 1 % Tween-20
PCR	Polymerase Chain Reaction
PE	Phycoerythrin
PI	Propidium Iodide
ROS	Reactive Oxygen Species
RNA	Ribonucleic Acid
SDS	Sodium Dodecyl Sulphate
TBS	tris-Buffered Saline
TBST	TBS with 1 % Tween-20
TEM	Transmission Electron Microscope
TPP	Sodium tri-polyphosphate
wtCD	Wildtype CD

Chapter 1

Introduction and Literature Review

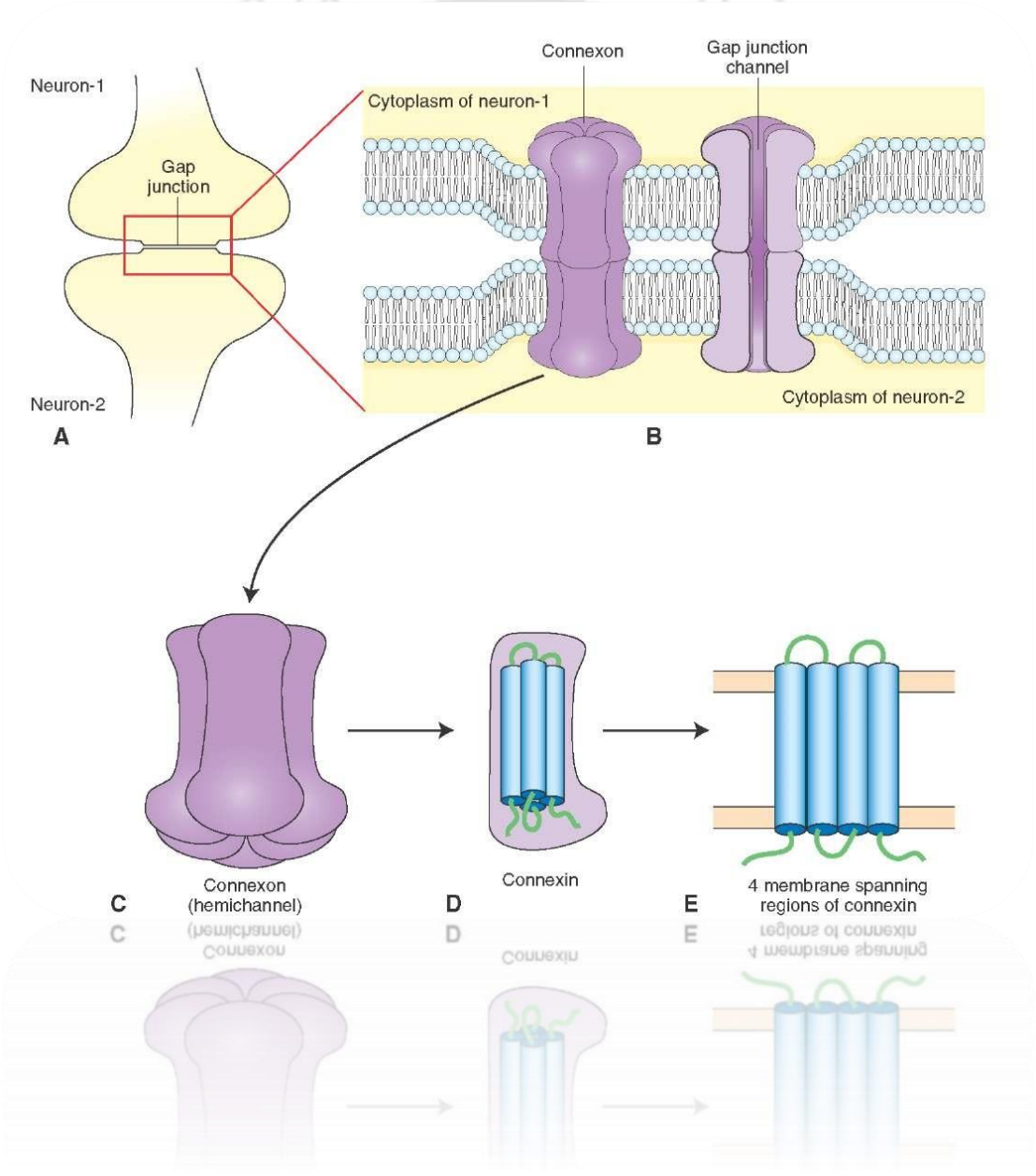

Chapter 1

Introduction and Literature Review

1.1 Introduction

During the period of evolution, multicellular organisms evolved from unicellular organisms and to accompany that transition complex genetic machinery and cellular functions had emerged. Unlike single-cell organisms, which survived environmental changes by adaptively responding to chemical (toxins, nutrients, toxicants) and physical (radiations, temperature) agents by intracellular signalling mechanisms, resulting in cell proliferation modifications, the multicellular organisms showed a delicate interplay of the regulation of cell proliferation for growth, tissue repair, wound healing, differentiation of cells, embryonic/fetal development, maturation, adulthood and aging. Such orchestration of specific cell/tissue/organ and organ system functions is referred to as "homeostasis".

Homeostasis is mechanistically regulated by three major communications in multicellular organisms: intercellular communication mediated by gap junction (GJ) channels, activated and modulated by intracellular communications through various secondary signalling messengers including c-AMP, diacylglycerol, Ca^{++}, pH, NO, ceramides, ROS and activated signal cascade triggered by extracellular communication via growth factors, hormones, cytokines and neurotransmitters.

Philosophically, the advent of malignancy, an event of homeostasis disruption in multicellular organisms, implied as though the appearance of carcinogenesis is a "throw-back" in the evolutionary process. The cancer cell in most of the part resemble single-cell organisms in their functionality and regulation, which survives by uncontrolled cell proliferation and cannot terminally differentiate. Cancer cells, which usually have abnormal apoptosis responses, do not terminally differentiate, do not have growth control and do not contact inhibit are frequently do not appear to have functional gap junctional intercellular communication (GJIC) [1-3]. Unicellular organisms do not have connexin genes while multicellular organisms do have. Is it

just happenstance that the terminal differentiation, cell growth regulation, and the appearance of apoptosis emerged when the GJIC genes showed up during the course of evolution of a multicellular organism or it may be accidental?

1.2 Cell-Cell Communication in Carcinogenesis

Multiple genetic modifications gradually accumulated in the cell during multistage carcinogenesis until it acquires a complete set of transformed genes crucial for neoplastic phenotype expression [4]. Most of the altered genes are often involved in cell growth control in human malignancies like p53 and Ras genes. In addition to those there are other set of genes get disrupted, which involved in maintaining harmony between cancer cells with their normal neighbour and maintaining the intercellular communication mechanism.

Except in very few cases such as platelets, red blood cells, neurons, spermatozoids and mature skeletal muscle fibre, GJs are present in all cell types of vertebrates [5]. Based on its ubiquity, GJs are often considered as fundamental structures necessary for tissular physiology, cell differentiation and normal functioning of the organ systems. Back in 1966, the first evidence was reported, which provided a direct link between GJ and cancer. Lowenstein and Kanno reported the loss of electrical coupling in both chemically-induced hepatomas as well as in rat transplanted hepatomas [6, 7]. During the same period, it was discovered that the lack of electrical coupling is the common phenomenon in differently induced (transplanted, chemically or spontaneous) and of different origin (hamster, rat, humans) solid tumours of unrelated origins (stomach, thyroid, liver). The data from the Lowenstein and its colleagues laboratory, established that cells derived from tumours of various origins are GJIC deficient contrary to their normal counterparts. In **figure 1.1**, the timeline shows key discoveries related to GJs and cancer.

Biochemical, ultrastructural and immunological study of number and size, cell-cell coupling of GJ and connexin expression provided an interesting finding about cell-cell communication in carcinogenesis. The majority of neoplastic cells have less number of GJs, smaller in size, low connexion expression, and reduced GJIC as compared to normal cells [8]. There are cancer cells having normal or increased GJ expression and cell-cell communication, but this does not result in normal cell

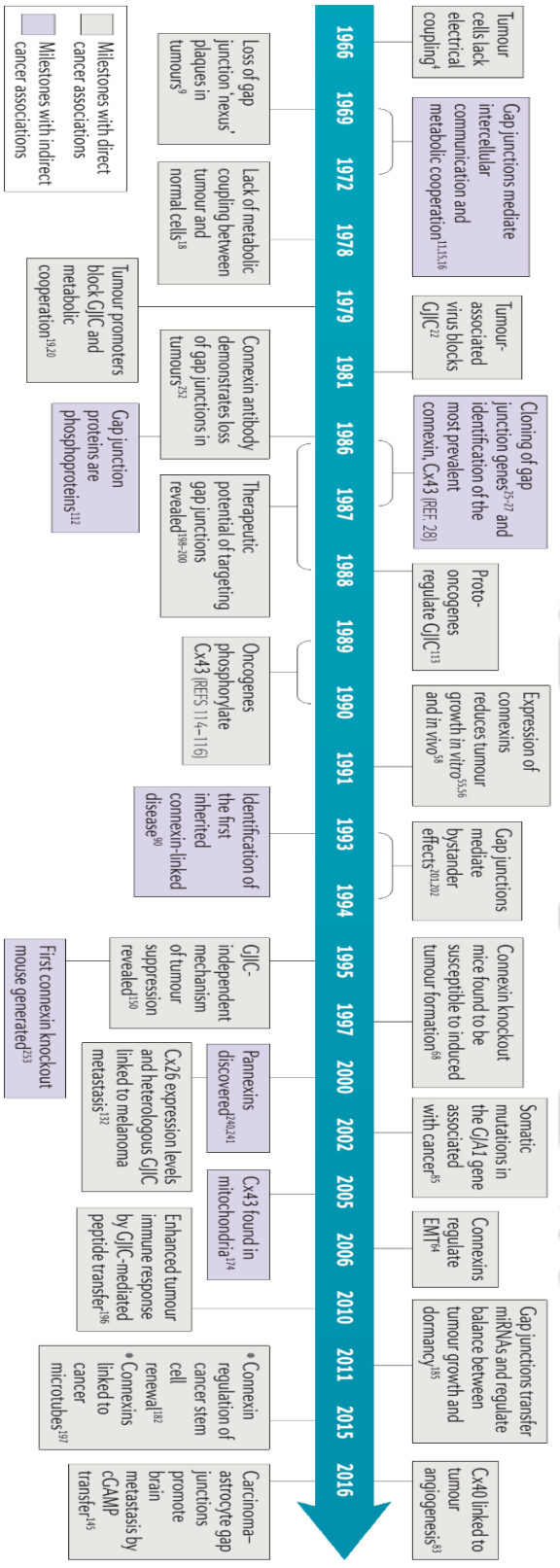

Figure 1.1. The Timeline shows key discoveries related to GJs and cancer. Milestones with less direct cancer associations are depicted in purple. cGAMP, 2′3′-cGMP–AMP; Cx, connexin; EMT, epithelial to mesenchymal transition; GJIC, GJ intercellular communication; miRNAs, microRNAs. Reproduced with Permission from Reference [9]. Copyright © 2016, Macmillan Publishers Limited, part of Springer Nature

communication. Cells may have defective GJIC at multiple instances as follows, a) they may lack functional GJ, b) they may have functional GJs amongst themselves, but are incapable to communicate between nontransformed cells, c) they may form functional cell-cell coupling among themselves, but are unable to respond to the GJ signals that mediate differentiation, opening and closing of GJ and phenotype of the cell.

1.3 The connexin Multigene Family

The functions and behaviour of individual cells are governed at two levels in multicellular organisms: a) within the cells and b) through intercellular communication. Cancer is a disease of "abnormal homeostasis" facilitated by irregularities in extra-, inter- and intracellular forms of communications. Intercellular communication between cells is achieved with the help of GJIC. GJIC plays a crucial role in maintaining cell-cell homeostasis by keeping growth control signals at equilibrium among GJIC connected cells [10]. Each GJ channel is composed of a pair of hemichannels or connexon and a single connexon is comprised of six protein subunits known as connexins [11]. All known connexins are the four pass transmembrane α-helical domains, two intracellular termini, two extracellular and one intracellular loop having cytoplasmic amino- and carboxyl- terminal. The membrane spanning regions lie in parallels. The carboxy tail of the most of the connexins are phosphorylated. A complete channel between neighbouring cells is formed when two connexons align end-to-end **(Fig. 1.2)**. Each channels have the measurement of approximately 1.5-2 nm diameter depending on the connexin proteins type. They allow many molecules and ions of small sizes (<2000 Da) to directly diffuse among the cells. Several small molecules including sugars, drugs, small peptides, fatty acids, amino acids, nucleotides, waters, ions and carcinogens are able to pass through these channels. However, RNA, polysaccharides, complex lipids, proteins and other large molecules are not.

Connexins, the GJ forming proteins are comprises of a multi-gene family with at least 21 connexins discovered so far [12]. They all share a common basic structure and vary due to the structural differences within the cytosolic areas [13]. The different connexins species are designated based on two nomenclature systems. First system associated the molecular weight of the connexins with the name (e.g. Cx43 has

molecular weight of 43 kDa), as deduce by the cDNA sequencing. The second system classified connexins into subclasses (a, h, g, or y) based on their sequence similarity and length of the cytoplasmic domain with added prefix "GJ" for GJ and assigned a number based on their order of discovery. Out of these two systems, molecular weight-based nomenclature is used most commonly. In an old nomenclature system, which was adopted in 1987 GJ meeting at Asilomar, connexins distinguishes based on their species of origin (e.g. r for rat, ch for chicken, xen for Xenopus, b for bovine, h for human, etc.) [14]. Out of all the connexins **(Table 1.1)**, most of the established cell lines express Cx43, while readily detectable amount of other connexins are found in very few cell lines. In addition, the downregulation of Cx43 has been elucidated and the mechanism behind it studied in detail in the cancer research area at molecular level [15].

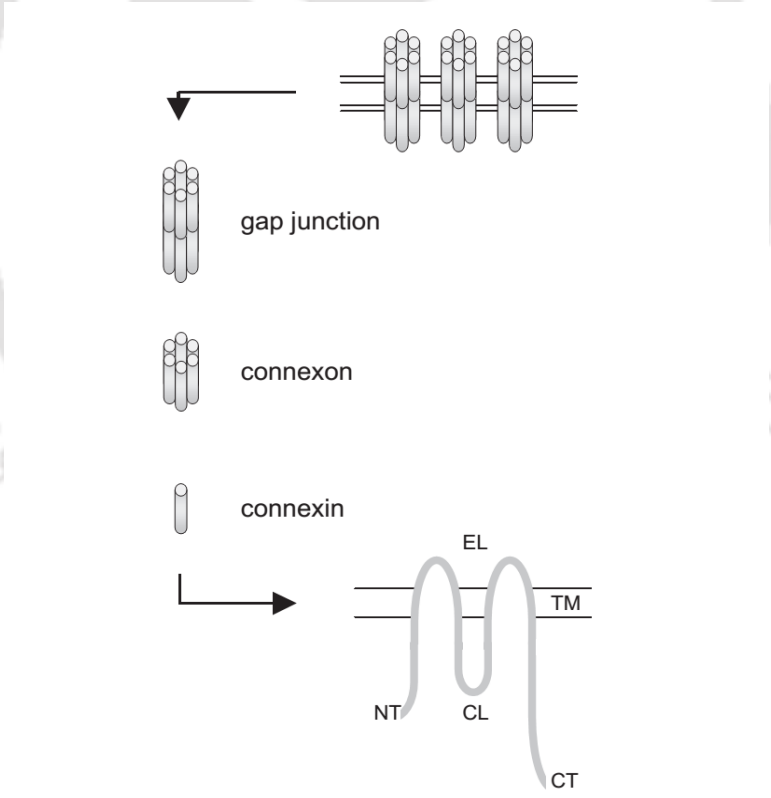

Figure 1.2. The connexin structure consists of two extracellular loops (EL), four membrane spanning domains (TM), one cytoplasmic loop (CL), one N-terminal tail (NT), and one C-terminal tail (CT). Reproduced with Permission from Reference [16]. Copyright © 2005 Elsevier Inc.

Table 1.1
The connexin gene family and its chromosomal distribution in mouse and human. This table reflects the current state of the sequence information available from the NCBI database (http://www.ncbi.nlm.nih.gov/genomes/static/euk_g.html). Reproduced with Permission from Reference [12]. Copyright © 2004, European Society of Cardiology

Mouse connexin			**Human connexin**		
Connexin	**GJ**	**chr**	**chr**	**GJ**	**Connexin**
mCx23		10	6		**hCx23**
			6		**hCx25**
mCx26	Gjb2	14	13	GJB2	**hCx26**
mCx29	Gje1	5	7	GJE1	**hCx30.2 (hCx31.3)**
mCx30	Gjb6	14	13	GJB6	**hCx30**
mCx30.2	Gja11	11	17	GJA11	**hCx31.9**
mCx30.3	Gjb4	4	1	GJB4	**hCx30.3**
mCx31	Gjb3	4	1	GJB3	**hCx31**
mCx31.1	Gjb5	4	1	GJB5	**hCx31.1**
mCx32	Gjb1	X	X	GJB1	**hCx32**
mCx33	Gja6	X			
mCx36	Gja9	2	15	GJA9	**hCx36**
mCx37	Gja4	4	1	GJA4	**hCx37**
mCx39		18	10		**hCx40.1**
mCx40	Gja5	3	1	GJA5	**hCx40**
mCx43	Gja1	10	6	GJA1	**hCx43**
mCx45	Gja7	11	17	GJA7	**hCx45**
mCx46	Gja3	14	13	GJA3	**hCx46**
mCx47	Gja12	11	1	GJA12	**hCx47**
mCx50	Gja8	3	1	GJA8	**hCx50**
			1	GJA10	**hCx59**
mCx57	Gja10	4	6		**hCx62**
Σ 20					**Σ 21**

1.4 Loss of GJIC and Connexins is an Early Event of Malignancy

The general observation that has been often claimed in carcinogenesis is a decreased expression of Cxs. However, it is difficult to deduce point out at which step of the multistage process it really does occur. Multiple tumour promoting agents and carcinogens (over 100) known to inhibit GJIC during carcinogenesis. TPA (12-O-tetradecanoylphorbol-13-acetate), pesticides, dietary additives, polyhalogenated hydrocarbons or cigarette components are such examples. Some oncogenes like Src and Ras regulate Cxs expression and phosphorylation [17-20]. The ability of inhibiting GJIC is one of the most common properties of the tumour promoters **(Fig. 1.3)**. However, the normal cells are less sensitive towards the GJIC inhibitory effects of tumour promoters as compare to the preneoplastic cells [21-23]. Similar effects have been seen in the protein products of the various oncogenes. In addition to deregulating growth control, gene regulation, signal transduction and other aspects of cellular and tissue homeostasis, they can block GJIC [24, 25]. When applied to cultured cells, many growth factors, such as transforming growth factor alpha, hepatic growth factor, basic fibroblast growth factor, platelet derived growth factor and epidermal growth factor inhibit GJIC [26]. In other case, few growth factors like transforming growth factor beta selectively enhance and inhibit GJIC depending on cell types [27]. Furthermore, some chemopreventive and antitumour promoting agents like retinoids, are known to enhance cell-cell comunications, providing additional mode of evidence for this relation.

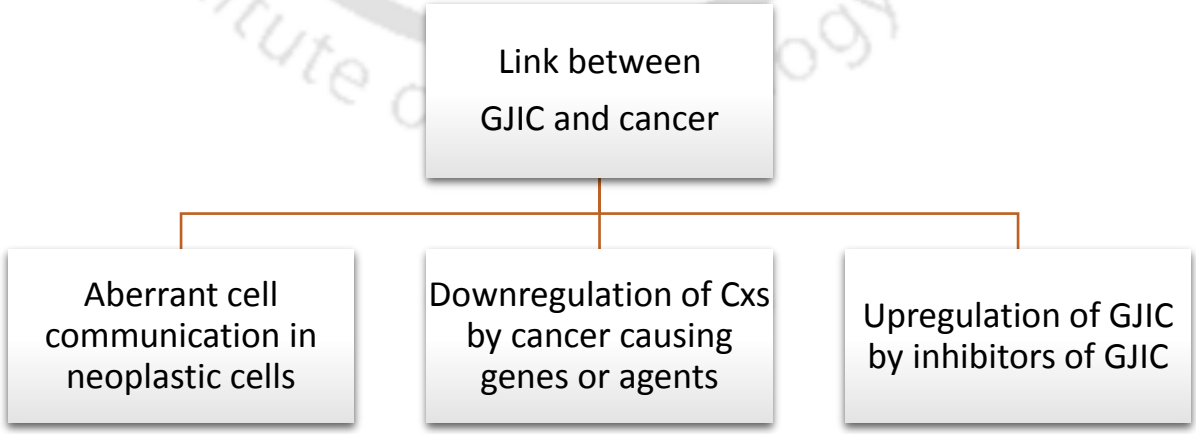

Figure 1.3. Relationship between GJIC and cancer.

Various mechanism is involved in modulating the GJIC during carcinogenesis. Apart from the basic regulatory mechanism, like post-translational modifications, translational control, mRNA splicing and transcription, which apply for most of the proteins, the Cxs functions also regulated at different control levels. For example, the connexons formed by the assembly of Cxs in the trans-Golgi apparatus and its movement to plasma membrane can also be regulated [28]. Moreover, the GJIC can be influenced by opening and closing of the channels under different circumstances, growth factors, extracellular matrix as well as cell adhesion molecules and mutations in Cxs genes. These are the most critical mechanisms, which is susceptible to carcinogenic insults.

1.5 Tumour Suppression by Connexins

Multiple evidences suggested the impairment of GJIC during carcinogenesis, therefore, a series of approaches have been designed to up-regulate Cxs expression to restore GJIC and control growth. Several studies have been reported the effect of retinoids on increasing GJIC and decreasing transformation and cell growth [29-31] . In further studies, a thorough examination of the role of increasing GJIC by increasing the expression of Cxs proteins on tumour suppression was performed by cloning various Cxs cDNAs. Functional analyses was carried out by transfecting specific Cx RNA into oocytes of Xenopus. The *in vitro* and *in vivo* transfection and expression of Cx40 [32], Cx26 [32, 33], Cx32 [34] and Cx43 [35-37] in various tumours resulting in increased GJIC. However, only few connexins established the relation between the level of expression and tumour suppression. In supported evidence, in which the chemically transformed human glioblastoma, mouse fibroblasts, human rhabdomyosarcoma and rat glioma cells, which are deficient in Cx43, loss there tumourigenicity and showed reduced cell growth after transfection with the Cx43 cDNA [35, 36]. Although, when the chemically transformed mouse fibroblasts cells and rat glioma cells, when transfected with Cx32, no reduction in tumour growth was observed [38]. There are evidences which showed that restoration of GJIC decrease the transformed phenotype of the cancer cells. Enforced expression of Cx43 in a canine kidney epithelial cell line altered the regulation of cell-cycle regulatory proteins, suggesting the involvement of Cx43 in altering the level of certain CDKs, thus

influencing cell cycle regulation directly or indirectly based on the mode of action, the anti-tumour activity of Cx43 have been divided into two groups:

1.5.1 GJIC-dependent Mechanism: the *Bystander Effect*

Recent strategy to combat cancer involves a process called "*bystander effect*" (BE). This strategy does not require the drug to reach all tumour cells; instead, triggering the death process in a single cell could be amplified by transfer of the cytotoxic signalling molecules via GJICs causing death of the interacting cells [39]. BE has been considered as an important mechanism, as it does not depend on the drugs to reach all tumour cells [40]. The BE potential directly depend on the extent of GJIC and levels of connexin expression. In particular, Cx43 mediates BE [41]. Connexins and GJs are tightly regulated even though connexins are capable of functions of their own [42]. In an interesting finding by Cottin S *et al* in 2008, it was showed that even though Cx43 is localized in the cytoplasm, it is still able to exhibit bystander effect [43]. The exact mechanism behind this is unknown till date.

To increase the therapeutic activity of BE, use of enzyme/prodrug strategy has shown a great potential. Numerous studies have shown that, the increase in cell killing by increasing the bystander effects, when connexins are over-expressed along with HSV-tk/GCV suicide gene therapy system. Co-culture of cells expressing connexins and those without connexins, when treated with HSV-tk/GCV, showed an increased cell death as compared to the number of cells that originally got HSV-tk [44]. While over expression of connexins has been shown to increase the BE in HSV-tk/GCV system, there is no such documentation available with cytosine deaminase (CD)/5-fluorouracil (5-FC) system **(Fig 1.4)**.

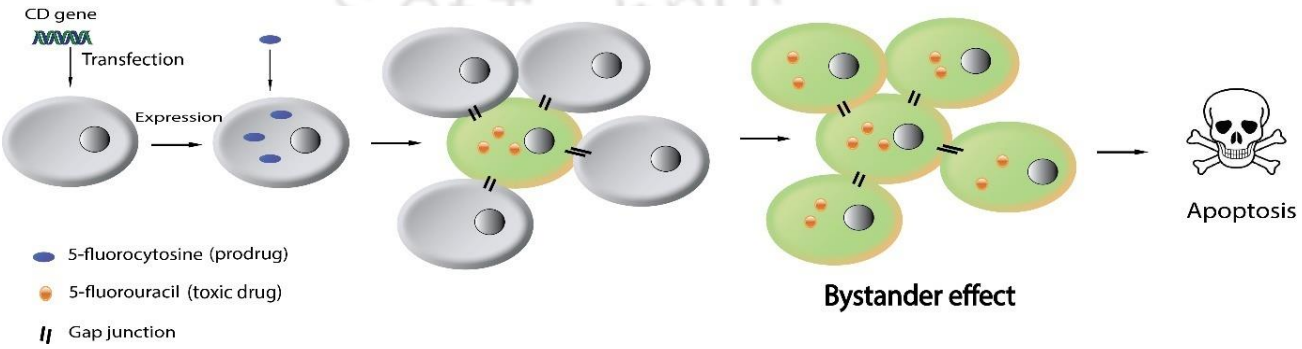

Figure 1.4. Bystander effect with CD/5-FC system.

1.5.2 GJIC Independent Mechanism: Modulation of Anti-tumour Proteins

It has long been known that Cx43 only involve in the formation of GJ and maintain GJIC among the cells, which further contribute in normal cell growth. Recently, the accumulating evidences suggested GJ-independent role of Cx43 in tumour suppression and regulating cell growth. Mesnil *et al* demonstrated that there was no correlation between the GJIC formed by different connexins and tumourigenicity. More studies acknowledge that the anti-tumour effect on cancer behaviour may rely on the connexin proteins itself, rather than on cell-cell coupling [45]. For example, the transfection of Cx43 gene into human glioblastoma cells reversed the transformed phenotype of the cells; however, the reversed transformed activity was found to be unrelated of GJIC [37].

The mechanistic aspects of the GJ-independent regulation of cancer cells by connexin proteins depends on its role in affecting tumourigenic cell cycle and signalling. The carboxyl terminal of Cx43 protein is known to regulate cell growth by interacting with the other anti-tumour proteins and transcription factors. The Cxs localized in cytoplasm and nucleus also exhibit cell growth suppression function [46, 47]. Connexin proteins influence the activity and production of many cell cycle regulatory proteins, such as FGF1, Src, ERK 1/2, cyclin D2, Cyclin D1, Cyclin A, p27kip1 and p21cip1 [48-52]. It has been reported that Cx43 downregulate Wnt signalling by interacting with the β-catenin at cell-cell contact areas and reduces the amount of β-catenin that is available for signalling resulting in inhibition of cell proliferation [53]. Several apoptotic genes, such as Bcl-2, Bcl-xL, and surviving are targeted in Wnt signalling [54-56]. Interestingly, it has been found that the Cx43 gene itself is the downstream target of β-catenin signal cascade, which imply that Cx43 can regulate its own production [57]. Recent findings suggest that connexin interacts with various proteins including actin, microtubules, cytoskeletons, N-cadherin, claudins, occluding and zonula occludens-1 [58-60]. In other report, the overexpression of Cx43 has been correlated with the accumulation of the hypophosphated retinoblastoma (Rb) protein and increase in the level of p27 proteins, a cyclin dependent kinase inhibitor [52]. The same group also showed the negative regulation of the human F-box protein S phase kinase-associated protein 2 (Skp2) by Cx43 protein. Skp2 is involved in the proteosomal degradation of p27 and p21 proteins [61]. The role of GJ independent

inhibitory action of Cx43 was demonstrated using GJ inhibitors. Even though, only C-terminus domain of the Cx43 protein, which does not form GJ channels exhibited the same inhibitory effect as full length Cx43 protein [62]. They postulated that the movement of cAMP through the GJ is involved in the GJ-dependent synthesis of p27 proteins while inhibition of Skp2 proteins is responsible for GJ-independent degradation of p27 protein.

1.6 Restoring Connexin Expression as a Therapeutic Approach

Cx protein inhibits the tumour growth and the downregulation of Cx protein in cancer. Therefore, the restoring connexins expression could provide an alternative therapeutic approach towards cancer treatment. Restoration of Cx can be achieved through different approaches listed below.

1.6.1 Gene Therapy

Gene therapy has assumed enormous significance in recent years as it can offer one-time solution for many genetic disorders including cancer. In cancer gene therapy both malignant and non-malignant cells can be the target. Efforts to treat cancer by gene therapy are being made in several ways like

- Transfer of gene to enhance the immune response towards tumour
- Transfer of tumour-suppressor genes that can replace the altered or missing gene
- Transfer of drug-resistance genes
- RNA Interference
- Transfer of suicide genes [63, 64]

Restoration of Cx with the help of gene therapy involved the cloning and transfection of cDNA into Cx deficient cells. The exogenous expression of Cx43 resulting into the formation of the functional GJIC among neighbouring cells. GJIC further help in increasing the drug penetration and dispersal in tumours. In addition of exchanging molecules between cells to permit metabolic cooperation; they also transmit stress signal, apoptosis signal, developmental signals and molecules affecting cellular regulation, including such second messengers as inositol 1,4,5-trisphosphate and Ca2+ [65].

1.6.2 Targeting Transcriptional Regulation of Connexins

In many cancer cells, inactivation of the Cx expression is found to be regulated at the transcriptional level. Histone deacetylase (HDAC), a group of enzymes that effect global gene expression and regulate chromatin remodelling are the targets of anti-cancer therapeutics. Several HDAC inhibitors (HDACi) have shown there anti-cancer potential, both *in vivo* as well as *in vitro*. The HDACi also showed its effect on the expression of connexins and formation of GJIC. For example, 4-phenylbutyrate (4-PB), a HDACi, established a functional GJ communication between adjacent pancreatic cells [66]. 4-PB showed over-additive effect in combination with nucleoside analogue gemcitabine in pancreatic cancer cells. The GJIC established after the 4-PB treatment potentiates GJ mediated bystander killing in glioma cells by HSV-tk/ganciclovir suicide gene therapy system [67]. In prostate cancer cells, the Cx43 expression and GJIC were restored using another HDACi, trichostatin A (TSA) [68]. In rat epithelial cells, sodium butyrate and TSA countered TPA and H_2O_2 induced inhibition of GJIC, as well as hyperphosphorylation and degradation of Cx43 [69].

In some instance, aberrant methylation is also responsible for the inactivation of Cxs genes to become another target for cancer therapy. Cx32 gene is downregulated in human renal cell carcinoma by promoter hypermethylation. 5-aza-2'-deoxycytidine (5-aza-C), a DNA demethylating agent, restored Cx32 expression and suppressed growth of renal cell carcinoma (RCC) in xenograft model [70].

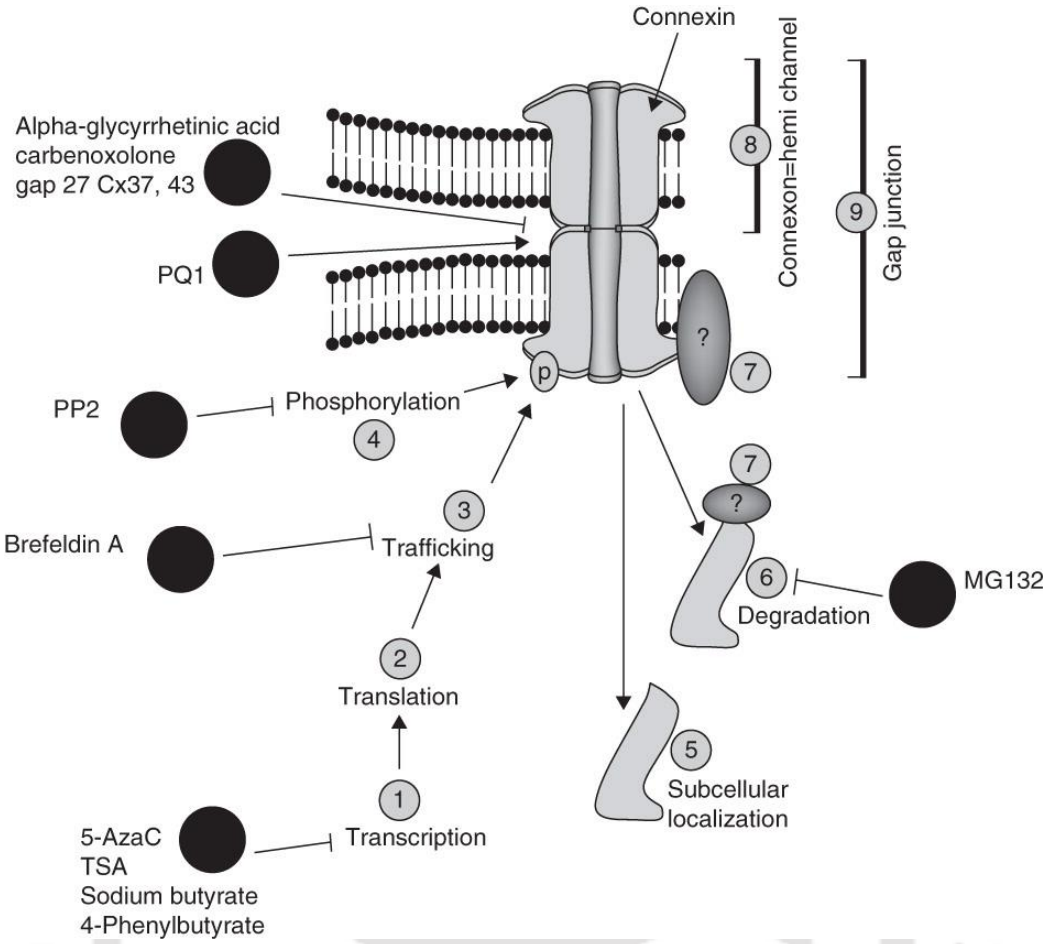

Figure 1.6. Illustration of different levels of potential therapeutic intervention to modulate the connexins (Cxs) expression and function. Transcription modulators (TM) including Histone deacetylase inhibitors (HDACi) such as Trichostatin A (TSA), Sodium butyrate and 4-phenylbutyrate, or demethylating agents such as 5-Aza-Cytidine (5-AzaC) are used to increase Cxs transcription (1). Although no drugs have yet been assessed for their effect on Cxs translation (2), these are important levels of post transcriptional regulation. Although not used in anti-cancer settings, the trafficking inhibitor (TI) brefeldin A, a small hydrophobic molecule that disassembles the Golgi, has been shown to interrupt Cx26 and Cx43 trafficking (3) to the cell membrane via the golgi [96]. Phosphorylation (4) is the best studied Cxs post-translational modification and can be affected by tyrosine kinase inhibitors (TKI) such as the Src inhibitor 4-amino-5-(4-chlorophenyl)-7-(t-butyl)pyrazolo[3,4-d]pyramidine (PP2). Due to the importance of Cxs subcellular localization (5) for its expression and function, this is important information to take into consideration when targeting Cxs. Of particular interest is the endocytic life of connexins and GJs [97]. The life of Cxs is also dependent on post-translational ubiquitination and degradation by the

proteasome (6), which offers an opportunity to increase their level by using proteasome inhibitors (PI) such as MG132. Also, the number of Cxs-interacting proteins (7) is still undetermined, although some interactors have been identified such as the cytoskeleton proteins (microtubules, actin filaments). In other respect, whether Cxs are involved in hemichannels (8), gap junction plaques (9) or acting alone, determining differences in their functions should condition the way they are manipulated for therapeutic purposes. Similarly, the impact of various GJ inhibitors (GJI) such as a-glycyrrehetinic acid, or activators (GJA) such as the Quinoline derivative PQ1 is still ill defined. Reproduced with Permission from Reference [71]. Copyright © 2010, Taylor & Francis.

1.7 Drug Delivery

Many chemotherapeutic drugs have problems of poor stability, low water solubility and low efficiency. To overcome these barriers, several nanocomposites have been designed to improve drug stability, solubility and efficiency. These modified polymeric nanodelivery system can also be engineered to target only cancer cells without affecting normal cells, using cancer cell specific biomarkers. Polymeric nanoparticles are colloidal solid particles synthesized from non-biodegradable polymers like PLGA (poly-lactic co-glycolic acid) and PLA (poly-lactic acid) or biodegradable polymers such as collagen, sodium alginate, albumin and chitosan [72-74]. Due to the advantage of small size (50-300 nm), these particles can easily take up by the cells and penetrate into the capillaries resulting in the accumulation of the drug at the target site of action. They have showed their potential as a promising nanocarriers for drug delivery by improving the specificity towards the target cell changing their physicochemical properties and pharmacokinetics [73]. Chitosan based-nanoparticle hold the immense potential in the field of drug delivery due to their biocompatibility, high loading efficiency, water-retention capabilities, and bio-adhesiveness. Chitosan is a natural, linear polysaccharide of deacetylated beta-1, 4-D-glucosamine obtained by the partial N-deacetylation of chitin, the second most abundant polysaccharide in Nature [75, 76].

To enable optical tracking and monitoring of the nanocarriers, fluorescent moieties may be attached to polymeric templates. The particles then discovered known as 'nanoclusters', which differ widely in physicochemical properties from their

nanoparticle counterparts. Fluorescent NPs are evolving as a promising tool for theranostic purposes [77].

1.8 Key Areas and Scope of Research

Based on the literature review in the field of GJ-dependent as well as GJ-independent anti- tumour activity of Cx43, the research areas with potential scope are summarized below:

- The role of GJIC in cancer cells, their potential clinical usage as well as the advantages they hold over current modes of cancer therapy
- The GJ-dependent as well as independent mode of anti-tumour property mediated by Cx43
- The role of GJIC in mediating 'bystander effect' in combination with chemotherapeutic drugs
- Molecular pathway behind the anti-tumour activity of Cx43
- Combination therapy involving different method of Cx43 expression and changes in chemotherapeutic drug sensitivity in the cancer cell

1.9 The present work

1.9.1 Objective

The main objectives of the present work are as follows:

- Studying the of establishment of functional GJIC by expressing Cx43, through different means in MCF-7 cells
- Targeting cancer cells via GJ-dependent as well as independent pathways
- Investigating the role of Cx43 in mediating "bystander effect"
- To study the effect of 4-phenylbutyrate (4-PB) on the expression of Cx43 GJ protein in MCF-7 cell line in combination with artesunate (ART)
- Studying the anti-tumour property of Cx43 in enhancing suicide gene therapy
- Evaluation of 4-PB bound nanocarrier and its activity on MCF-7 cells based spheroid model

1.9.2 Significance and Salient Features of the Present Study

The significance and salient features of the present study are summarized below:

- Cloning of Cx43 gene and its stable expression was performed in MCF-7 cells
- Therapeutic implications of Cx43 in enhancing the tumour suppressing activity of artesunate via GJ-dependent as well as independent pathways in human breast cancer cells was studied
- GJIC mediated bystander cell death after treatment with ART and the transfer of ROS between the neighbouring cancer cells not exposed to ART was demonstrated by performing co-culture experiment
- Use of 4-PB in forceful expression of Cx43 and its synergistic interaction with ART both in MCF-7 cells as well as in DLA bearing mice was demonstrated
- Comparative analysis between wtCD and F186W transfected A549 cells were performed by assessing cell viability after 5-FC treatment in suicide gene therapy
- Improvement in the cytotoxic activity of the F186W mutant in conjunction with the Cx43 has been reported
- Fabrication of a versatile novel 4-PB bound composite nanoparticles has been demonstrated and the efficacy of the 4-PB bound nanocarrier was also evaluated in spheroids based model of cancer cells

1.10 References

[1] W.R. Loewenstein, Permeability of membrane junctions, Ann N Y Acad Sci 137(1) (1966) 441-472.

[2] Y. KANNO, Modulation of cell communication and carcinogenesis, The Japanese journal of physiology 35(5) (1985) 693-707.

[3] H. Yamasaki, M. Mesnil, Y. Omori, N. Mironov, V. Krutovskikh, Intercellular communication and carcinogenesis, Mutation Research/Fundamental and Molecular Mechanisms of Mutagenesis 333(1) (1995) 181-188.

[4] E.R. Fearon, B. Vogelstein, A genetic model for colorectal tumourigenesis, Cell 61(5) (1990) 759-767.

[5] K. Willecke, J. Eiberger, J. Degen, D. Eckardt, A. Romualdi, M. Güldenagel, U. Deutsch, G. Söhl, Structural and functional diversity of connexin genes in the mouse and human genome, Biol Chem 383(5) (2002) 725-737.

[6] W.R. Loewenstein, Y. Kanno, Intercellular communication and the control of tissue growth: lack of communication between cancer cells, Nature 209(5029) (1966) 1248-1249.

[7] W.R. Loewenstein, Y. Kanno, Intercellular communication and tissue growth, The Journal of cell biology 33(2) (1967) 225-234.

[8] J.W. Holder, E. Elmore, J.C. Barrett, Gap Junction Function and Cancer, Cancer Research 53(15) (1993) 3475-3485.

[9] T. Aasen, M. Mesnil, C.C. Naus, P.D. Lampe, D.W. Laird, Gap junctions and cancer: communicating for 50 years, Nat Rev Cancer 16(12) (2016) 775-788.

[10] W.R. Loewenstein, B. Rose, The cell-cell channel in the control of growth, Seminars in Cell Biology 3(1) (1992) 59-79.

[11] T. White, R. Bruzzone, D. Paul, The connexin family of intercellular channel forming proteins, Kidney international 48(4) (1995) 1148-1157.

[12] G. Söhl, K. Willecke, Gap junctions and the connexin protein family, Cardiovasc Res 62(2) (2004) 228-232.

[13] P.E.M. Martin, G. Blundell, S. Ahmad, R.J. Errington, W.H. Evans, Multiple pathways in the trafficking and assembly of connexin 26, 32 and 43 into gap junction intercellular communication channels, J Cell Sci 114(21) (2001) 3845-3855.

[14] H. Yamasaki, C.C. Naus, Role of connexin genes in growth control, Carcinogenesis 17(6) (1996) 1199-1213.

[15] C.C. Naus, Gap junctions and tumour progression, Can J Physiol Pharmacol 80(2) (2002) 136-141.

[16] M. Vinken, T. Vanhaecke, P. Papeleu, S. Snykers, T. Henkens, V. Rogiers, Connexins and their channels in cell growth and cell death, Cell Signal 18(5) (2006) 592-600.

[17] J.L. Brissette, N.M. Kumar, N.B. Gilula, G.P. Dotto, The tumour promoter 12-O-tetradecanoylphorbol-13-acetate and the ras oncogene modulate expression and phosphorylation of gap junction proteins, Mol Cell Biol 11(10) (1991) 5364-5371.

[18] E. Leithe, E. Rivedal, Epidermal growth factor regulates ubiquitination, internalization and proteasome-dependent degradation of connexin43, J Cell Sci 117(7) (2004) 1211-1220.

[19] M.H. Tai, B.L. Upham, L.K. Olson, M.S. Tsao, D.N. Reed, J.E. Trosko, Cigarette smoke components inhibited intercellular communication and differentiation in human pancreatic ductal epithelial cells, Int J Cancer 120(9) (2007) 1855-1862.

[20] E. Peterson-Roth, C.M. Brdlik, P.M. Glazer, Src-Induced cisplatin resistance mediated by cell-to-cell communication, Cancer Res 69(8) (2009) 3619-3624.

[21] J. Klaunig, R. Ruch, C. Weghorst, J. Hampton, Role of inhibition of intercellular communication in hepatic tumour promotion, In Vitro Toxicol. 3(1) (1990) 91-107.

[22] V. Krutovskikh, M. Mesnil, G. Mazzoleni, H. Yamasaki, Inhibition of rat liver gap junction intercellular communication by tumour-promoting agents in vivo. Association with aberrant localization of connexin proteins, Laboratory investigation; a journal of technical methods and pathology 72(5) (1995) 571-577.

[23] I.V. Budunova, S. Carbajal, T.J. Slaga, Effect of diverse tumour promoters on the expression of gap-junctional proteins connexin (Cx) 26, Cx31. 1, and Cx43 in SENCAR mouse epidermis, Mol Carcinog 15(3) (1996) 202-214.

[24] H. Yamasaki, Gap junctional intercellular communication and carcinogenesis, Parallels in Cell to Cell Junctions in Plants and Animals, Springer1990, pp. 115-127.

[25] M.R. Na, S.K. Koo, D.Y. Kim, S. Dai Park, K.W. Kang, C.O. Joe, In vitro inhibition of gap junctional intercellular communication by chemical carcinogens, Toxicology 98(1) (1995) 199-206.

[26] R.J. Ruch, The role of gap junctional intercellular communication in neoplasia, Advances in Oncobiology 1 (1996) 119-141.

[27] E. Van Zoelen, L. Tertoolen, Transforming growth factor-beta enhances the extent of intercellular communication between normal rat kidney cells, J Biol Chem 266(18) (1991) 12075-12081.

[28] L.S. Musil, D.A. Goodenough, Biochemical analysis of connexin43 intracellular transport, phosphorylation, and assembly into gap junctional plaques, The Journal of cell biology 115(5) (1991) 1357-1374.

[29] H. Yamasaki, F. Katoh, Further evidence for the involvement of gap-junctional intercellular communication in induction and maintenance of transformed foci in BALB/c 3T3 cells, Cancer Res 48(12) (1988) 3490-3495.

[30] P.P. Mehta, J.S. Bertram, W.R. Loewenstein, The actions of retinoids on cellular growth correlate with their actions on gap junctional communication, The Journal of cell biology 108(3) (1989) 1053-1065.

[31] J.S. Bertram, A.L. Vine, Cancer prevention by retinoids and carotenoids: independent action on a common target, Biochimica et Biophysica Acta (BBA)-Molecular Basis of Disease 1740(2) (2005) 170-178.

[32] M. Mesnil, V. Krutovskikh, C. Piccoli, C. Elfgang, O. Traub, K. Willecke, H. Yamasaki, Negative growth control of HeLa cells by connexin genes: connexin species specificity, Cancer Res 55(3) (1995) 629-639.

[33] C. Tomasetto, M.J. Neveu, J. Daley, P.K. Horan, R. Sager, Specificity of gap junction communication among human mammary cells and connexin transfectants in culture, The Journal of cell biology 122(1) (1993) 157-167.

[34] S.L. Bond, J.F. Bechberger, N. Khoo, C. Naus, Transfection of C6 glioma cells with connexin32: the effects of expression of a nonendogenous gap junction protein, Cell growth & differentiation: the molecular biology journal of the American Association for Cancer Research 5(2) (1994) 179-186.

[35] D. Zhu, S. Caveney, G. Kidder, C. Naus, Transfection of C6 glioma cells with connexin 43 cDNA: analysis of expression, intercellular coupling, and cell proliferation, Proceedings of the National Academy of Sciences 88(5) (1991) 1883-1887.

[36] R. Huang, Y. Lin, C.C. Wang, J. Gano, B. Lin, Q. Shi, A. Boynton, J. Burke, R.-P. Huang, Connexin 43 suppresses human glioblastoma cell growth by down-regulation of monocyte chemotactic protein 1, as discovered using protein array technology, Cancer Res 62(10) (2002) 2806-2812.

[37] R.-P. Huang, Y. Fan, M.Z. Hossain, A. Peng, Z.-L. Zeng, A.L. Boynton, Reversion of the neoplastic phenotype of human glioblastoma cells by connexin 43 (cx43), Cancer Res 58(22) (1998) 5089-5096.

[38] B. Eghbali, J. Kessler, L. Reid, C. Roy, D. Spray, Involvement of gap junctions in tumourigenesis: transfection of tumour cells with connexin 32 cDNA retards growth in vivo, Proceedings of the National Academy of Sciences 88(23) (1991) 10701-10705.

[39] I.J. van Dillen, N.H. Mulder, W. Vaalburg, E.F.J. de Vries, G.A.P. Hospers, Influence of the Bystander Effect on HSV-tk / GCV Gene Therapy. A Review, Current Gene Therapy 2(3) (2002) 307-322.

[40] I.J. van Dillen, N.H. Mulder, W. Vaalburg, E.F. de Vries, G.A. Hospers, Influence of the bystander effect on HSV-tk/GCV gene therapy. A review, Curr Gene Ther 2(3) (2002) 307-322.

[41] R.A. McMasters, R.L. Saylors, K.E. Jones, M.E. Hendrix, M.P. Moyer, R.R. Drake, Lack of bystander killing in herpes simplex virus thymidine kinase-transduced colon cell lines due to deficient connexin43 gap junction formation, Hum Gene Ther 9(15) (1998) 2253-2261.

[42] M. Mesnil, S. Crespin, J.-L. Avanzo, M.-L. Zaidan-Dagli, Defective gap junctional intercellular communication in the carcinogenic process, Biochimica et biophysica acta 1719(1-2) (2005) 125-145.

[43] S. Cottin, K. Ghani, M. Caruso, Bystander effect in glioblastoma cells with a predominant cytoplasmic localization of connexin43, Cancer gene therapy 15(12) (2008) 823-831.

[44] T. Jimenez, W.P. Fox, C.C.G. Naus, J. Galipeau, D.J. Belliveau, Connexin Over-Expression Differentially Suppresses Glioma Growth and Contributes to the Bystander Effect Following HSV-Thymidine Kinase Gene Therapy, Cell Communication and Adhesion 13(1-2) (2006) 79-92.

[45] L. Cronier, S. Crespin, P.-O. Strale, N. Defamie, M. Mesnil, Gap junctions and cancer: new functions for an old story, Antioxid Redox Signal 11(2) (2009) 323-338.

[46] C. Moorby, M. Patel, Dual functions for connexins: Cx43 regulates growth independently of gap junction formation, Exp Cell Res 271(2) (2001) 238-248.

[47] X. Dang, B.W. Doble, E. Kardami, The carboxy-tail of connexin-43 localizes to the nucleus and inhibits cell growth, Cardiac Cell Biology, Springer2003, pp. 35-38.

[48] G. Olbina, W. Eckhart, Mutations in the second extracellular region of connexin 43 prevent localization to the plasma membrane, but do not affect its ability to suppress cell growth, Mol Cancer Res 1(9) (2003) 690-700.

[49] F. Princen, P. Robe, D. Gros, T. Jarry-Guichard, J. Gielen, M.-P. Merville, V. Bours, Rat gap junction connexin-30 inhibits proliferation of glioma cell lines, Carcinogenesis 22(3) (2001) 507-513.

[50] H. Qin, Q. Shao, T. Thomas, J. Kalra, M.A. Alaoui-Jamali, D.W. Laird, Connexin26 regulates the expression of angiogenesis-related genes in human breast tumour cells by both GJIC-dependent and-independent mechanisms, Cell communication & adhesion 10(4-6) (2003) 387-393.

[51] H. Qin, Q. Shao, H. Curtis, J. Galipeau, D.J. Belliveau, T. Wang, M.A. Alaoui-Jamali, D.W. Laird, Retroviral delivery of connexin genes to human breast tumour cells inhibits in vivo tumour growth by a mechanism that is independent of significant gap junctional intercellular communication, J Biol Chem 277(32) (2002) 29132-29138.

[52] Z. You-Wei, I. Morita, M. Ikeda, M. Kai-Wen, S. Murota, Connexin43 suppresses proliferation of osteosarcoma U2OS cells through post-transcriptional regulation of p27, Oncogene 20(31) (2001) 4138.

[53] Z. Ai, A. Fischer, D.C. Spray, A.M. Brown, G.I. Fishman, Wnt-1 regulation of connexin43 in cardiac myocytes, J Clin Investig 105(2) (2000) 161.

[54] P.J. Kim, J. Plescia, H. Clevers, E.R. Fearon, D.C. Altieri, Survivin and molecular pathogenesis of colorectal cancer, The Lancet 362(9379) (2003) 205-209.

[55] H. Xie, Z. Huang, M.S. Sadim, Z. Sun, Stabilized β-catenin extends thymocyte survival by up-regulating Bcl-xL, The Journal of Immunology 175(12) (2005) 7981-7988.

[56] Q. Li, W.-M. Dashwood, X. Zhong, H. Nakagama, R.H. Dashwood, Bcl-2 overexpression in PhIP-induced colon tumours: cloning of the rat Bcl-2 promoter and characterization of a pathway involving β-catenin, c-Myc and E2F1, Oncogene 26(42) (2007) 6194.

[57] M. Van der Heyden, M.B. Rook, M. Hermans, G. Rijksen, J. Boonstra, L. Defize, O. Destree, Identification of connexin43 as a functional target for Wnt signalling, J Cell Sci 111(12) (1998) 1741-1749.

[58] B.N. Giepmans, I. Verlaan, T. Hengeveld, H. Janssen, J. Calafat, M.M. Falk, W.H. Moolenaar, Gap junction protein connexin-43 interacts directly with microtubules, Curr Biol 11(17) (2001) 1364-1368.

[59] X. Xu, W. Li, G. Huang, R. Meyer, T. Chen, Y. Luo, M. Thomas, G. Radice, C. Lo, Modulation of mouse neural crest cell motility by N-cadherin and connexin 43 gap junctions, The Journal of cell biology 154(1) (2001) 217-230.

[60] H.S. Duffy, M. Delmar, D.C. Spray, Formation of the gap junction nexus: binding partners for connexins, Journal of Physiology-Paris 96(3) (2002) 243-249.

[61] Y.-W. Zhang, K. Nakayama, K.-I. Nakayama, I. Morita, A novel route for connexin 43 to inhibit cell proliferation: negative regulation of S-phase kinase-associated protein (Skp 2), Cancer Res 63(7) (2003) 1623-1630.

[62] Y.-W. Zhang, M. Kaneda, I. Morita, The gap junction-independent tumour-suppressing effect of connexin 43, J Biol Chem 278(45) (2003) 44852-44856.

[63] K. Yazawa, W.E. Fisher, F.C. Brunicardi, Current Progress in Suicide Gene Therapy for Cancer, World Journal of Surgery 26(7) (2002) 783-789.

[64] G. Vassaux, P. Martin-Duque, Use of suicide genes for cancer gene therapy: study of the different approaches, Expert Opinion on Biological Therapy 4(4) (2004) 519-530.

[65] J.C. Saez, J.A. Connor, D.C. Spray, M. Bennett, Hepatocyte gap junctions are permeable to the second messenger, inositol 1, 4, 5-trisphosphate, and to calcium ions, Proceedings of the National Academy of Sciences 86(8) (1989) 2708-2712.

[66] O. Ammerpohl, A. Trauzold, B. Schniewind, U. Griep, C. Pilarsky, R. Grutzmann, H. Saeger, O. Janssen, B. Sipos, G. Kloppel, Complementary effects of HDAC inhibitor 4-PB on gap junction communication and cellular export mechanisms support restoration of chemosensitivity of PDAC cells, Br J Cancer 96(1) (2007) 73.

[67] O. Ammerpohl, D. Thormeyer, Z. Khan, I.B. Appelskog, Z. Gojkovic, P.M. Almqvist, T.J. Ekström, HDACi phenylbutyrate increases bystander killing of HSV-tk transfected glioma cells, Biochem Biophys Res Commun 324(1) (2004) 8-14.

[68] M. Hernandez, Q. Shao, X.J. Yang, S.P. Luh, M. Kandouz, G. Batist, D.W. Laird, M.A. Alaoui-Jamali, A histone deacetylation-dependent mechanism for transcriptional repression of the gap junction gene cx43 in prostate cancer cells, The Prostate 66(11) (2006) 1151-1161.

[69] J.-W. Jung, S.-D. Cho, N.-S. Ahn, S.-R. Yang, J.-S. Park, E.-H. Jo, J.-W. Hwang, O.I. Aruoma, Y.-S. Lee, K.-S. Kang, Effects of the histone deacetylases inhibitors sodium butyrate and trichostatin A on the inhibition of gap junctional intercellular communication by H 2 O 2-and 12-O-tetradecanoylphorbol-13-acetate in rat liver epithelial cells, Cancer Lett 241(2) (2006) 301-308.

[70] H. Hagiwara, H. Sato, Y. Ohde, Y. Takano, T. Seki, T. Ariga, N. Hokaiwado, M. Asamoto, T. Shirai, Y. Nagashima, 5-Aza-2′-deoxycytidine suppresses human renal carcinoma cell growth in a xenograft model via up-regulation of the connexin 32 gene, Br J Pharmacol 153(7) (2008) 1373-1381.

[71] M. Kandouz, G. Batist, Gap junctions and connexins as therapeutic targets in cancer, Expert Opin. Ther. Targets 14(7) (2010) 681-692.

[72] N.A. Ochekpe, P.O. Olorunfemi, N.C. Ngwuluka, Nanotechnology and drug delivery part 2: nanostructures for drug delivery, Tropical Journal of Pharmaceutical Research 8(3) (2009).

[73] W. Qiao, B. Wang, Y. Wang, L. Yang, Y. Zhang, P. Shao, Cancer therapy based on nanomaterials and nanocarrier systems, Journal of Nanomaterials 2010 (2010) 7.

[74] J.S. Hrkach, M.T. Peracchia, A. Bomb, R. Langer, Nanotechnology for biomaterials engineering: structural characterization of amphiphilic polymeric nanoparticles by 1H NMR spectroscopy, Biomaterials 18(1) (1997) 27-30.

[75] A. Chaudhury, S. Das, Recent advancement of chitosan-based nanoparticles for oral controlled delivery of insulin and other therapeutic agents, Aaps Pharmscitech 12(1) (2011) 10-20.

[76] M.A. Islam, J. Firdous, Y.-J. Choi, C.-H. Yun, C.-S. Cho, Design and application of chitosan microspheres as oral and nasal vaccine carriers: an updated review, Int. J. Nanomedicine 7 (2012) 6077.

[77] R. Bardhan, S. Lal, A. Joshi, N.J. Halas, Theranostic nanoshells: from probe design to imaging and treatment of cancer, Acc. Chem. Res. 44(10) (2011) 936-946.

Chapter 2

Connexin-43 enhances tumour suppressing activity of artesunate via gap junction-dependent as well as independent pathways in human breast cancer cells

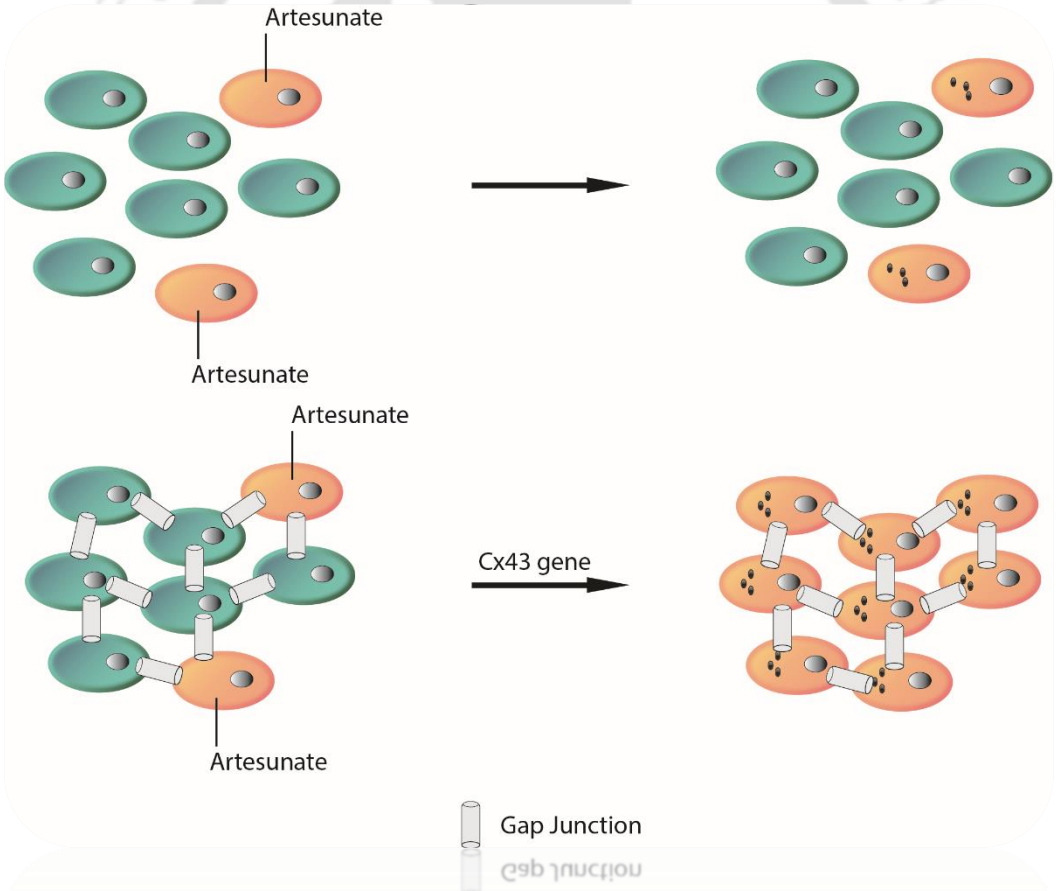

Chapter 2

Connexin-43 enhances tumour suppressing activity of artesunate via gap junction-dependent as well as independent pathways in human breast cancer cells

2.1 Introduction

Gap junctions (GJs) are the fundamental entities for intercellular communications that contribute to cell differentiation, maintenance of normal cell growth, embryonic development, and tissue homeostasis [1, 2]. The first link between GJs and cancer was established when it was found that the rat hepatomas were devoid of GJIC [3]. Understanding the intricate association between GJs and cancer may shed considerable light on possible modes of cancer therapy. In this regard, a deeper comprehension of the role of connexins (Cxs), the building block of GJs, is desirable. Cxs are documented as tumour suppressor proteins as their re-expression into tumour cells decreases their tumourigenicity and reverses the transformed phenotypes of these tumour cells. Independent studies have shown tumour-suppressing effects of several Cxs (e.g. Cx26, Cx32, and Cx43) [4]. Among these, Cx43 has been studied extensively because of its widespread expression [5]. The tumour suppressive activity of Cx43 is not only limited to the exchange of specific molecules between normal cells and the tumour cells, but in some cases has also been found to be via GJ independent pathways [6-9]. In addition, GJ dependent mechanism of Cx43 helps in the spreading of prodrug (bystander effect) [10] as well as small regulating signalling molecules in the neighbouring cells. Even though the transmission of stress signal from irradiated to non-irradiated cells was reported earlier, the responsible molecule(s) is yet to be identified [11].

Due to the adverse side effects of the chemotherapeutic drugs, plant-based active anti-cancer compounds may provide a better alternative. Artemisinin, a plant derivative, has been widely used as an antimalarial agent in the last few decades.

However, its strong anticancer activity has been only explored recently [12-14]. ART is a semi-synthetic derivative of artemisinin, developed to overcome the pharmacokinetic limitations of artemisinin [15]. In addition, ART is recommended by World Health Organization due its good clinical efficacy and tolerability. Mode of action of ART involves the presence of endoperoxide bond, that is believed to be activated by reduced heme or ferrous iron (FeII), resulting in generation of cytotoxic ROS, which are strong alkylating agents [16, 17]. Also, the tumour cells are prone to ROS mediated damages as they exhibit downregulation of several antioxidant enzymes [18]. Normally, the dosage of ART required to have a cytotoxic response on tumour cells is much higher than those needed to exterminate malarial parasites. Consequently, an effective mode of co-therapy will be needed to counter the dose-dependent side effects of ART [19].

Here, an endeavour has been made to delineate that overexpression of Cx43 sensitised the MCF7 cells towards ART treatment. Also, an investigation has been made to study the GJIC established between the neighbouring cells helped in the bystander killing of the cells after ART treatment. This is the first expedition aimed at illustrating evidences in favour of the contribution of ROS generated by ART, in suppressing the growth of the neighbouring cells.

2.2 Materials and Methods

2.2.1 Reagents and chemicals

All the chemicals, reagents, and kits used in the following experiments were purchased from Sigma-Aldrich, unless otherwise mentioned.

2.2.2 Cell culture and drug treatment

ACHN and MCF7 cells were procured from the National Centre for Cell Science (NCCS), Pune, India. Both the cell lines were grown in Dulbecco's modified Eagle's medium (DMEM high glucose), containing 10% fetal bovine serum (FBS) and 1% penicillin/streptomycin (100 U/ml; 0.1 mg/ml), in humidified air containing 5% CO_2 at 37° C. ART was made as a stock solution of 100 mM in dimethyl sulfoxide (DMSO). Carbenoxolone (CBX), a GJ inhibitor, was prepared as a 100 mM stock solution

dissolved in water. Treatments with ART were performed (usually for 48 h) at varying concentrations.

2.2.3 Cloning, transfection, and expression analysis

The total RNA was isolated from Human renal adenocarcinoma cells (ACHN) using the GenElute Mammalian Total RNA Miniprep Kit. Furthermore, 1 µg of isolated RNA was used to generate cDNA library by using Verso cDNA Kit (Thermo Scientific, Waltham, MA, USA) following the manufacturer's protocol. A semi-quantitative polymerase chain reaction (PCR) was performed with Cx43 forward and reverse primers having *EcoRI* and *ApaI* restriction sequence overhangs, respectively, using cDNA of the ACHN cells. The amplified Cx43 gene was cloned in pGEM-T Easy vector using gene-specific primers. Further, the gene was sub-cloned into pEGFP-N1, a mammalian expression vector. DNA sequence and sense insertion were confirmed by performing restriction digestion and sequencing.

Stable transfection of Cx43 was performed as described previously in [20]. The overexpression of Cx43 was assessed by semi-quantitative PCR and quantitative real-time PCR (qPCR; primer sequences provided in supplementary info). qPCR was performed using SYBR Green as reporter dye (Power SYBR Green PCR master mix, Applied Biosystem) in Rotor-Gene Q (Qiagen). β-actin was taken as the endogenous control. ΔΔCt method was used to calculate the relative Cx43 mRNA expression.

2.2.4 Immunocytochemistry and laser scanning confocal microscopy

Cells were grown on a glass coverslip in 35-mm dishes until they reached sub-confluency. After washing with phosphate buffered saline (PBS) (pH 7.4), cells were fixed with 4% paraformaldehyde (HiMedia Inc.), permeabilised using 0.5% v/v Triton X-100 and blocked using 1% w/v bovine serum albumin (BSA) in PBS at room temperature. Further, the cells were incubated overnight at 4 ºC with 1:500 dilution of mouse anti-Cx43 monoclonal antibody. After three washes with PBS, the cells were then incubated with a fluorescein isothiocyanate (FITC)-conjugated anti-mouse antibody at a dilution of 1:200 in blocking buffer (PBS with 0.1% tween 20) for 1 h at room temperature. Coverslips were mounted on a glass slide and imaged using Zeiss LSM 880 laser scanning confocal microscope system (Carl Zeiss Germany Ltd.).

2.2.5 GJIC functional assay

The functionality of GJIC was assessed by dye transfer assay using calcein-AM (acetoxymethyl ester) and PKH26 dyes. Cells were grown in a 12-well plate to their confluency. Another population of cells were labelled with 5 µM calcein-AM (30 min at 37 ºC) and 2 µM PKH26 (10 min at 25 ºC) dyes. Dual stained cells were trypsinised and plated on top of the cells grown in a 12-well plate at a ratio of 1:50 (labelled: unlabelled). After 6 h of incubation, the cells were visualised using fluorescence microscope (Nikon Eclipse Ti-U, Tokyo, Japan).

2.2.6 Assessment of cell viability

MCF7 and Cx43-MCF7 cells were plated in 96-well plate at a density of 7 x 10^3 cells per well in serum-supplemented DMEM media and allowed to adhere for 24 h. The cell populations were exposed to increasing concentrations of ART (10 to 200 µM) or ART in combination with CBX (100 µM) or DMSO (control) or catalase (2,000 units/mL) for 48 h. After the onset of treatment period, the anti-cell viability activity of ART was assessed by the 3-(4,5-dimethylthiazol-2-yl)2,5-diphenyltetrazolium-bromide (MTT) assay (HiMedia, Mumbai, India). Fractional cell survival was assessed by taking absorbance at 570 nm (Bio-Rad, Hercules, CA, USA) and normalising the background measurement at 650 nm at each drug concentration. Each experiment was performed in triplicates and repeated at least four times. The viability of the untreated cells (or control group) was normalised at 100%.

2.2.7 Apoptotic cell assessment

The healthy, early apoptotic, and late apoptotic cells were distinguished by using phycoerythrin (PE) Conjugated Annexin V/7-aminoactinomycin D (7-AAD), following treatment with 20 µM ART. MCF7 and Cx43-MCF7 cells were grown and treated with ART for 48 h. After the treatment duration was over, the cells were collected by trypsinisation, washed with PBS, and stained with PE Annexin V and 7-AAD, following the manufacturer's protocol (BD Biosciences). Finally, the cells were analysed using CytoFLEX flow cytometer (Beckman Coulter). The morphology of apoptotic cell surface was also visualised under Field Emission Scanning Electron Microscope (FESEM; Carl-Zeiss). The data presented are the results from at least three independent experiments.

2.2.8 Antibodies and Western blotting

The technique of Western blotting was applied to assess different signalling pathways involved. MCF7 cell lysate was electrophoresed on 12% SDS-PAGE. Thereafter, whole cell lysate was prepared from treated and untreated cells, with RIPA buffer, supplemented with 1 mM PMSF and 1 mM EDTA. Total protein content was estimated with Lowry assay and 12% SDS-PAGE was done after loading equal amounts of protein for each sample. In all cases, protein was electroblotted onto a PVDF membrane for 3 h at constant voltage, followed by blocking with 4% BSA in PBST for 2 h. Next, the membrane was incubated overnight with the respective primary antibodies under cold conditions. Subsequently, membrane was washed six times with PBST, before being incubated with horseradish peroxidase (HRP) conjugated secondary antibody for 2 h. Then, it was washed six times with PBST and developed with chemiluminescence peroxidase substrate kit. It should be mentioned here that for probing phospho-proteins, TBST was used in all steps, instead of PBST. Anti-Skp2, anti-p27 ^{Kip1} and anti- p21^{Cip1} were procured from Sigma-Aldrich (Steinheim, Germany). Mouse anti- Cx43 was purchased from BD Transduction Laboratories (India). DNA damage antibody sampler kit (#9947) was bought from Cell Signalling Technology (Danvers, MA). Western blotting was performed as described previously [21]. CBX (100 µM) was added in the Cx43-MCF7 growing medium to assess GJ independent expression of Skp2, p27 ^{Kip1} and p21^{Cip1} proteins. The Western blot images are representative of three independent experiments.

2.2.9 Cell proliferation assay

The proliferation of MCF7 and CX43-MCF7 cells were measured by flow cytometric analysis of CFSE (carboxyfluorescein diacetate, succinimidyl ester or CFDA-SE) loaded cells [22]. In brief, the MCF7 and Cx43-MCF7 cells were incubated with 5 µM of CFSE in serum-free medium for 30 min at 37 ºC. Subsequently, the labelled cells were incubated in 6-well plate and after 24 h of seeding, cells were analysed in flow cytometer. This time point was considered as 0 h in analysis. After 72 h, the cells were again harvested and the data were aquired in CytoFLEX flow cytometer (Beckman Coulter) and analysed using FCS Express 6 software (De Novo software). The acquired histogram of CFSE fluorescence intensity were unimodal, therefore a simplified calculation for doubling time estimation was used. Assuming no cell death during the

course of our study and all the cells are dividing, the mean doubling time of the cell population were estimated using $T_d = T/\log_2 (F_0)/(F_T)$; here, F_0 and F_T are geometric mean fluorescence intensity at 0 h and 72 h, respectively. T_d was taken as 72 h.

2.2.10 Cell cycle analysis

The cell cycle analysis of untreated and treated (36 h with 20 µM ART) MCF7 and Cx43-MCF7 cells were performed as described previously [20] with little modifications. The cells were synchronised using serum-free medium for 24 h. After the completion of the treatment duration, cells were harvested, fixed and subjected to flow cytometric evaluation. The data were acquired using CytoFLEX flow cytometer (Beckman Coulter) at an excitation wavelength of 488 nm, and emission was recorded in PE-A channel. The data were then analysed using ModFit LT software (Verity Software House).

2.2.11 Intracellular ROS detection

The level of intracellular ROS was estimated using 2',7'–dichlorofluorescein diacetate (DCFH-DA) assay. Briefly, MCF7 and Cx43-MCF7 cells were cultured at a density of 5 X 10^4 cells per well of a 6-well plate and incubated overnight for attachment. Thereafter, the cells were treated with 20 µM of ART with or without 500 µM of N-acetylcysteine (NAC) in the serum-enriched medium for 6 h. Subsequently, the cells were washed with 1X PBS and incubated with 1 µM of DCFH-DA for 30 min at 37 ºC in serum-free media. After labelling with DCFH-DA, the cells were washed repeatedly with PBS and harvested for flow cytometric evaluation. The data were then acquired using CytoFLEX flow cytometer (Beckman Coulter) at an excitation wavelength of 488 nm, and emission was recorded in FITC-H channel. The data were analysed using WinList 3D 9.0.1 software (Verity Software House).

2.2.12 Fluorescent dye based assessment of bystander effect

The fluorescein-based dye CFSE was used for cell labelling. Cx43-MCF7 cells were first treated with 20 µM of ART for 6 h at 37 ºC in a 6-well plate (50% confluence). After the treatment period was completed, the ART containing medium was replaced with fresh medium containing 10% serum. Another population of MCF7 or Cx43-MCF7 cells was labelled with 5 µM of CFSE in serum-free medium for 30 min at 37 ºC. After extensive washing, the CFSE-labelled cells were added to each well containing ART

pre-treated Cx43-MCF7 cells. CBX (100 μM) was used to block GJIC. To assess the possible involvement of H_2O_2, cells were also pre incubated with 2,000 units/mL of catalase. The ratio of ART pre-treated cells to CFSE-labelled untreated cells was ~3:1. Untreated cells were cocultured with CFSE labelled cells as a negative control. After 48 h of being cocultured, the cells were exposed to propidium iodide (PI; 1 μg/ml) to assess cell death. The ART pre-treated cells showed red nuclei while the bystander CFSE labelled cells nuclei appeared yellow due to green fluorescent CFSE dye. Quantitation of yellow nuclei were performed by taking multiple images using the fluorescence inverted microscope (Nikon Eclipse Ti-U, Tokyo, Japan).

To assess the effect of ART on the growth rate and proliferation of the bystander cells, the CFSE labelled cells were cocultured in a 12-well plate with ART pre-treated Cx43-MCF7 cells. Coculture of CFSE labelled MCF7 or Cx43-MCF7 cells with untreated Cx43-MCF7 cells was taken as control. CFSE-labelled cells were counted using fluorescence microscope 4 h after plating (baseline) and 48 h after cocultured. Experiment was performed in triplicates and cells were counted in three separate areas of 0.4 mm^2 per field in each well. Thus, the number of cells/ mm^2 (cell density) was calculated as the mean of nine separate measurements.

2.2.13 Statistical analysis

Data points were obtained from at least three different set of experiments in triplicates and expressed as the mean ± SD (SD = standard deviation). To calculate the statistical significance of differences, the two-way analysis of variance (ANOVA) and Tukey's post hoc test were used for pairwise comparisons. Data were analysed using Prism, version 5.01 (GraphPad Software Inc., San Diego, CA, USA). Statistically significant values were taken as *p< 0.05, **p< 0.01, ***p< 0.001 and ****p< 0.0001. Non-linear curve regression analysis was used to assess the IC_{50} value for ART cytotoxicity.

2.3 Results

2.3.1 Overexpression of Cx43 in MCF7 cells formed a functional GJIC

The ACHN cells were screened for the endogenous expression of Cx43. The 1.2 kb long CDS of Cx43 encoded a protein of 382 amino acids with an estimated molecular mass of 43 kDa (GenBank accession no. CAG46461.1) **(Fig. 2.1)**.The pEFGP-N1-Cx43 construct was then stably transfected into MCF7 cells. RT-PCR of cDNA library of Cx43-MCF7 lysate using Cx43 specific primers, amplified a gene having a size of 1.2 kb, which corresponds to the Cx43 gene **(Fig. 2.2)**. The relative expression analysis of Cx43 in MCF7 and Cx43-MCF7 cells showed the 157-fold increase in the expression of Cx43 in Cx43-MCF7 cells relative to the Cx43 expression in MCF-7 **(Fig. 2.3)**. The above PCR-based analysis confirmed the transfection and expression of Cx43 gene with the formation of Cx43 mRNA.

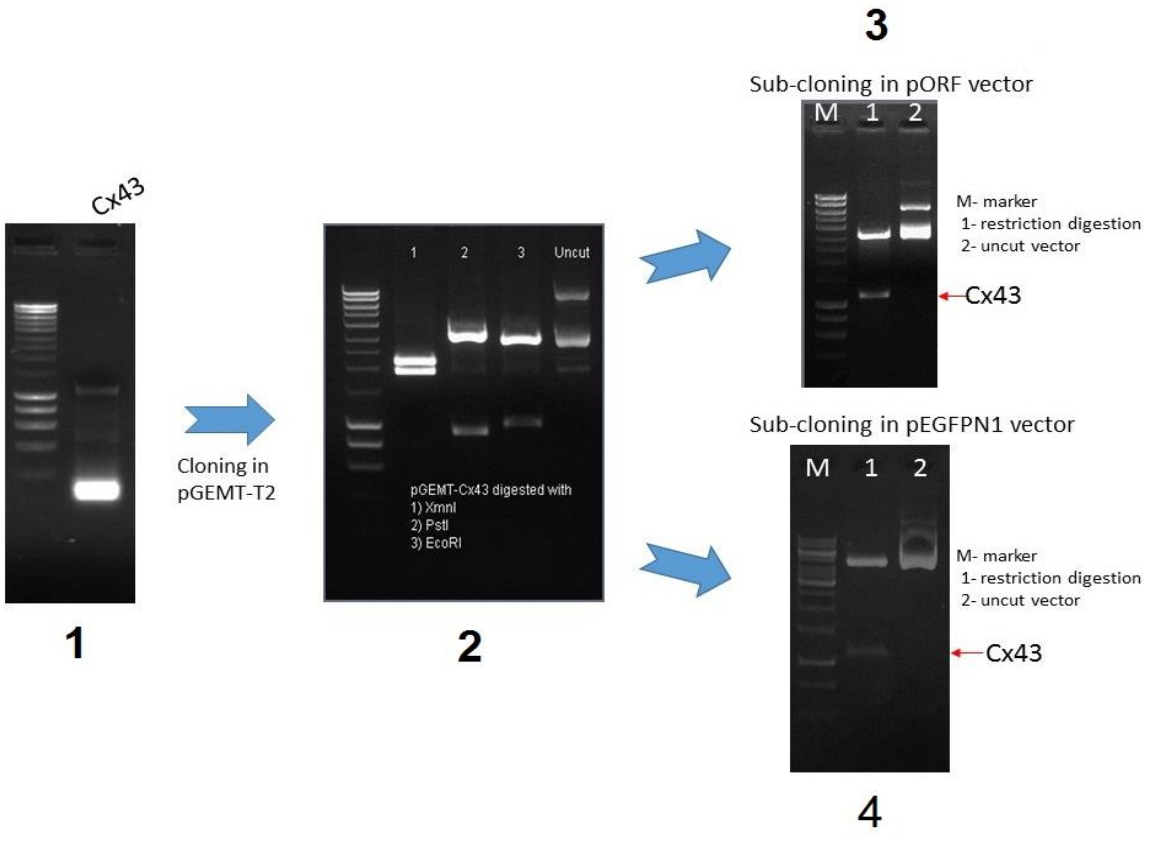

Figure 2.1. Cloning of Cx43 gene from the cDNA pool of ACHN cell line. **1)** Cx43 gene was amplified from cDNA pool of ACHN cell line using Cx43 specific primers. **2)** Cx43 gene was then subcloned in pGEMT vector. **3)** subcloning was also performed in pORF and 4) pEFGFN1 mammalian expression vector.

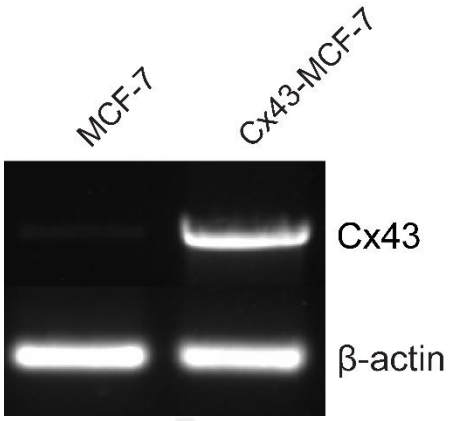

Figure 2.2. Expression level of Cx43 gene was initially examined by semi-quantitative PCR using cDNA library of MCF7 and Cx43 transfected MCF7 cells. The Cx43 gene band has been cropped and merged on top of the β-actin.

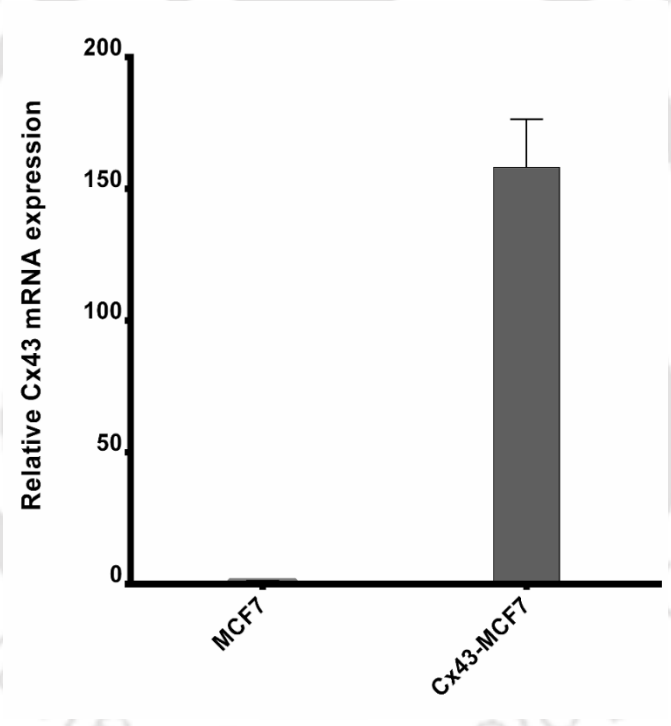

Figure 2.3. The comparative analysis of Cx43 mRNA expression in MCF7 and Cx43-MCF7 cells were analysed by using real-time PCR. The Cx43 mRNA expression in MCF7 was normalised to 1.

Expression of Cx43 protein in MCF7 and Cx43-MCF7 was examined by Western blotting with anti-Cx43 antibody using whole cell lysate **(Fig. 2.4)**. An intense immunoreactive band at 43 kDa corresponding to Cx43-MCF7 cell lysate suggested the overexpression of the Cx43 protein in the transfected cells. The band corresponding to the MCF7 cell lysate revealed basal expression of Cx43 protein in

the cells. To examine the sub-cellular localisation of Cx43 more precisely, the Cx43-MCF7 cells were subjected to immunofluorescence reactions. In Cx43-MCF7 cells, patchy fluorescence with the granular appearance on cell surface suggested the varied localisation of the Cx43 proteins in the cytoplasm and the cell to cell junctions. However, the fluorescence density was highest in the areas of intercellular contact depicting the presence of Cx43 proteins, as shown in **figure 2.5**.

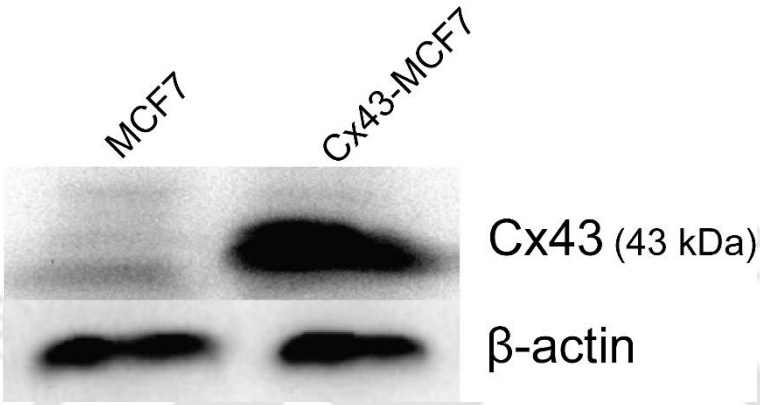

Figure 2.4. The Cx43 protein formation was assessed by immunoblotting using anti-Cx43 antibody taking β-actin as endogenous control.

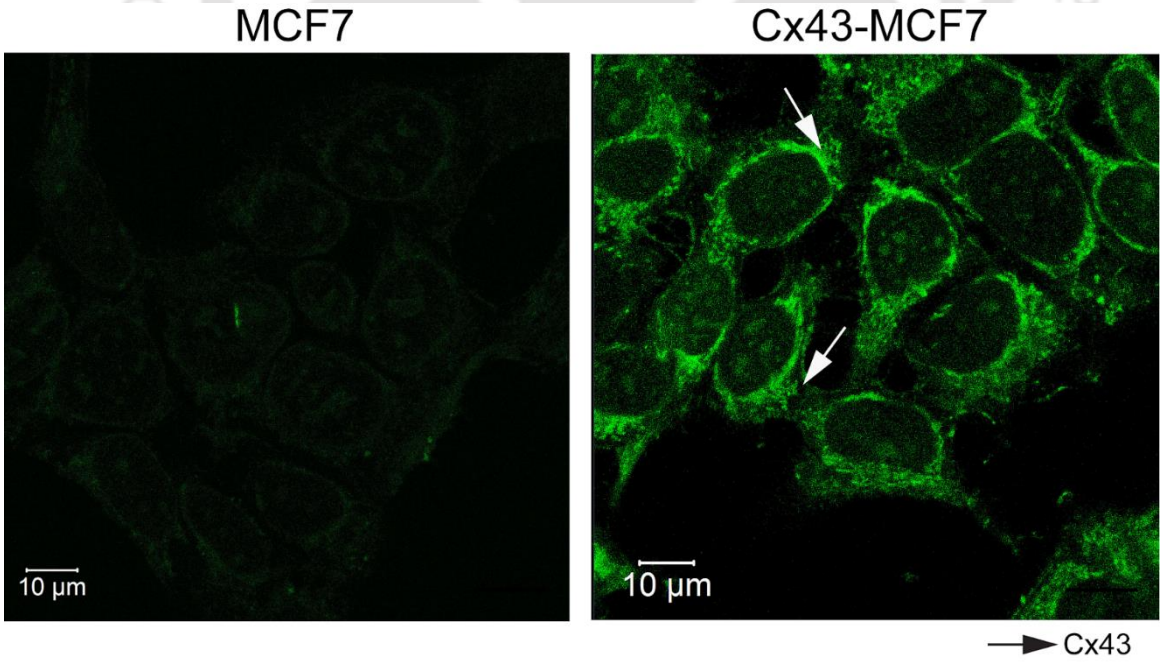

Figure 2.5. The immunocytochemical analysis of Cx43 proteins in Cx43 transfected MCF7 cells revealed its presence at cell-cell contact points (arrows) and also in lesser extent inside cytoplasm. Bar = 10 µm.

In order to study the functionality of GJIC, MCF7 and Cx43-MCF7 cells were labelled with two different fluorescent dyes, PKH26 and calcein-AM. Due to its linkage with the cell membrane, PKH26 cannot be transferred from one cell to another. On the contrary, calcein, a green fluorescent dye generated from the calcein-AM when subjected to hydrolyse intracellularly by nonspecific esterases, can diffuse via GJ channels to the neighbouring cells as a marker for functional GJ coupling activity. Dual labelled MCF7 cells or Cx43-MCF7 cells were co-cultured with unlabelled Cx43-MCF7 cells; they settled on top of the unlabelled Cx43-MCF7 cells and got attached within 4 hour of plating. The extent of dye transfer after 4 h from MCF7 cells to Cx43-MCF7 cells was limited to one or no cell without any significant visual dye transfer. However, co-culture of dual-stained Cx43-MCF7 cells with the plated unlabelled Cx43-MCF7 cells showed a substantial increase in dye transfer among neighbouring cells, as about 15-30 unlabelled cells showed green fluorescence by sequential transfer of calcein from a single donor cell **(Fig. 2.6)**. PKH26 was retained by both the donor cells without any dye transfer.

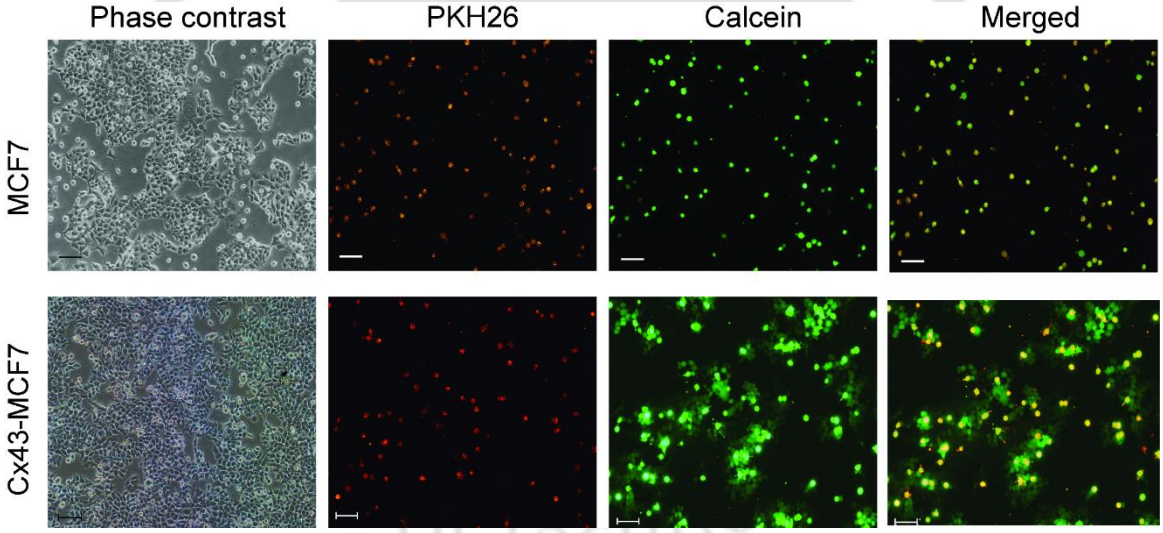

Figure 2.6. Functionality of GJIC was determined by dye transfer assay using two different fluorescent probes viz. PKH26 and calcein AM. Bar = 100 µm.

2.3.2 Overexpression of Cx43 in MCF7 cells sensitised it toward ART treatment

The sensitivity of MCF7 and Cx43-MCF7 cells towards the cytotoxicity of ART was examined by MTT assay. The MCF7 and Cx43-MCF7 cells were exposed to varying concentrations of ART for 48 h. Following treatment with ART, the Cx43 transfected cells showed a significant dose-dependent decrease in cell viability compared to

untransfected MCF7 cells **(Fig. 2.7)**. Addition of GJ inhibitor, CBX, in combination with ART doses did not affect the dose-dependent decrease in cell viability of ART treated Cx43-MCF7 cells. Thus, the possibility of the involvement of GJs in the enhanced cytotoxicity of ART on Cx43-MCF7 cells was ruled out. The toxicity level (measured as IC_{50}) induced by ART in Cx43-MCF7 was about 5-fold higher than that of untransfected MCF7 cells **(Fig. 2.8)**. In particular, it has been observed that 58.98 ± 1.16 μM of ART concentration was required to reach its IC_{50} in MCF7 cells, while for Cx43-MCF7 cells, the IC_{50} concentration significantly reduced to only 11.22 ± 2.04 (mean ± S.D.; $p < 0.05$). The occurrence of apoptosis was further corroborated by FESEM imaging, in which membrane blebbing could be prominently visualised in the ART-treated Cx43-MCF7 cells as depicted in **figure 2.9**.

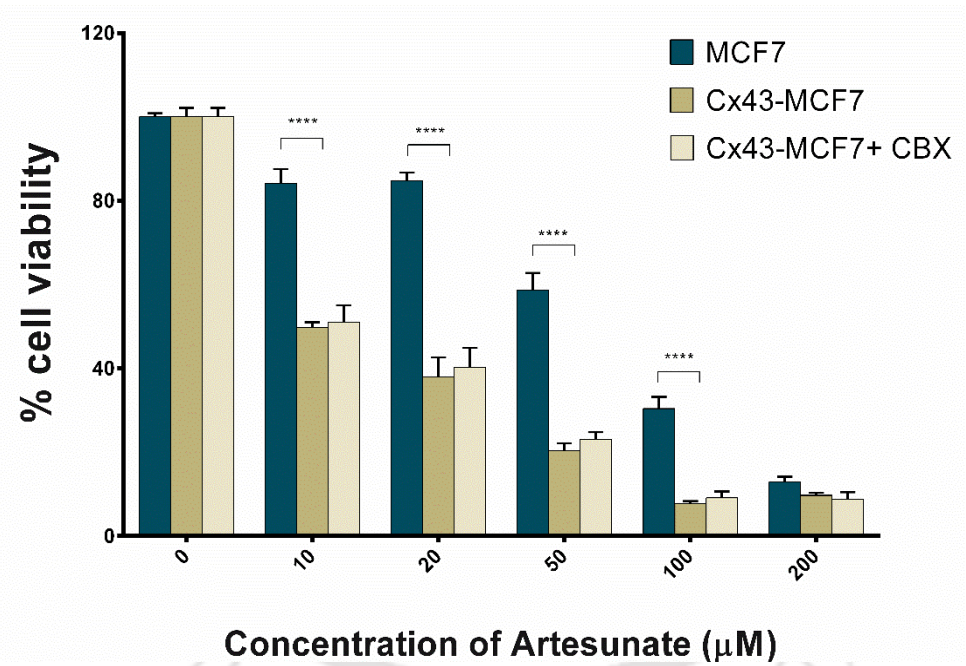

Figure 2.7. Both MCF7 and Cx43-MCF7 cells were subjected to treatment with increasing dose of ART or ART with 100 μM of CBX for 48 h. At the end of treatment duration, cell viability was assessed by MTT assay.

In order to establish whether the enhanced sensitivity to ART induced by overexpression of Cx43 was associated with the progression of drug-induced apoptosis, performed PE Annexin V/7-AAD FACS-based assay had been performed. MCF7 and Cx43-MCF7 cells were subjected to treatment with 20 μM ART for 48 h. After the treatment duration was completed, cells were stained with PE Annexin V

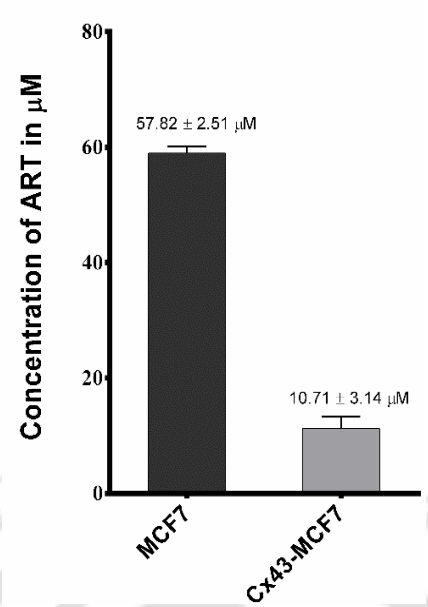

Figure 2.8. IC_{50} Value of MCF-7 and Cx43-MCF-7 Treated with ART.

and 7-AAD (which measure early and late apoptotic events, respectively) and analysed their fluorescence in flow cytometer **(Fig. 2.10)**. Untreated MCF7 and Cx43-MCF7 cells showed a low level of staining with either PE Annexin V or 7-AAD or both (2-4%). In contrast, ART-treated Cx43-MCF7 cells showed higher percentage of apoptotic cells (38.24%) when compared with ART treated MCF-7 cells (27.41%). Thus, the expression of Cx43 in MCF7 cells led to a substantial increase in the apoptotic cell population compared to untransfected MCF7 cells. Moreover, use of CBX with the ART did not reduce the extent of apoptosis, which, supported the concept of gap junction independent sensitisation of MCF7 cells after Cx43 transfection.

2.3.3 GJ independent regulation of pro-apoptotic genes by Cx43 increased doubling time and induced G1 arrest in MCF7 cells

To elucidate the mechanism by which Cx43 facilitate the enhancement of ART activity, the expression of anti-proliferative genes expression was initially checked. Initial investigation ascertained the expression of Skp2 in MCF7 and Cx43-MCF7 cells, and found that the expression of Cx43 led to the downregulation of Skp2 protein **(Fig. 2.11)**. The downregulation of Skp2 further prevents the degradation of $p27^{Kip1}$ and $p21^{Cip1}$ proteins [6, 23]. Both $p27^{Kip1}$ and $p21^{Cip1}$ proteins are regarded as potent tumour suppressor proteins as their upregulation leads to the cell cycle regulation

and cells become more responsive towards DNA damage response. Interestingly, addition of CBX in the Cx43-MCF7 growing medium (48 h) does not abrogated the expression of the above mentioned proteins, which inferred the GJ independent antitumour mechanism of Cx43.

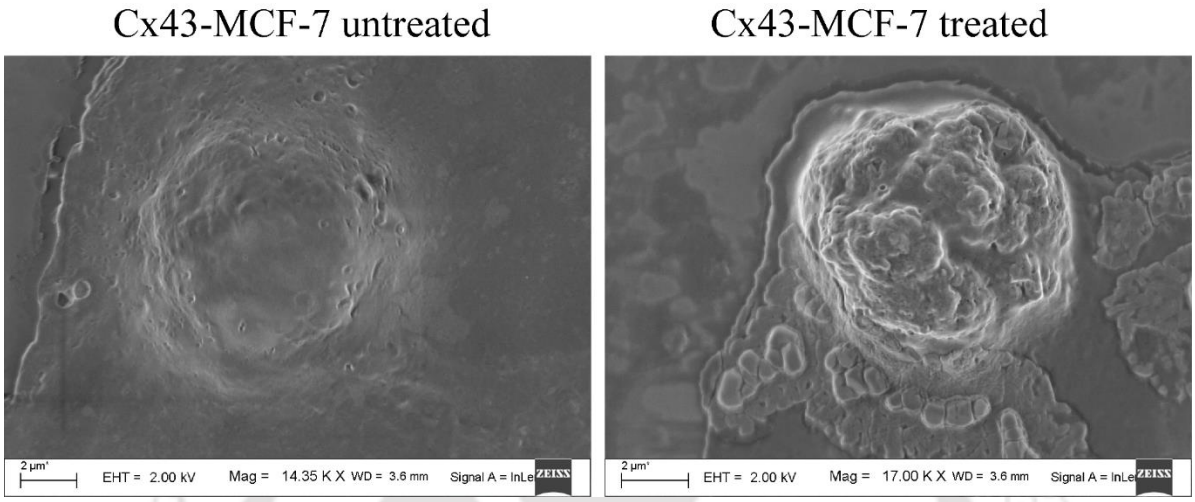

Figure 2.9. FESEM image of control and ART treated cell. Onset of apoptosis in the form of membrane blebbing was prominent on ART treated MCF7 cell.

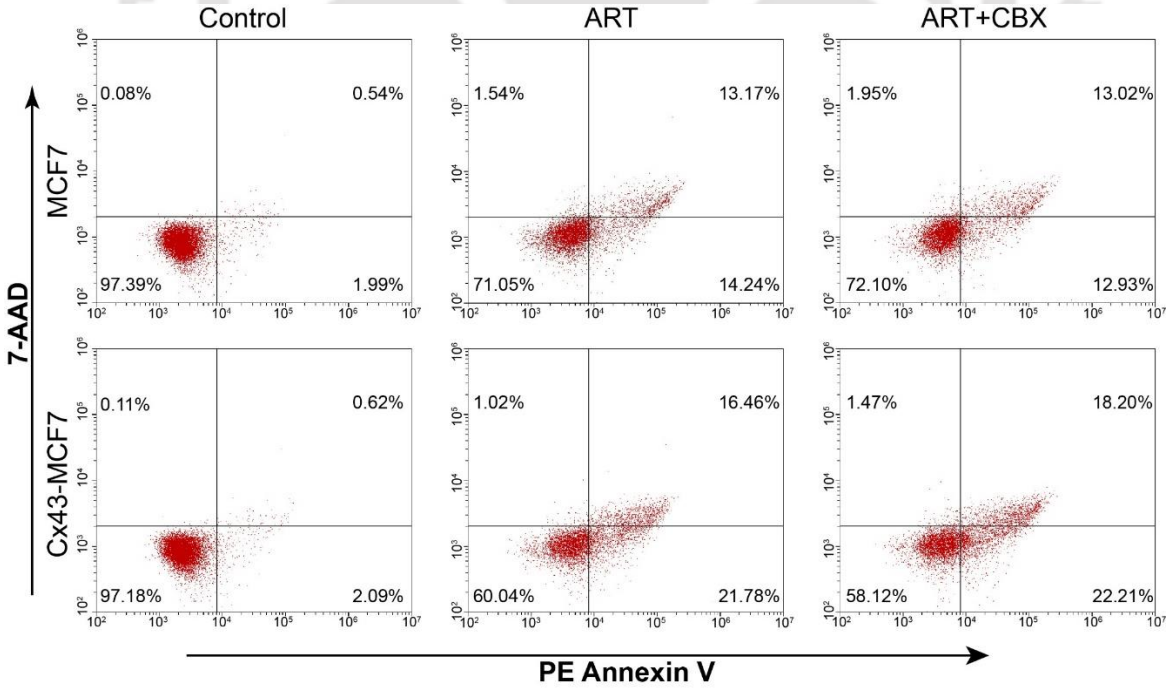

Figure 2.10. Flow cytometry analysis of the cytotoxic effect of ART on MCF7 and Cx43-MCF7 cells determined by PE Annexin V and 7-AAD staining.

The observation that Cx43 enhanced the expression of p27 ^{Kip1} and p21^{Cip1} protein, raised two possibilities. First, it is possible that the expression of these anti-tumour proteins leads to the reduction in the cells doubling time. Second, it is possible that these proteins help in the cell cycle arrest after DNA damage cause by ART treatment. To identify the delay in cell division, CFSE was used to pulse-label the MCF7 and Cx43-MCF7 cells. At two different time points, samples were collected and analysed in flow cytometer. Division of CFSE labelled cells led to a decrease in the dye fluorescence due to dye dilution **(Fig. 2.12)**. However, the unimodal peak shifting in Cx43 cells after 72 h was less when compared with MCF7 cells. This indicated that Cx43-MCF7 cells had lesser number of cell divisions in contrast to MCF7 cells in 72 h. After applying the equation as described in Materials and Methods section, it was observed that the expression of Cx43 in MCF7 cells led to an increase in the doubling time of Cx43-MCF7 cells from 26 ± 2.75 h to 34 ± 3.12 h.

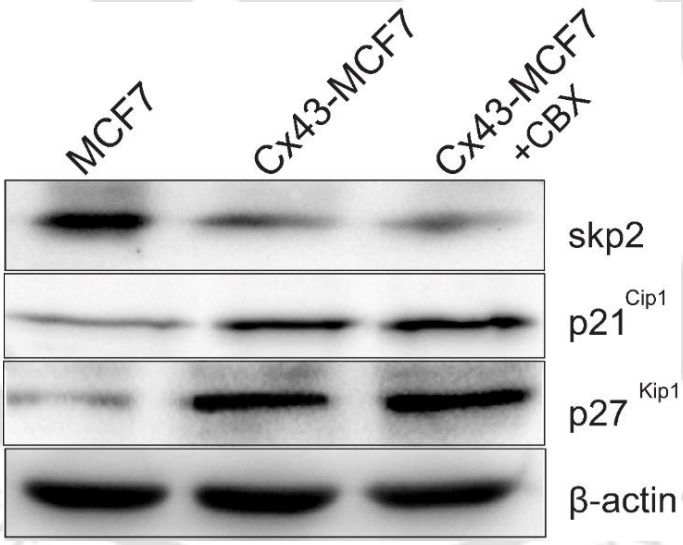

Figure 2.11. Regulation of anti-tumour proteins Skp2, p27, and p21 were determined after overexpression of Cx43 in MCF7 cells.

As the increase in the division time of Cx43-MCF7 cells was observed, it is important to determine the alteration in cell cycle profile behind it. It was reported earlier that, increase in the expression of p27 ^{Kip1} and p21^{Cip1} proteins makes cell susceptible to G1 arrest [24, 25]. Based on these reports, analysis of the DNA content of the cell population for cell cycle analysis using PI was performed. **Figure 2.13** showed the FACS data analysed in ModFit LT software, revealing a considerate amount of cell population present in G1 phase of cell cycle when treated with ART, as

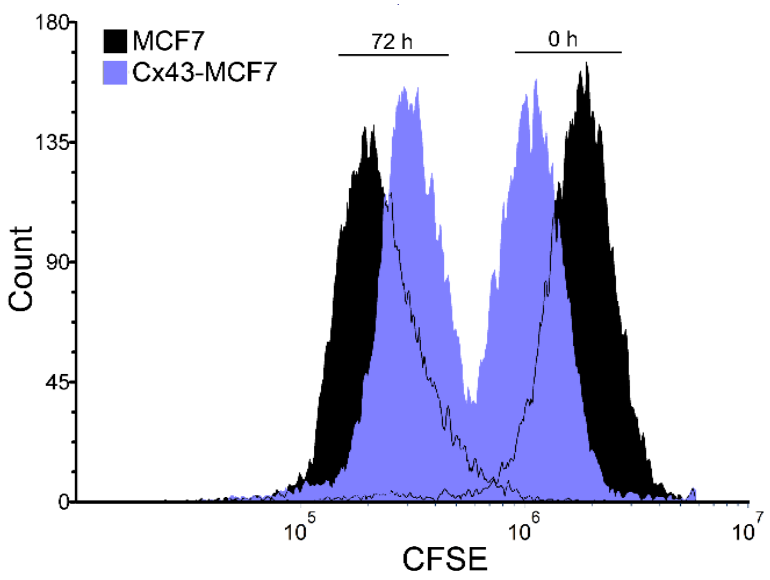

Figure 2.12. CFSE fluorescence intensity histogram of MCF7 and Cx43-MCF7 in a representative experiment. The histogram moved leftward after 72 h of incubation, indicating dye dilution due to cell division.

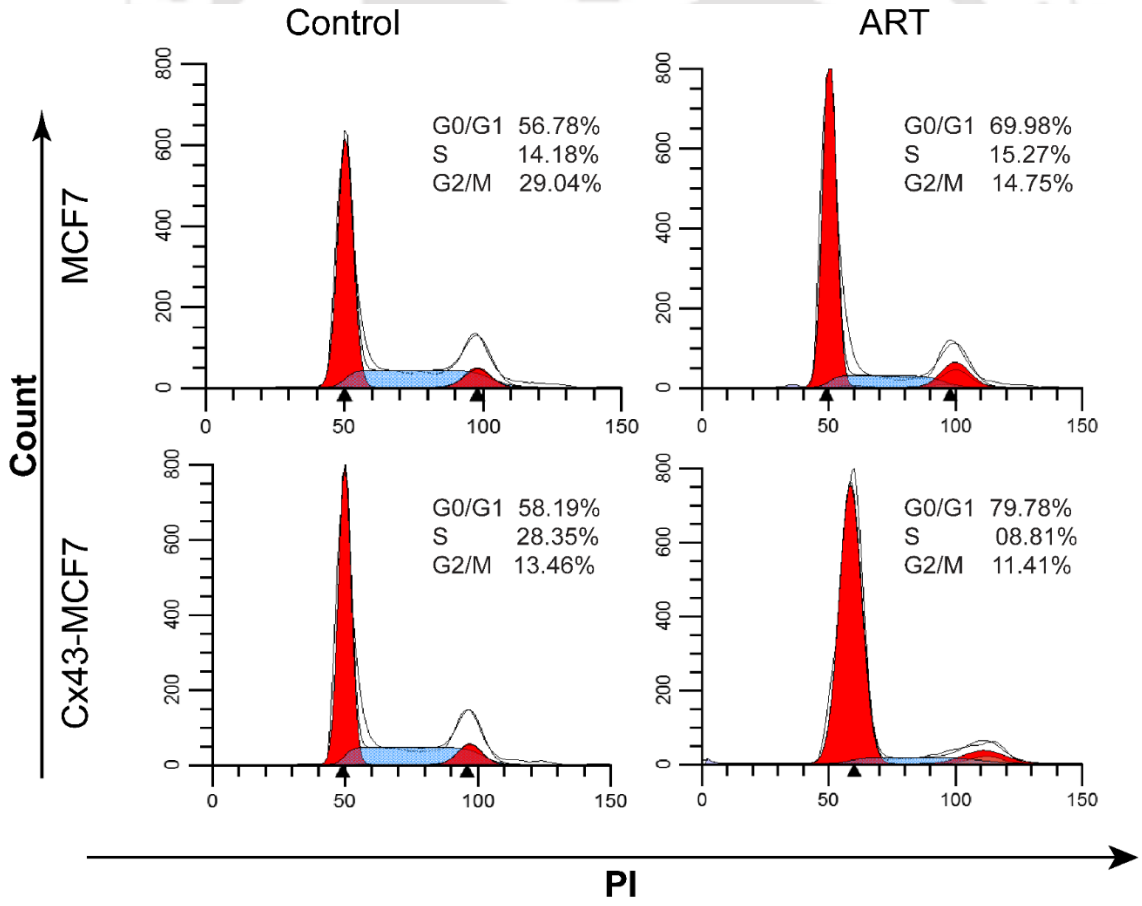

Figure 2.13. Cell cycle profiling of MCF7 and Cx43-MCF7 cells after treatment with ART. Data were analysed using ModFit LT software.

reported earlier [26]. However, the G1 population present in the treated Cx43-MCF7 cells (79.78 %) were much higher when compared to treated MCF7 (69.98 %) cells. Such difference in the G1 population suggesting that the Cx43-MCF7 cells were more susceptible to G1 arrest after treatment.

2.3.4 DNA damaging ROS generated by ART in MCF7 cells initiated DNA damage response pathways in MCF7 cells

To evaluate the role of ROS in ART-induced cell death, the intracellular ROS levels using intracellular peroxide-dependent oxidation of DCFH-DA to form fluorescent DCF was determined. Intracellular ROS clearly increased when both MCF7 and Cx43-MCF7 cells were treated with 20 µM of ART for 6 h at 37 ºC. Fluorescent intensity of

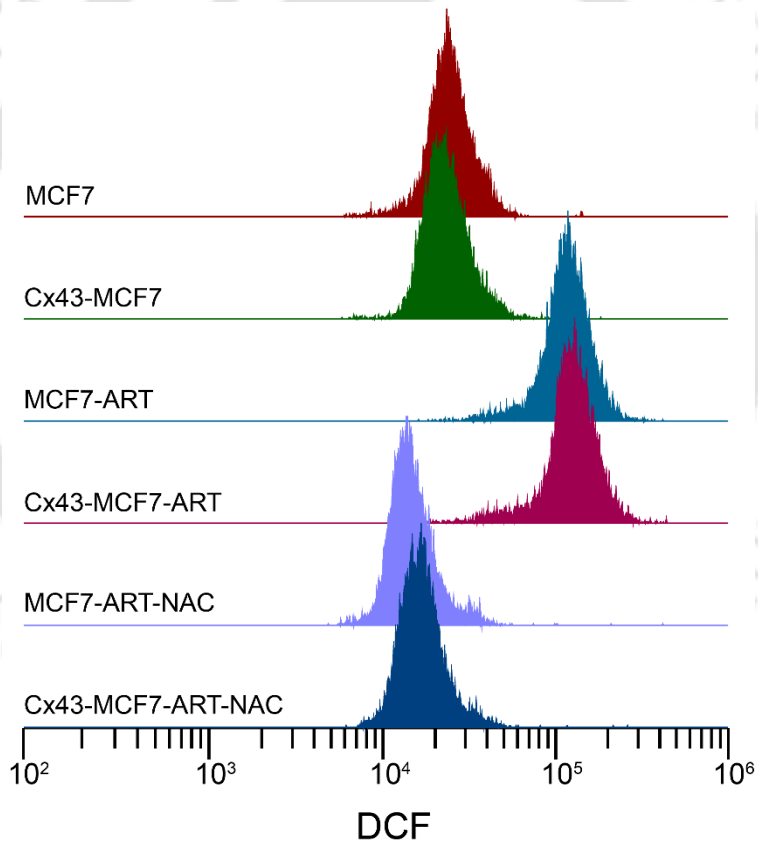

Figure 2.14. Generation of ROS in MCF7 and Cx43-MCF7 cells were assessed by measuring DCF fluorescence using flow cytometer. Untreated MCF7 and Cx43-MCF7 cells were taken as control and cells were treated in presence or absence of antioxidant NAC (5 mM).

DCF is directly proportional to the level of ROS generated inside the cells. In **figure 2.14**, the increase in the fluorescence of DCF in ART-treated MCF7 and Cx43-MCF7 cells compared to untreated MCF7 and Cx43-MCF7 cells clearly suggested the

generation of the ROS in treated cells. Also, the fluorescence intensity of DCF was nearly the same in both treated MCF7 and Cx43-MCF7 cells, thus implying that there is no role of Cx43 in increasing the ROS generation after the treatment. Furthermore, to confirm that the increase in fluorescent intensity of DCF was due to ROS generation inside the cells, NAC was used. Addition NAC in the treatment medium reduced the DCF fluorescence intensity, thus confirming the production of ROS inside the cells brought about by ART treatment.

A previous report suggested that increased ROS formation by ART induces DNA damage response in the cells [27]. Initially, ROS mediated DNA damage was analysed by agarose gel electrophoresis. To further confirm the apoptosis induced by DNA damage, immunoblot for the proteins involved in major checkpoints in response to DNA damages were performed **(Fig. 2.15)**. MCF7 cells were treated with 20 μM of ART for 24 h. At the end of the treatment period, the cells were lysed and subjected to Western blotting experiment. Increase in the expression of phospho-ATM (Ser1981) and phospho-ATR (Ser428) in ART-exposed cells indicated the DNA double-strand break and DNA single-strand break, respectively. Once the DNA damage response pathway was initiated by ATM and ATR, the downstream response proteins were also activated by phosphorylation. Chk1 and Chk2, the downstream protein kinases of ATM/ATR, get phosphorylated by ATM/ATR at Ser280 and Thr68, respectively. The histone H2A.X gets phosphorylated at Ser139 by ATM [28]. p53 and BRCA1 also get phosphorylated by upstream kinases. Phosphorylation of these signalling checkpoints proteins in response to DNA damage plays an important role in DNA damage checkpoint control, tumour suppression, and embryonic development.

2.3.5 ART induced cytotoxic bystander effect via GJIC

We speculated that the ROS and DNA damage response induced by ART might spread among the neighbouring cells through GJ. To test the above possibility, the Cx43-MCF7 cells were plated to its sub-confluency and treated with 20 μM ART for 6 h. At the end of the treatment period, drug-containing medium was repeatedly washed and replaced with the fresh medium. Another untreated population of MCF7 or Cx43-MCF7

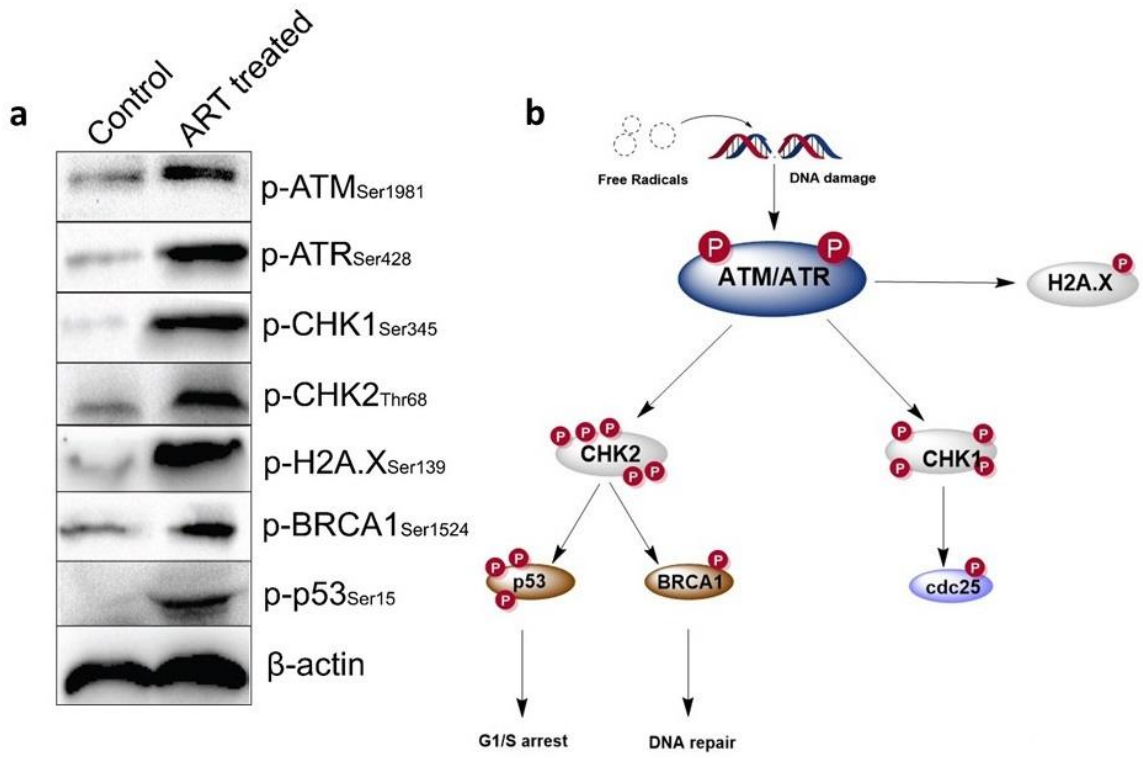

Figure 2.15. a) ART induced DNA damage response in MCF7 cells upon exposure. Phosphorylation of ATM, ATR, Chk1, Chk2, histone H2A.X, BRCA1, and p53 was determined 8 h after the onset of treatment. β-actin was used as an endogenous control and to ensure equal proteins levels. **b)** Schematic of DNA damage response pathway.

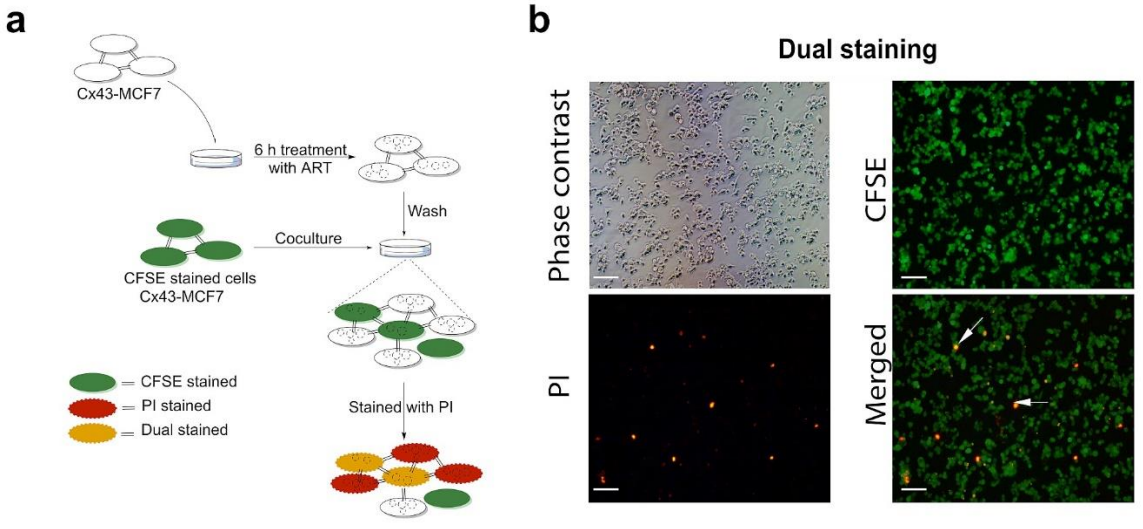

Figure 2.16. a) Scheme of the experimental protocol used to delineate the bystander effect of ART. **b**) After the onset of 48 h of coculture, the cells were stained with PI to examine the dead or membrane compromised cells. Nucleus of ART pre-treated dead cells appeared red while CFSE labelled membrane compromised cells showed yellow nucleus stain (arrow). Bar = 100 µm.

cells were labelled with non-toxic green fluorescent dye CFSE and then after trypsinisation, co-cultured with washed pre-treated Cx43-MCF7 cells. Cells were stained with PI after 48 h of co-culture. Membrane compromised or dead cells that were ART-treated exhibited red nuclei whereas the CFSE labelled bystander cells showed yellow nuclei due to colabelling with green (CFSE) and red (PI) dyes **(Fig. 2.16 a & b)**. **Figure 2.17a** represents quantitative analyses of multiple images taken after 48 h of coculture revealing that the mean percentage of PI-labelled cells among the CFSE-labelled bystander cells was increased over 7-fold from 0.23 % in untreated cocultured MCF7 cells to 1.64 % in the treated cocultured MCF7 cells. Whereas, when Cx43-MCF7 cells were used instead of MCF7 cells for coculturing, the mean percentage of PI-labelled cells among the CFSE-labelled bystander cells were showed to have over 14.5-fold increase in the apoptotic cells. A significant drop of over 7.5-fold was observed in the mean percentage of cells with yellow nuclear staining among the CFSE-labelled cells when CBX was used in the media. Moreover, to investigate the

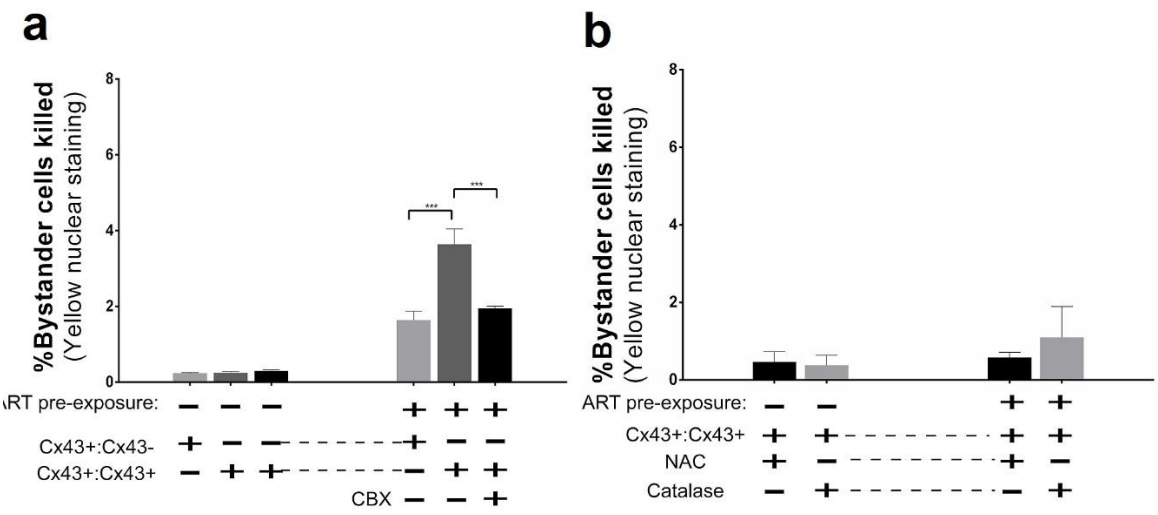

Figure 2.17. a) Quantitation of red and yellow nuclei after 48 h of coculture in ART pre-treated Cx43-MCF7 cells in presence or absence of CBX are presented. **b)** NAC and catalase were also used to prove the involvement of ROS in mediating bystander cell toxicity. The percentage of PI-labelled yellow nucleus cells counted from multiple fields (n = 6) was plotted.

involvement of the ROS in mediating the cytotoxic bystander effect, the ART pre-treated Cx43-MCF7 cells were cocultured with CFSE labelled Cx43-MCF7 cells in presence or absence of NAC or catalase in the medium. The reduction in the percentage of bystander cells in presence of NAC or catalase provided the evidence

for the involvement of the ROS in mediating cytotoxic bystander effect of ART **(Fig. 2.17b)**. Abolishment of the cytotoxic bystander effect of ART by using catalase in the medium strongly suggests the role of H_2O_2 in the process.

2.3.6 Inhibition of bystander cell proliferation was enhanced by GJIC

Apart from lethal damage to the neighbouring cells, it is probable that ROS generated by ART might help in the decreasing the proliferation of the bystander cells. To test the above possibility, the MCF7 or Cx43-MCF7 cells were labelled with CFSE dye and

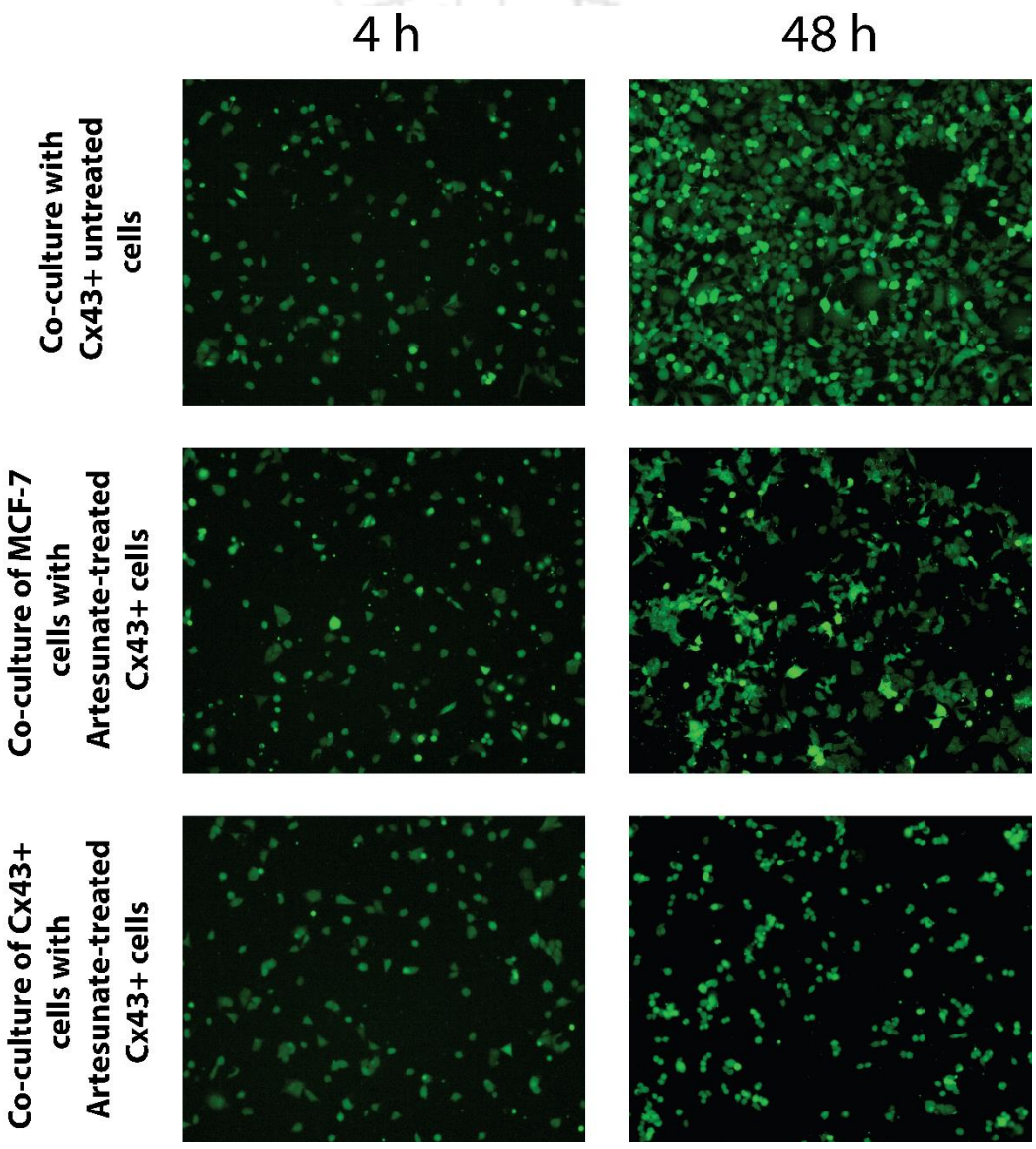

Figure 2.18. Image represented the density of CFSE labelled MCF7 or Cx43-MCF 7 cells after 4 h and 48 h of coculture with ART treated or not unlabelled Cx43-MCF7 cells. Bar = 100 µm.

plated on top of the Cx43-MCF7 cells, which were pre-treated with or without 20 μM of ART. Quantitative measurement of CFSE labelled cells (number of green cells/mm^2) after 48 h of coculture provided the density of the cells grown. The density of CFSE labelled MCF7 or Cx43-MCF7 cells increased significantly from 223.67 ± 9.1 to 1055.3 ± 106.25 and 221.3 ± 14.57 to 938.67 ± 50.2 cells per mm^2 after 48 h of coculture with untreated Cx43-MCF7 cells (control), respectively. Further, when the CFSE labelled MCF7 or Cx43-MCF7 cells were grown with ART pre-treated Cx43-MCF7 cells, there was a significant decrease or inhibition of the cell proliferation **(Fig. 2.18 & 2.19)**. After 48 h of coculture, the density of MCF7 cells grown with the pre-treated Cx43-MCF7 cells was found to be 403.3 ± 47.5 cells per mm^2. Interestingly, the density of Cx43-MCF7 cells grown with the pre-treated Cx43-MCF7 cells was shown to have significant impact on the cell proliferation of the bystander cells as only 197.3 ± 18.5 green cells per mm^2 were alive.

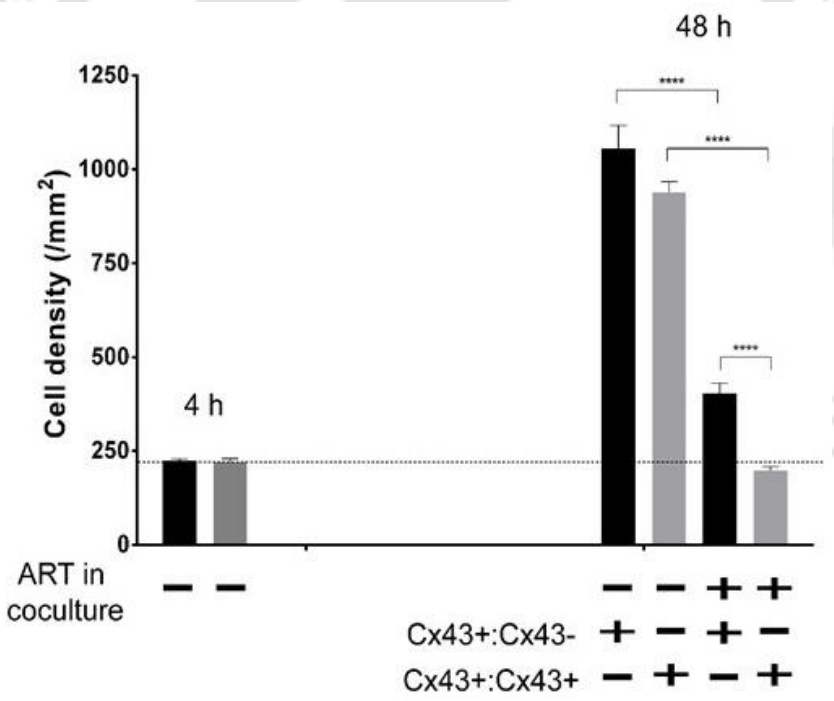

Figure 2.19. Bystander cells in cocultured were quantified in three independent experiments performed in triplicates.

2.4 Discussion

Lack of GJIC is more often found in various human tumours compared with adjacent normal tissues. Restoration of Cxs and /or GJIC in these tumour cells, particularly in early stage diseases, has been documented to have some unique therapeutic advantages in several *in vitro* and *in vivo* models [29]. In the present study, the tumour-suppressing property of Cx43 overexpression via GJ dependent as well as GJ independent pathways was exploited. In the present study, it has been found that the enforced expression of Cx43 in MCF7 cells increased its sensitivity towards ART treatment. ART has been most widely used as an anti-malarial drug since decades. We used a GJ deficient cell line MCF7 for the study of the mode of action of ART after forced establishment of GJIC and assessed the ART cytotoxicity through GJ dependent as well as GJ independent pathways. Here it has been showed, for the first time that overexpression of Cx43 in MCF7 cells increased its ART-based cytotoxicity independent of GJ, and also the established GJIC helped ART in causing apoptosis and arresting proliferation of neighbouring untreated cells.

The transfection of Cx43-pEGFP-N1 into MCF7 cells led to the establishment of a stable cell line expressing Cx43. After transfection, the level of expression of Cx43 mRNA was checked and compared it with untransfected MCF7 cells, after that it was found that the mRNA of Cx43 was upregulated in Cx43-MCF7 cells, when compared with MCF7 cells alone. Consequently, the transcribed mRNA of Cx43 was translated into Cx43 protein, which was confirmed by Western blotting. The transfection of Cx43-pEGFP-N1 in MCF7 led to the overexpression of Cx43 proteins inside the cells. These proteins mostly localised on the surface and on the cell to cell contact formed a functional GJ. Cx43 proteins present on the point of cell-cell contact, formed a functional GJ, which established an active GJIC between neighbouring cells. The spread of calcein dye from stained Cx43-MCF7 cells to the unstained Cx43-MCF7 cells confirmed the functionality of GJIC.

In addition to GJIC, there are multiple pieces of evidence portraying the GJ-independent roles of Cx43 in the control of cell growth and the suppression of tumourigenicity. Huang *et al* [30] showed that the tumour suppressive effect of Cx43 was unrelated to the activity of GJIC. To delve deeper into this facet, the combined effect of Cx43 overexpression in MCF7 cells and ART treatment was examined. Recent

experimental evidences suggest that anti-malarial ART may be a therapeutic alternative in highly aggressive cancers with rapid dissemination, without developing drug-based resistance [31, 32]. Although, a few reports of toxicities in cell lines and laboratory animals have raised concerns about the high doses and prolonged use of ART [19], these findings have not been reported in humans taking numerous doses of artemisinin till date.

In this study, it was deduced that the IC_{50} of ART treatment on MCF7 cells have significantly reduced when Cx43 was overexpressed in the cells. The dose required to reach IC_{50} in Cx43-MCF7 cells is ~5 fold less than that of MCF7 cells alone. Even though, when a specific GJ inhibitor, CBX, was used, it did not abrogate ART-based cytotoxicity, as examined by cell viability assay and PE Annexin V/7 AAD assay. The IC_{50} of ART for Cx43-MCF7 remained almost the same. The above result suggested that the Cx43-mediated enhancement of cytotoxicity is independent of GJ function.

Since it was delineated above that the overexpression of Cx43 in MCF7 cells enhances the cytotoxicity of ART, the activation of underlying mechanism associated with it was delineated. Among the various cell cycle signalling proteins, downregulation of $p27^{Kip1}$ and $p21^{Cip1}$, an inhibitor of cyclin-dependent kinases, is linked with poor prognosis in many cancers. Both $p27^{Kip1}$ and $p21^{Cip1}$ promote cell cycle arrest in response to various stimuli [33, 34]. When the expression of these proteins in Cx43-MCF7 cells were checked, it was found that there was a substantial decrease in the expression of Skp2 protein, while expression of both $p27^{Kip1}$ and $p21^{Cip1}$ was augmented, compared to the untransfected MCF7 cells. To rule out the possibility of the involvement of GJ in the expression levels of the above mentioned proteins, CBX in the medium was added for 48 h to inhibit GJIC and then assessed the proteins expression. Interestingly, resulting data showed CBX had no effect on the protein expression. Thus, it can infer that Cx43 inhibited the expression of Skp2, which regulates the ubiquitination of $p27^{Kip1}$ and $p21^{Cip1}$, independent of GJIC. Therefore, the data suggest that Cx43 may be involved in the sensitisation of Cx43-MCF7 cells towards the ART treatment by controlling the expression of Skp2, thereby increasing the level of tumour suppressor proteins, $p27^{Kip1}$ and $p21^{Cip1}$. Flow cytometric evaluation of the fluorescent intensity of CFSE labelled cells at different time intervals suggested an increase in the division time of Cx43-MCF7 cell population

compared to the MCF cells. Based on the observation of increase in the expression of p27 Kip1 and p21Cip1, a cell cycle profiling of treated cell population was performed. The cell cycle profile suggested that the G1 arrest was more pronounced in Cx43-MCF7 cells. This might be one of the causes of the increase of ART sensitivity in Cx43-MCF7 cells.

It was postulated that iron-activated ART, which is considered as a prodrug, generates ROS such as hydroxyl radicals, superoxide anions, and highly alkylating carbon-centred free radicals [35, 36]. MCF7 cells provided an excellent model for our present study as it is devoid of Cx43 proteins and therefore GJIC. Also, the bioactivity of ART requires Fe(II), and it was previously reported that MCF7 cells express high concentration (5-15 times more than normal breast cells) of transferrin receptors on the cell surface and have a substantial amount of Fe(III) ion uptake into cells [37]. When treated with ART, MCF7 and Cx43-MCF7 cells showed a high level of ROS production as depicted in **figure 2.14**. Free radicals and ROS have been known to cause DNA damage in cells [28]. Intrigued by this, the DNA damage response pathway in Cx43-MCF7 cells after ART treatment was assessed. The generation of H_2O_2 inside the cell was determined by using catalase. The MTT assay showed a considerable increase in cell viability when catalase was used with ART in medium, suggesting the role of H_2O_2 in mediating the bystander effect. The expression analyses of ATM/Chk2 and ATR/Chk1 pathways, which get activated in DNA damage responses was delineated. Overexpression of phospho-ATM and phospho-ATR after ART treatment indicated double-strand break and single-strand break of DNA, respectively. Once phosphorylated, the ATM and ATR phosphorylates a large number of downstream proteins [38]. Immunoblot data showed the overexpression of such proteins like phospho-Chk1 and phospho-Chk2. After it gets phosphorylated, Chk2 further activates p53 and BRCA1 proteins. BRCA1 helps in the double-strand break repair of DNA and cell cycle arrest in the S-phase, while p53 triggers cell cycle arrest in the G1-phase or cell death. We also found overexpression of phospho-Histone H2A.X, a novel biomarker of DNA damage response. ATM has been found to be the major protein that phosphorylates H2AX [39].

One of the striking features of the Cx43 expression is the formation of GJIC among cells. The basic strategy in GJIC-based therapies relied on the spreading of the

cytotoxic molecules or signals in neighbouring cells, called 'bystander effect'. Several studies have suggested a role of ART in the treated cancer cells, but whether ART treatment affects neighbouring cells remains elusive. Our study showed that even at the low clinically relevant concentration, ART induced cytotoxic bystander effect to the neighbouring cells. By using two different cocultured experiments it was illustrated that the GJIC helped ART in causing apoptosis as well as ceasing proliferation of the bystander cells. In the dual staining coculture experiment, over 14.5-fold increase in the neighbouring untreated Cx43-MCF7 apoptotic cells was found. Although, a significant percentage of apoptosis in untreated neighbouring MCF7 cells was observed which do not form GJIC with treated Cx43-MCF7 cells, it can be speculate that it might be because of an extracellular release of ROS. The increase in the percentage of apoptotic cells in Cx43-MCF7 cells was dependent on the GJIC, as exhibited by the use of CBX in the medium, which brought about a significant drop in the percentage of apoptotic cells. It is worth noting that, as Cx43-MCF7 cells were more sensitive towards ART treatment, the percentage of apoptosis was more pronounced in these bystander cells compared to MCF7 cells alone. Moreover, the addition of NAC and catalase in the coculture medium abolished the bystander effect of ART. This suggested the possible involvement of H_2O_2 in mediating the cytotoxic bystander effect of ART. Although, the effect was more pronounced in case of NAC than catalase, this could be because of the involvement of some other ROS, possibly long lived radicals species [40, 41]. Further, It is worth mentioning that GJs also transmits cell-death signal from the dying cell to the healthy neighbouring cell, thus spreading the effect to large number of cell population [42]. Moreover, it was also found that ART completely inhibited the proliferation of the bystander cells. This could be because of the presence of H_2O_2 in the medium. A possible mechanism underlying our experimental findings has been portrayed in the **figure 2.20**. Overall, through a well-orchestrated interplay between GJ dependent as well as GJ independent action of Cx43, a new perspective of the effective ART treatment was discovered in conjunction with Cx43 overexpression in MCF7 cells.

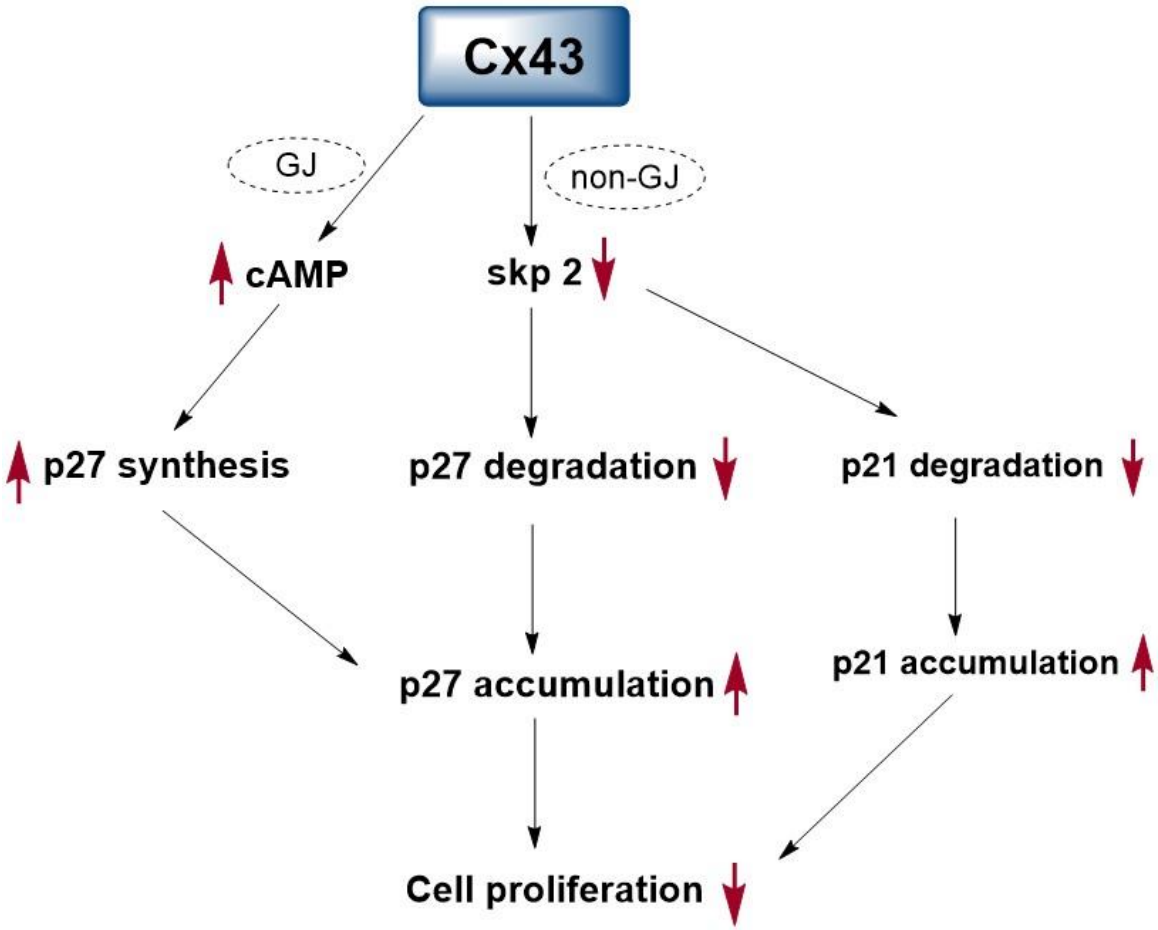

Figure 2.20. Schematic for the role of Cx43 in enhancing GJ dependent as well as GJ independent cytotoxicity of ART.

2.5 References

[1] K. Willecke, J. Eiberger, J. Degen, D. Eckardt, A. Romualdi, M. Güldenagel, U. Deutsch, G. Söhl, Structural and Functional Diversity of Connexin Genes in the Mouse and Human Genome, Biol Chem, 2002, p. 725.

[2] B. Constantin, L. Cronier, Involvement of gap junctional communication in myogenesis, Int Rev Cytol, Academic Press2000, pp. 1-65.

[3] W.R. Loewenstein, Y. Kanno, Intercellular Communication and the Control of Tissue Growth: Lack of Communication between Cancer Cells, Nature 209(5029) (1966) 1248-1249.

[4] M. Mesnil, S. Crespin, J.-L.L. Avanzo, M.-L.L. Zaidan-Dagli, Defective gap junctional intercellular communication in the carcinogenic process, Biochim Biophys Acta 1719(1-2) (2005) 125-145.

[5] M. Kandouz, G. Batist, Gap junctions and connexins as therapeutic targets in cancer, Expert Opin. Ther. Targets 14(7) (2010) 681-692.

[6] Y.-W.W. Zhang, M. Kaneda, I. Morita, The gap junction-independent tumour-suppressing effect of connexin 43, The Journal of biological chemistry 278(45) (2003) 44852-44856.

[7] J.Z. Zhou, J.X. Jiang, Gap junction and hemichannel-independent actions of connexins on cell and tissue functions--an update, FEBS Lett 588(8) (2014) 1186-1192.

[8] C. Moorby, M. Patel, Dual functions for connexins: Cx43 regulates growth independently of gap junction formation, Exp Cell Res 271(2) (2001) 238-248.

[9] M. Vinken, E. Decrock, L. Leybaert, G. Bultynck, B. Himpens, T. Vanhaecke, V. Rogiers, Non-channel functions of connexins in cell growth and cell death, Biochim Biophys Acta 1818(8) (2012) 2002-2008.

[10] T. Asklund, I.B. Appelskog, O. Ammerpohl, I.A. Langmoen, S.M. Dilber, A. Aints, T.J. Ekström, P.M. Almqvist, Gap junction-mediated bystander effect in primary cultures of human malignant gliomas with recombinant expression of the HSVtk gene, Exp Cell Res 284(2) (2003) 183193.

[11] E.I. Azzam, S.M. de Toledo, J.B. Little, Direct evidence for the participation of gap junction-mediated intercellular communication in the transmission of damage signals from alpha - particle irradiated to nonirradiated cells, Proc Natl Acad Sci U S A 98(2) (2001) 473-478.

[12] T. Efferth, H. Dunstan, A. Sauerbrey, H. Miyachi, C.R. Chitambar, The anti-malarial artesunate is also active against cancer, Int J Oncol 18(4) (2001) 767-773.

[13] T. Efferth, A. Sauerbrey, A. Olbrich, E. Gebhart, P. Rauch, H.O. Weber, J.G. Hengstler, M.-E. Halatsch, M. Volm, K.D. Tew, D.D. Ross, J.O. Funk, Molecular Modes of Action of Artesunate in Tumour Cell Lines, Mol Pharmacol 64(2) (2003) 382-394.

[14] T. Efferth, Willmar Schwabe Award 2006: antiplasmodial and antitumour activity of artemisinin--from bench to bedside, Planta Med 73(4) (2007) 299-309.

[15] M. Ashton, N.D. Sy, N. Van Huong, T. Gordi, T.N. Hai, D.X. Huong, N.T. Niêu, L.D. Công, Artemisinin kinetics and dynamics during oral and rectal treatment of uncomplicated malaria, Clin Pharmacol Ther 63(4) (1998) 482-493.

[16] S.R. Meshnick, A. Thomas, A. Ranz, C.-M. Xu, H.-Z. Pan, Artemisinin (qinghaosu): the role of intracellular hemin in its mechanism of antimalarial action, Mol. Biochem. Parasitol. 49(2) (1991) 181-189.

[17] P.L. Olliaro, R.K. Haynes, B. Meunier, Y. Yuthavong, Possible modes of action of the artemisinin-type compounds, Trends Parasitol 17(3) (2001) 122-126.

[18] D.G. Bostwick, E.E. Alexander, R. Singh, A. Shan, J. Qian, R.M. Santella, L.W. Oberley, T. Yan, W. Zhong, X. Jiang, Antioxidant enzyme expression and reactive oxygen species damage in prostatic intraepithelial neoplasia and cancer, Cancer 89(1) (2000) 123-134.

[19] T. Gordi, E.-I. Lepist, Artemisinin derivatives: toxic for laboratory animals, safe for humans?, Toxicol. Lett. 147(2) (2004) 99-107.

[20] A. Raza, V. Kohila, S.S. Ghosh, Redesigned Escherichia coli cytosine deaminase: a new facet of suicide gene therapy, The journal of gene medicine 17(6-7) (2015) 132-139.

[21] A. Ghoshal, U. Goswami, A.K. Sahoo, A. Chattopadhyay, S.S. Ghosh, Targeting Wnt Canonical Signaling by Recombinant sFRP1 Bound Luminescent Au-Nanocluster Embedded Nanoparticles in Cancer Theranostics, ACS Biomaterials Science & Engineering 1(12) (2015) 1256-1266.

[22] B.J. Quah, H.S. Warren, C.R. Parish, Monitoring lymphocyte proliferation in vitro and in vivo with the intracellular fluorescent dye carboxyfluorescein diacetate succinimidyl ester, Nat. Protoc. 2(9) (2007) 2049-2056.

[23] G. Bornstein, J. Bloom, D. Sitry-Shevah, K. Nakayama, M. Pagano, A. Hershko, Role of the SCFSkp2 ubiquitin ligase in the degradation of p21Cip1 in S phase, J Biol Chem 278(28) (2003) 25752-25757.

[24] S. Bates, K.M. Ryan, A.C. Phillips, K.H. Vousden, Cell cycle arrest and DNA endoreduplication following p21Waf1/Cip1 expression, Oncogene 17(13) (1998) 1691-1703.

[25] H. Toyoshima, T. Hunter, p27, a novel inhibitor of G1 cyclin-Cdk protein kinase activity, is related to p21, Cell 78(1) (1994) 67-74.

[26] Y. Li, F. Shan, J.-M. Wu, G.-S. Wu, J. Ding, D. Xiao, W.-Y. Yang, G. Atassi, S. Léonce, D.-H. Caignard, Novel antitumour artemisinin derivatives targeting G1 phase of the cell cycle, Bioorg Med Chem Lett 11(1) (2001) 5-8.

[27] A.M. Gopalakrishnan, N. Kumar, Antimalarial action of artesunate involves DNA damage mediated by reactive oxygen species, Antimicrob Agents Chemother 59(1) (2015) 317-325.
[28] N. Berdelle, T. Nikolova, S. Quiros, T. Efferth, B. Kaina, Artesunate induces oxidative DNA damage, sustained DNA double-strand breaks, and the ATM/ATR damage response in cancer cells, Mol Cancer Ther 10(12) (2011) 2224-2233.
[29] L. Cronier, S. Crespin, P.-O.O. Strale, N. Defamie, M. Mesnil, Gap junctions and cancer: new functions for an old story, Antioxid Redox Signal 11(2) (2009) 323-338.
[30] R.-P. Huang, Y. Fan, M.Z. Hossain, A. Peng, Z.-L. Zeng, A.L. Boynton, Reversion of the neoplastic phenotype of human glioblastoma cells by connexin 43 (cx43), Cancer Res 58(22) (1998) 5089-5096.
[31] M.P. Crespo-Ortiz, M.Q. Wei, Antitumour Activity of Artemisinin and Its Derivatives: From a Well-Known Antimalarial Agent to a Potential Anticancer Drug, BioMed Research International 2012 (2011).
[32] T. Efferth, H. Dunstan, A. Sauerbrey, H. Miyachi, C. Chitambar, The anti-malarial artesunate is also active against cancer, Int J Oncol 18(4) (2001) 767-773.
[33] C. Catzavelos, N. Bhattacharya, Y.C. Ung, J.A. Wilson, L. Roncari, C. Sandhu, P. Shaw, H. Yeger, I. Morava-Protzner, L. Kapusta, Decreased levels of the cell-cycle inhibitor p27Kip1 protein: prognostic implications in primary breast cancer, Nat. Med. 3(2) (1997) 227-230.
[34] T. Waldman, K.W. Kinzler, B. Vogelstein, p21 is necessary for the p53-mediated G1 arrest in human cancer cells, Cancer Res 55(22) (1995) 5187-5190.
[35] A.E. Mercer, I.M. Copple, J.L. Maggs, P.M. O'Neill, K.B. Park, The Role of Heme and the Mitochondrion in the Chemical and Molecular Mechanisms of Mammalian Cell Death Induced by the Artemisinin Antimalarials, J Biol Chem 286(2) (2011) 987-996.
[36] A.E. Mercer, J.L. Maggs, X.-M. Sun, G.M. Cohen, J. Chadwick, P.M. O'Neill, B.K. Park, Evidence for the involvement of carbon-centered radicals in the induction of apoptotic cell death by artemisinin compounds, J Biol Chem 282(13) (2007) 9372-9382.
[37] P. Reizenstein, Iron, free radicals and cancer, Med. Oncol. 8(4) (1991) 229-233.
[38] S. Matsuoka, B.A. Ballif, A. Smogorzewska, E.R. McDonald, K.E. Hurov, J. Luo, C.E. Bakalarski, Z. Zhao, N. Solimini, Y. Lerenthal, ATM and ATR substrate analysis reveals extensive protein networks responsive to DNA damage, Science 316(5828) (2007) 1160-1166.
[39] S. Burma, B.P. Chen, M. Murphy, A. Kurimasa, D.J. Chen, ATM phosphorylates histone H2AX in response to DNA double-strand breaks, J Biol Chem 276(45) (2001) 42462-42467.
[40] J. Simpson, S. Narita, S. Gieseg, S. Gebicki, J. Gebicki, R. Dean, Long-lived reactive species on free-radical-damaged proteins, Biochem J 282(3) (1992) 621-624.

[41] N. Hamada, H. Matsumoto, T. Hara, Y. Kobayashi, Intercellular and intracellular signaling pathways mediating ionizing radiation-induced bystander effects, J Radiat Res 48(2) (2007) 87-95.

[42] V.A. Krutovskikh, C. Piccoli, H. Yamasaki, Gap junction intercellular communication propagates cell death in cancerous cells, Oncogene 21(13) (2002) 1989.

Chapter 3

4-phenylbutyrate Manifests Synergistic Interaction with Artesunate by Suppressing DNA Repair Activity

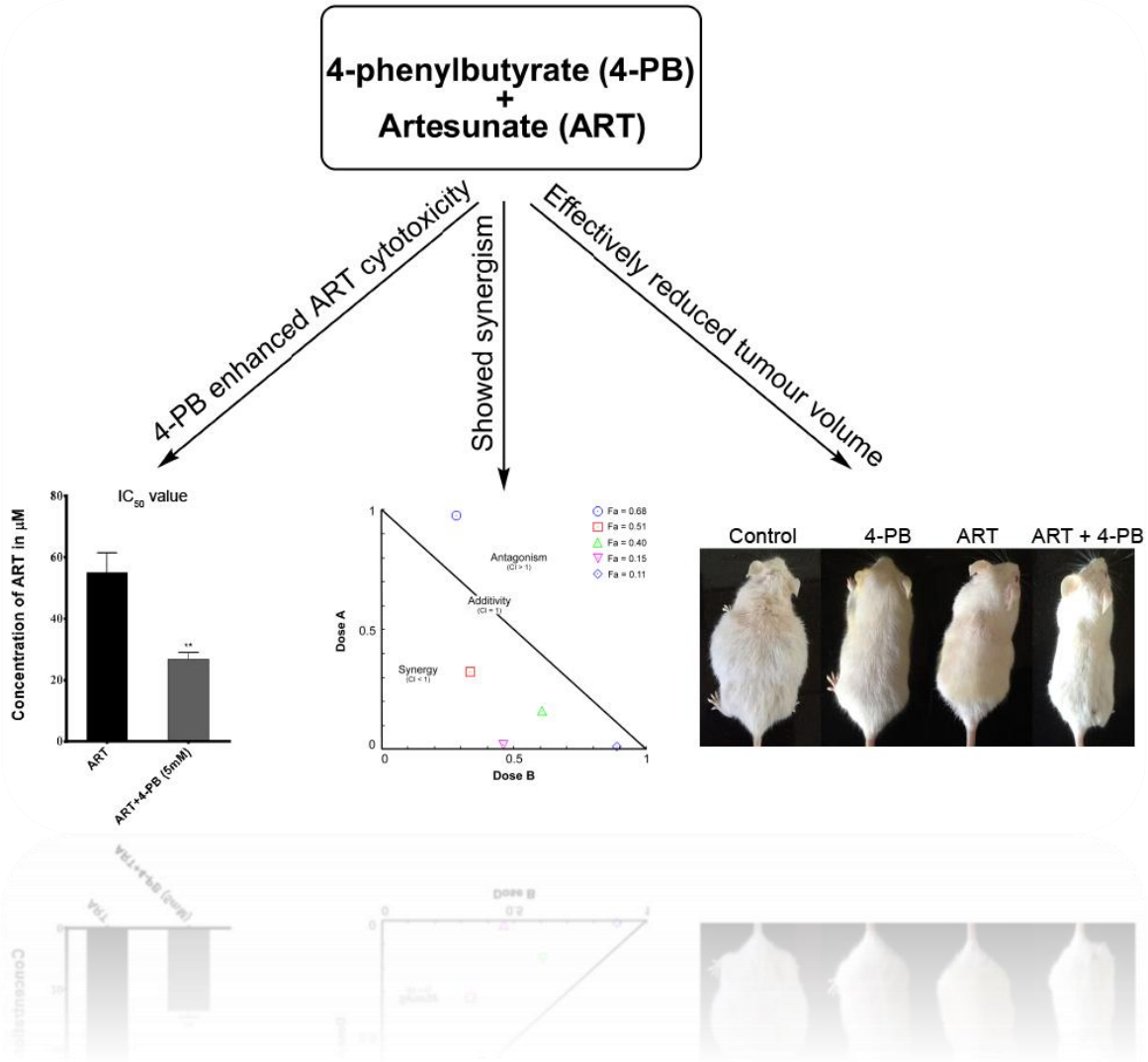

Chapter 3

4-phenylbutyrate Manifests Synergistic Interaction with Artesunate by Suppressing DNA Repair Activity

3.1 Introduction

In cellular oncogenesis, aberrant activity of histone deacetylases (HDACs) and histone acetyltransferases (HATs) was observed in various instances. Multiple evidences suggest that the inactivation of HATs and abnormal HDACs expression results in the suppression of several antiproliferative genes in cancer cells, which further mediate the tumour onset or progression [1, 2]. Apart from regulating acetylation of histones, HDACs also participate in the modifications of various non-histone proteins, including repression of several transcription factors, chaperones, and signalling molecules, which may contribute to cancer cell survival [3].

HDACs modulates chromatin structure, resulting in the relaxation of chromatin and making it easier for transcription factors to load onto the DNA [4]. This further regulates the expression of various tumour related genes involved in the cell cycle control and apoptosis of the cancer cells [5]. Histone deacetylase inhibitors (HDACi) have been known to inhibit cancer cell progression and instigate apoptosis in cancer cells both *in vivo* and in several pre-clinical models. Various HDACi have shown their potential as anti-cancer drugs, particularly in combination with other chemotherapeutic drugs in clinical studies [6].

4-phenylbutyrate (4-PB), a non-cytotoxic stable short chain fatty acid HDACi, which is known for its characteristics to act as ammonia sink and a chemical chaperone [7]. Till date, 4-PB has been effectively tried in patients having a myelodysplastic disorder or recurring malignant gliomas in clinical trials. Furthermore, 4-PB has been approved by FDA and recommended as well-tolerated drug for patients with hyperammonemia and several urea cycle disorders, consequently being an enticing possibility for cancer treatments with less or no side

effects [8]. Moreover, HDACi has been known to suppress the capacity of the cell to repair ionising radiation- induced DNA damage, both at the level of DDR signalling and by affecting the essential DNA damage repair (DDR) pathways (NHEJ and HR), in the wide range of cell types in vitro [9]. Thus, it complimented the effect of radiation-induced DNA damage and enhanced its efficacy. Moreover, several reports suggested the role of 4-PB in enhancing the GJIC among cancer cells by increasing expression of Cx43 protein [10-12]. The increased GJ communication was correlated with the increase in the chemosensitivity of the cancer cells. However, the mechanism behind it was not properly investigated. For the reason that HDACi disrupt vital cell processes, it is also possible that combinations of these drugs with other cancer treatments may provide a therapeutic advantage.

Keeping these in mind, the role of 4-PB on ROS-mediated DNA damage and the complementing effect of 4-PB with artesunate on the human breast cancer cell line, MCF-7, was explored. Artesunate (ART) is a semi-synthetic derivative of plant-based anti-malarial drug artemisinin that has been used to treat malaria since ages [13]. The recent exploration of its strong anti-cancer activity makes it a better choice for the combination therapies [14]. Because artesunate gives rise to ROS leading to oxidative DNA damage [15], it is tempting to hypothesise that the ART-induced DNA damage may be enhanced by the DDR suppressing activity of 4-PB, which ultimately accounts for the enhancement of cytotoxic activity observed in cancer cells. Also, the required dosage of ART to substantially affect tumour cells is considerably higher than that required to terminate malarial parasites. Consequently, an effective mode of combination therapy will be required to limit the dose-dependent adverse effects of ART [16].

In the current study, a combination therapy involving 4-PB & ART was designed and investigated its efficacy both *in vitro* as well as *in vivo.* An experimental investigation was made to assess the effect of 4-PB on GJIC in MCF-7 cells and the mechanism underlying it. In addition, whether 4-PB and ART act synergistically in inducing apoptosis in MCF-7 cells was also studied. The outcome of this study could provide information about the potentiality of these two drug combinations as an effective and less toxic treatment for cancer.

3.2 Materials and Methods

3.2.1 Chemicals and reagents

All the chemicals, reagents, and kits used as a part of the accompanying investigations were obtained from Sigma-Aldrich, unless specified.

3.2.2 Cell culture and drug treatment

MCF-7 (human breast adenocarcinoma) cells were purchased from the National Centre for Cell Science (NCCS), Pune, India. The cell line was routinely maintained in 10% fetal bovine serum (FBS) supplemented with Dulbecco's modified Eagle's medium (DMEM high glucose) containing 1% penicillin/streptomycin (100 U/ml; 0.1 mg/ml). The cells were grown in the humidified air containing 5% CO_2 at 37 °C. 4-PB was prepared as 100 mM stock in PBS freshly, before each use. ART was resuspended in DMSO as a stock solution of 100 mM.

3.2.3 Cx43 expression analyses

The total RNA was isolated from MCF-7 cell line using the GenElute Mammalian Total RNA Miniprep Kit, after treatment with the 5 mM of 4-PB. Furthermore, 1 µg of isolated RNA was used to generate cDNA library by using Verso cDNA Kit (Thermo Scientific, Waltham, MA, USA) following the manufacturer's protocol. A semi-quantitative polymerase chain reaction (PCR) was performed with Cx43 forward and reverse primers using cDNA of the MCF-7 cells to assess Cx43 mRNA expression after treatment. Further, to confirm Cx43 protein expression, Western blotting was done using anti-Cx43 antibody procured from BD Transduction Laboratories (India).

3.2.4 Immunocytochemistry and laser scanning confocal microscopy

Cells were grown on a glass coverslip in 35-mm dishes until they reached sub-confluency. After washing with PBS (pH 7.4), cells were fixed with 4% paraformaldehyde (HiMedia Inc.), permeabilised using 0.5% v/v Triton X-100 and blocked using 1% w/v bovine serum albumin (BSA) in PBS at room temperature. Further, the cells were incubated overnight at 4 ºC with 1:500 dilution of mouse anti-Cx43 monoclonal antibody. After three washes with PBS, the cells were then incubated with a fluorescein isothiocyanate (FITC)-conjugated anti-mouse antibody

at a dilution of 1:200 in blocking buffer (PBS with 0.1% tween 20) for 1 h at room temperature. Coverslips were mounted on a glass slide and imaged using Zeiss LSM 880 laser scanning confocal microscope system (Carl Zeiss Germany Ltd.).

3.2.5 GJIC functional assay

The functionality of GJIC was assessed by dye transfer assay using calcein-AM (acetoxymethyl ester) and PKH26 dyes. Cells were grown in a 12-well plate to their confluency. Another population of cells were labelled with 5 µM calcein-AM (30 min at 37 ºC) and 2 µM PKH26 (10 min at 25 ºC) dyes. Dual stained cells were trypsinised and plated on top of the cells grown in a 12-well plate at a ratio of 1:50 (labelled: unlabelled). After 8 h of incubation, the cells were visualised using fluorescence microscope (Nikon Eclipse Ti-U, Tokyo, Japan).

3.2.6 Assessment of cell viability

The cell cytotoxicity activity of 4-PB and ART were assessed by the 3-(4,5-dimethylthiazol-2-yl)2,5-diphenyltetrazolium-bromide (MTT) assay (HiMedia, Mumbai, India) as previously described [17]. Briefly, 7 X 10^3 cells were seeded in 96-well plate in triplicates (n=4). After 24 h of seeding, the cells were treated with varying dose of drugs and its combinations (keeping 5 mM of 4-PB constant) for 48 h. Fractional cell survival was assessed by taking absorbance at 570 nm (Infinite® 200 PRO, Tecan, Switzerland) and normalising the background measurement at 650 nm. The viability of the untreated cells (or control group) was normalised at 100%.

3.2.7 HDAC inhibition assay

4-PB induced HDAC inhibition was estimated using fluorometric HDAC Activity Assay Kit. Briefly, cells were incubated with 5 mM of 4-PB and/ or 50 µM ART for 4 h. The cells were then lysed using the buffer containing 50 mM HEPES, 150 mM NaCl, and 0.1% Triton X-100 supplemented with protease inhibitor cocktail. Resulting cell lysates were sonicated and proceeded as per manufacturer's protocol. Fluorescence intensity was measured in a plate reader (Infinite® 200 PRO, Tecan, Switzerland) taking excitation at 350 nm and emission at 440 nm.

3.2.8 Propidium iodide (PI) apoptosis assay

The apoptotic population of the cells were analysed using the protocol described earlier [18]. MCF-7 cells were treated with 4-PB and/or ART for 48 h. After the completion of the treatment duration, the cells were collected, fixed in 70 % ethanol and processed following the protocol mentioned above. The cells were then analysed by using CytoFLEX flow cytometer (Beckman Coulter) using 488 nm laser line for excitation. Red fluorescence of PI was measured in PE-A channel.

3.2.9 Fluoremetric analyses of apoptotic cells using PE Annexin V and 7-AAD

The different apoptotic cell populations were quantified using PE (phycoerythrin) Annexin V and 7-AAD (7-aminoactinomycin D), following treatment with 5 mM 4-PB and/or 50 µM ART. In brief, MCF-7 cells were grown and treated with 4-PB and/or ART for 48 h. After the end of the treatment duration, the cells were collected by trypsinization and stained with PE Annexin V and 7-AAD, following the manufacturer's protocol (BD Biosciences). Further, the extent of apoptosis in the cells were analysed using flow cytometer (CytoFLEX, Beckman Coulter).

3.2.10 Combination Index (CI) curve and Isobologram Analyses

The data generated in the cell viability experiment were analysed in COMPUSYN software to study the type of interaction between 4-PB and ART. The normalized isobologram generated by the software, which is based on Median-Effect Equation (Chou) and the Combination Index Theorem (Chou-Talalay), were then analysed. The CI was used to express antagonism (CI > 1), additivity (CI = 1) or synergism (CI < 1). The analyses repeated up to 4 times. The average effect values (fa's) was used to plot Fa-Log (CI) curve.

3.2.11 Intracellular ROS measurement

The levels of ROS generated after the treatment with drugs were assessed by using the dichlorodihydrofluorescein diacetate (DCF-DA) method. Briefly, cells were treated with the 4-PB and/or ART for 6 h in presence or absence of 500 µM of N-acetylcysteine (NAC) in the medium. Further, the cells were washed multiple times with PBS and incubated in the serum-free medium containing 1 µM of DCFH-DA for 30 min at 37 ºC. The data were then acquired using CytoFLEX flow cytometer

(Beckman Coulter) and analysed using WinList 3D 9.0.1 software (Verity Software House).

3.2.12 Cell cycle analysis

The MCF-7 cells were synchronised by serum starvation for 24 h. Further, the cells were treated with 5mM 4-PB and/or 50 µM ART for 36 h. After the completion of treatment duration, the cells were fixed using 70 % ethanol and stained with the 25 µM of propidium iodide stain following RNAse (10 µg/ml) and 0.1% triton X-100 treatment. The data were acquired using CytoFLEX flow cytometer (Beckman Coulter) and analysed using ModFit LT software (Verity Software House).

3.2.13 Relative mRNA expression analysis

Quantitative real-time PCR (qPCR) was performed to estimate the fold change in the expression of Ku70, Ku80, XRCC4, and DNA-PKcs using SYBR Green as a reporter dye (iTaq Universal SYBR Green Supermix, Bio-Rad) in Rotor-Gene Q (Qiagen). β-actin was taken as the endogenous control. ΔΔCt method was used to calculate the relative mRNA expression of Ku70, Ku80, XRCC4, and DNA-PKcs in LinRegPCR software.

3.2.14 In Vivo Study:

3.2.14.1 Animals:

Male Swiss albino mice of four months old weighing 22-25 g were purchased from Chakraborty enterprise (1443/PO/b/11/CPCSEA), Kolkata, India. All the animals were acclimatised for the laboratory environment at the Central animal facility, Institute of Advanced Study in Science and Technology (IASST), Guwahati, Assam before conducting experiments. Animals were kept in polypropylene cages and maintained at ambiguous environment (22 ± 2 ºC and 60–70% relative humidity) with 12 h light–dark cycle. Throughout the experimental period, the animals were fed with the standard rodent pellet diet (Provimi Animal Nutrition India Pvt. Ltd., India). All the protocols were approved by the Institutional Animal Ethics Committee (IAEC) of IASST (IASST/IAEC/2016-17/002) and conducted by following the guidelines of Committee for the Purpose of Control and Supervision of Experiments on Animals (CPCSEA), Government of India.

3.2.14.2 Dalton's Ascites Lymphoma development in mice:

1×10^6 viable Dalton's ascites lymphoma (DLA) cells were injected into the mice through the intraperitoneal (I. P.) route. The tumour growth was confirmed by the belly swelling and increased in body weight of mice, which was visible from 8-10 days of post transplantation.

3.2.14.3 In vivo Experimental design:

A total of 46 swiss albino mice were selected for this study (n=10), where for group-I n = 6. ART and 4-PB doses were scaled up according to the *in vitro* results. To develop the DLA tumour, 0.2 ml of 1×10^6 DLA cells/mice were inoculated in each mice. Drug treatments were started from the 8^{th} day of DLA induction and continued for 8 days with 24 h interval.

Group-I: Animals with no DLA tumour + 0.2 ml PBS (I.P).

Group-II: Animals with DLA tumour + 0.2 ml PBS (I.P).

Group-III: Animals with DLA tumour + 20 mg/kg ART (I.P).

Group-IV: Animals with DLA tumour + 50 mg/kg 4-PB (I.P).

Group-V: Animals with DLA tumour + 50 mg/kg 4-PB (I.P) + 20 mg/kg ART (I.P).

Body weight changes were measured throughout the experimental period and cells from all treatment groups except Group-I were collected at the 16th day of the experiment to measure the cell viability. At 17th day five animals from each group were sacrificed through decapitation and the specimen of blood, liver and kidney were collected to determine the biochemical and histopathological analysis. The other five animals were observed for a period of 50 days to estimate the mean survival time (MST) and % increase in lifespan (% ILS).

3.2.14.4 Histopathological Analysis:

Pathological changes in liver and kidney were observed through histopathology analysis (Leica Biosystems, Germany). The livers and kidneys were collected in 10 % buffered formaldehyde and kept at least for 24 h. Further, the tissues were undergone for dehydration procedure by gradient alcohol concentrations (50, 70, 90 & 100 %) and xylene (1 h in each concentration). Further, the tissues were transferred to melted

paraffin and kept for 1 h and proceeded to embed into paraffin blocks. A thing 5 µm sections were prepared through microtome and stained the section in hematoxylin and eosin. Stained sections were observed under the light microscope (10 X) to observe the pathological changes.

3.2.14.5 Cell viability assay:

Trypan blue assay was conducted to determine the cell viability and to observe the cell cytotoxicity. Briefly, 0.1 ml of trypan blue (0.4 %) solution was mixed with 0.1 ml of DLA cells that were collected on day 17th. Further, the cells were quantified using automated cell counter (Countess II FL, Life Technologies, USA). The percentage of viable cells were calculated through the following formula-

$$\% \text{ cell cytotoxicity} = 100 - \frac{\text{number of viable cells in the treated group}}{\text{number of viable cells in the untreated control group}} \text{ X } 100$$

3.2.14.6 Measurement of percent survival fraction:

Five animals in each group (Except G-I) were observed for 50 days to measure mortality. Kaplan-Meier curve was plotted to represent percent survival fraction using Prism, version 6.01 (GraphPad Software Inc., San Diego, CA, USA)

3.2.14.7 Haematological and biochemical profiling

Blood was collected in ethylene diamine tetra acetic acid (EDTA) coated tubes and the blood components like red blood cells (RBC), white blood cells (WBC) and haemoglobin (Hb) were measured through haematology analyser (Sysmex, Japan). All the results were expressed in mean ± S.D.

For biochemical profiling, a part of blood from the animals in all the treatment groups was collected in vials with no anticoagulant. The serum was separated through centrifuging the blood at 1500 RPM for 10 min at 4°C. The supernatant was collected in a separate tubes and Aspartate transaminase (AST), Alanine transaminase (ALT) and Alkaline phosphatase (ALP) levels were measured using biochemical kits from Accurex, India. The protocols were adopted as per manufacturer instructions.

3.2.15 Statistical analysis

The IC_{50} dose was calculated using non-linear curve regression analysis and the level of significance were calculated using unpaired two-tailed t-test. Data points were expressed as the mean ± SD (SD = standard deviation) and experiments were performed at least thrice in triplicates. To assess the statistical significance of differences, the one- and two-way analysis of variance (ANOVA) and Tukey's post hoc test were used for pairwise comparisons. Data were analysed using Prism, version 6.01 (GraphPad Software Inc., San Diego, CA, USA). Statistically significant values (p-value) for unpaired two-tailed t-test were provided in the result section while for one- and two-way analysis of variance (ANOVA) the p-value corresponds to *p< 0.05, **p< 0.01, ***p< 0.001 and ****p< 0.0001.

3.3 Results

3.3.1 4-PB modulated Cx43 protein expression and its subcellular distribution in MCF-7 cells

Treatment of MCF-7 cells with 5 mM 4-PB led to increase expression of Cx43 gene. The mRNA expression of Cx43 was enhanced drastically after 4-PB treatment. RT-PCR of cDNA library of 4-PB treated MCF-7 lysate using Cx43 specific primers, amplified a gene having a size of 1.2 kb, which corresponds to the Cx43 gene **(Fig. 3.1)**. Expression

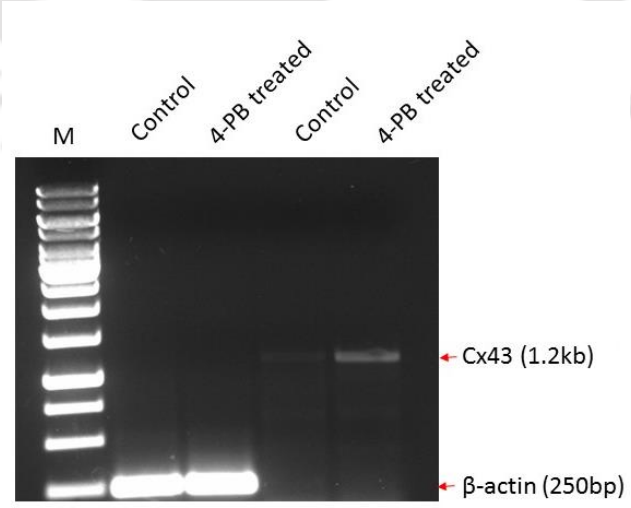

Figure 3.1. Expression of Cx43 mRNA was assessed using semi-quantitative PCR, after treating MCF-7 cells with 4-PB.

of Cx43 protein in 4-PB treated MCF7 cells was examined by Western blotting with anti-Cx43 antibody using whole cell lysate **(Fig. 3.2)**. An intense immunoreactive band at 43 kDa corresponding to treated MCF7 cell lysate suggested the overexpression of

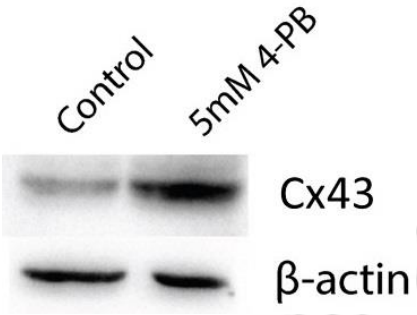

Figure 3.2. The Cx43 protein formation was examined by immunoblotting using anti-Cx43 antibody taking β-actin as endogenous control.

the Cx43 protein in the 4-PB treated MCF-7 cells. The band corresponding to the untreated MCF-7 cell lysate revealed basal expression of Cx43 protein in the cells. To examine the sub-cellular localisation of Cx43 more precisely, the treated MCF7 cells were subjected to immunofluorescence reactions. In treated MCF7 cells, patchy fluorescence with the granular appearance on cell surface suggested the varied localisation of the Cx43 proteins in the cytoplasm and the cell to cell junctions. However, the fluorescence density was highest in the areas of intercellular contact depicting the presence of Cx43 proteins, as shown in **figure 3.3**.

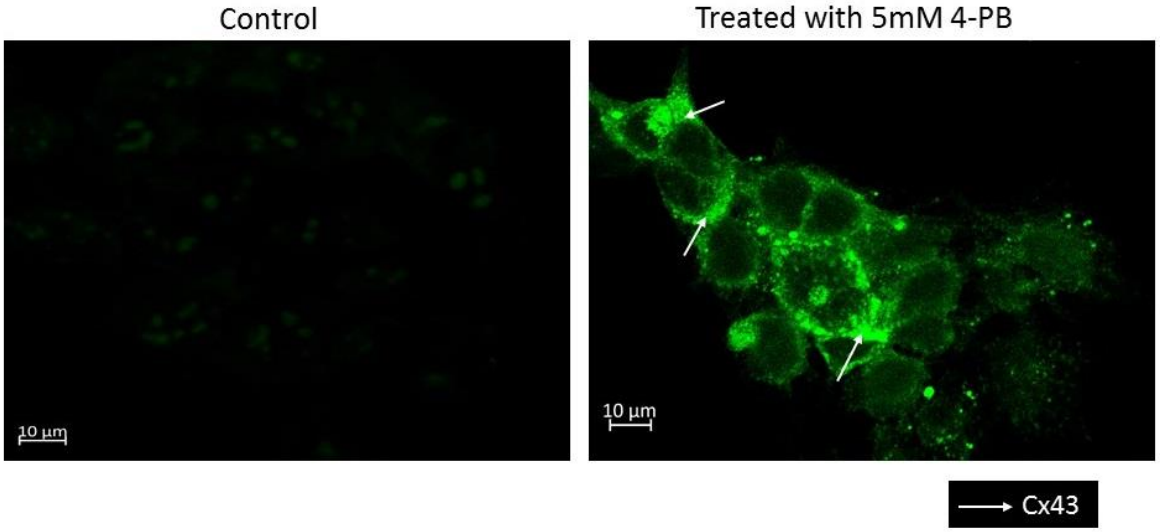

Figure 3.3. The immunocytochemical analysis of Cx43 proteins in 4_PB treated or untreated MCF7 cells revealed its presence at cell-cell contact points (arrows) and also in lesser extent inside cytoplasm. Bar = 10 µm.

3.3.2 Establishment of functional GJIC after 4-PB treatment

In order to study the functionality of GJIC, treated and untreated MCF7 were labelled with two different fluorescent dyes, PKH26 and calcein-AM. Dual labelled treated MCF7 cells or untreated MCF7 cells were co-cultured with unlabelled treated MCF7 cells; they settled on top of the unlabelled treated MCF7 cells and got attached within 8 hour of plating. The extent of dye transfer after 4 h from untreated MCF7 cells to treated MCF7 cells was limited to one or no cell without any significant visual dye transfer. However, co-culture of dual-stained treated MCF7 cells with the plated unlabelled treated MCF7 cells showed a substantial increase in dye transfer among neighbouring cells, as about 15-30 unlabelled cells showed green fluorescence by sequential transfer of calcein from a single donor cell **(Fig. 3.4)**. PKH26 was retained by both the donor cells without any dye transfer.

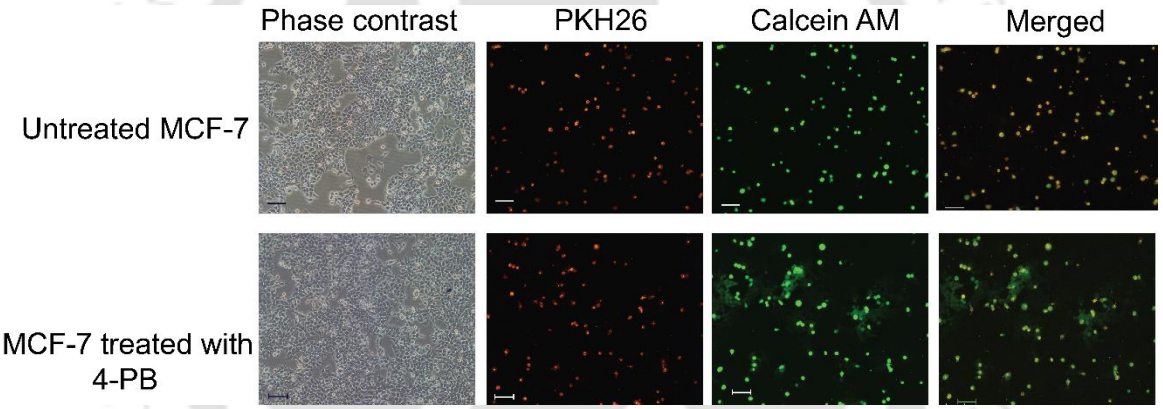

Figure 3.4. Functionality of GJIC was determined by dye transfer assay using two different fluorescent probes viz. PKH26 and calcein AM. Bar = 100 µm.

3.3.1 4-PB cytotoxicity on MCF-7 cells as a consequence of HDAC activity inhibition

Initial data of MTT assay suggested that the 4-PB significantly reduced the cell viability of MCF-7 cells at varying concentrations when administered for 48 h **(Fig 3.5)**. Using 1 mM concentration of 4-PB, 84% cell viability was observed, which further decreased to 68% at 5 mM concentration. An intermediate dose of 5 mM of 4-PB was chosen to further assess the synergism of 4-PB with ART.

As the 4-PB-mediated growth inhibition was known to act by inhibiting HDAC [19], HDAC activity assay was performed by treating the MCF-7 cells with 4-PB with or without ART **(Fig. 3.6)**. HDAC activity analysis using treated MCF-7 cell lysate

showed a significant drop in the 4-PB (P = 0.0079) and 4-PB with ART (P = 0.0082) treated cells when compared with untreated control lysate fluorescence. No inhibition of HDAC was observed in only ART-treated cells.

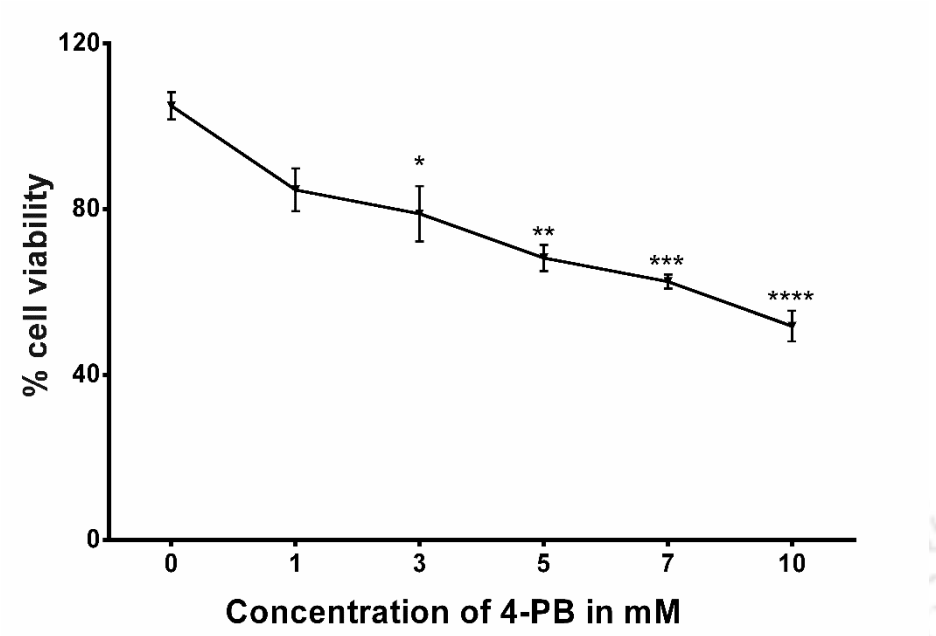

Figure 3.5. Reduction in cell viability was assessed after treating MCF-7 cells with different concentrations of 4-PB.

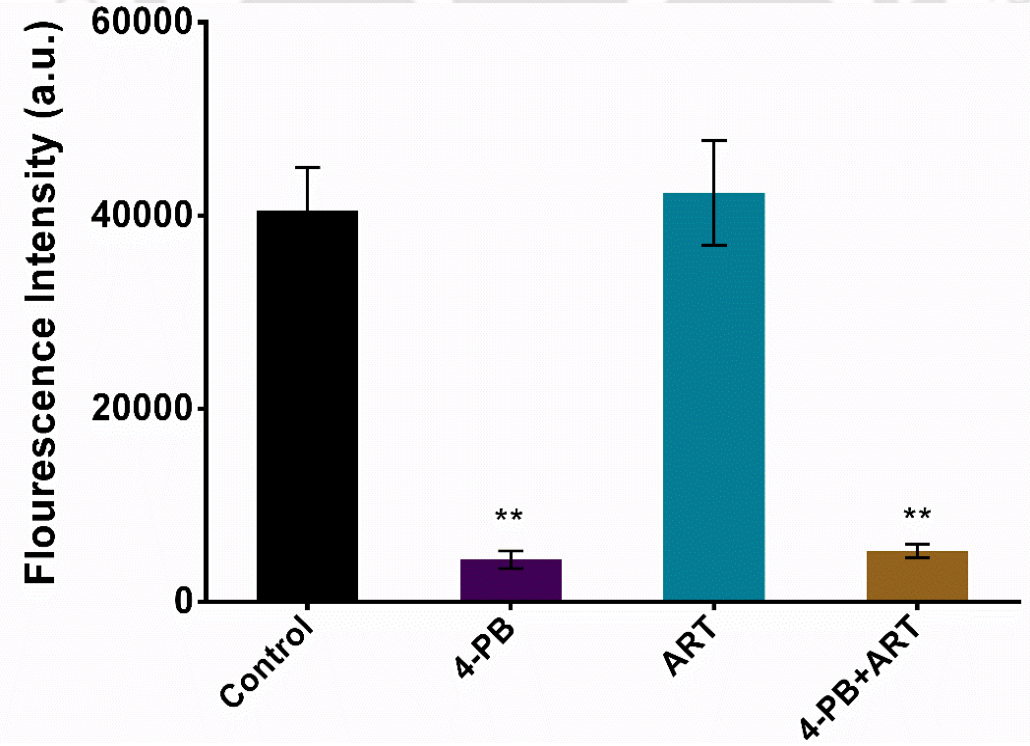

Figure 3.6. 4-PB acted by inhibiting HDAC activity in MCF-7 cells.

3.3.2 4-PB enhanced the dose-dependent cytotoxicity of ART

To probe into the effect of ART on MCF-7 cells, cell viability assay was performed. MCF-7 cells were treated with varying doses of ART in presence or absence of a constant dose of 4-PB (5-mM). Initially, ART treatment for 48 h showed a dose-dependent decrease in the cell viability of MCF-7 cells as depicted in f**igure 3.7**. However, a significant (P = 0.0020) enhancement in the cell cytotoxicity of MCF-7 cells was observed when the similar treatment was performed in the presence of 4-PB. In particular, it was observed that 55.56 ± 5.21 µM of ART concentration was required to reach its IC_{50}, while for ART + 4-PB the IC_{50} concentration significantly reduced to only 24.71 ± 3.44 µM **(Fig. 3.8)**.

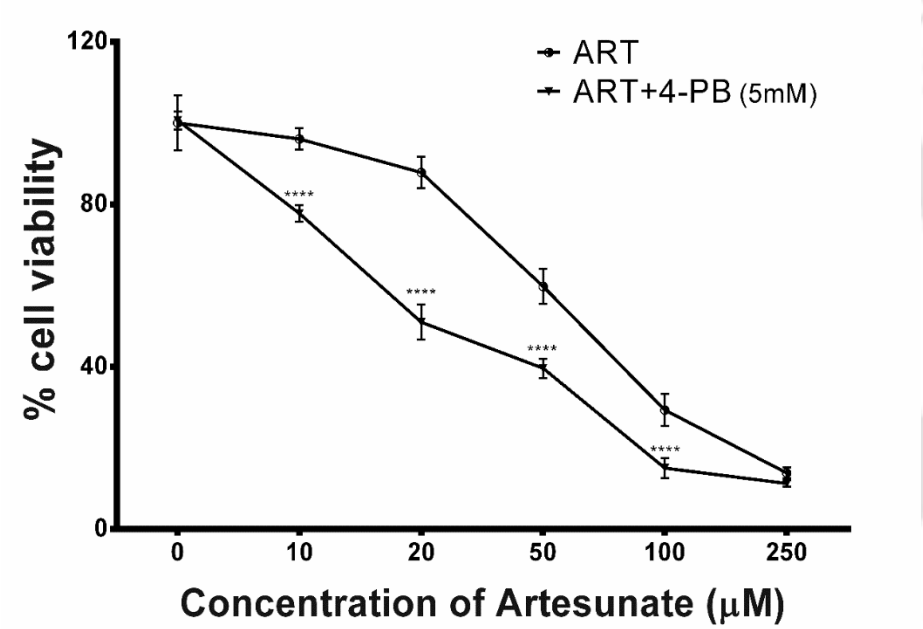

Figure 3.7. Dose dependent cell viability of ART and in combination with 5 mM 4-PB was examined by MTT based cell viability assay.

3.3.3 Induction of apoptosis by ART and/or 4-PB

In order to establish that ART and/or 4-PB treated cells were undergoing apoptosis, two different sets of flow cytometry based experiments have been performed. First, the analysis of apoptotic nuclei was done using PI dye and second, the early apoptotic, late apoptotic and necrotic cells were differentiated using PE Annexin V and 7-AAD assay.

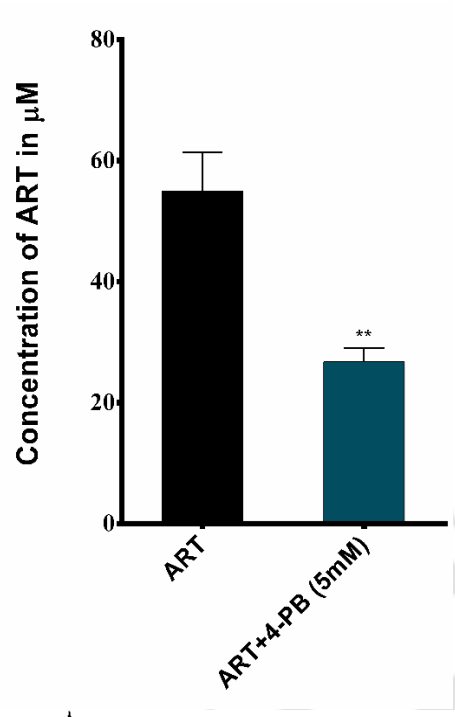

Figure 3.8. IC_{50} value of ART and ART in combination with 5 mM 4-PB was calculated using non-linear curve regression analysis and the level of significance were calculated using unpaired two tailed t-test (n = 3, p = 0.0020).

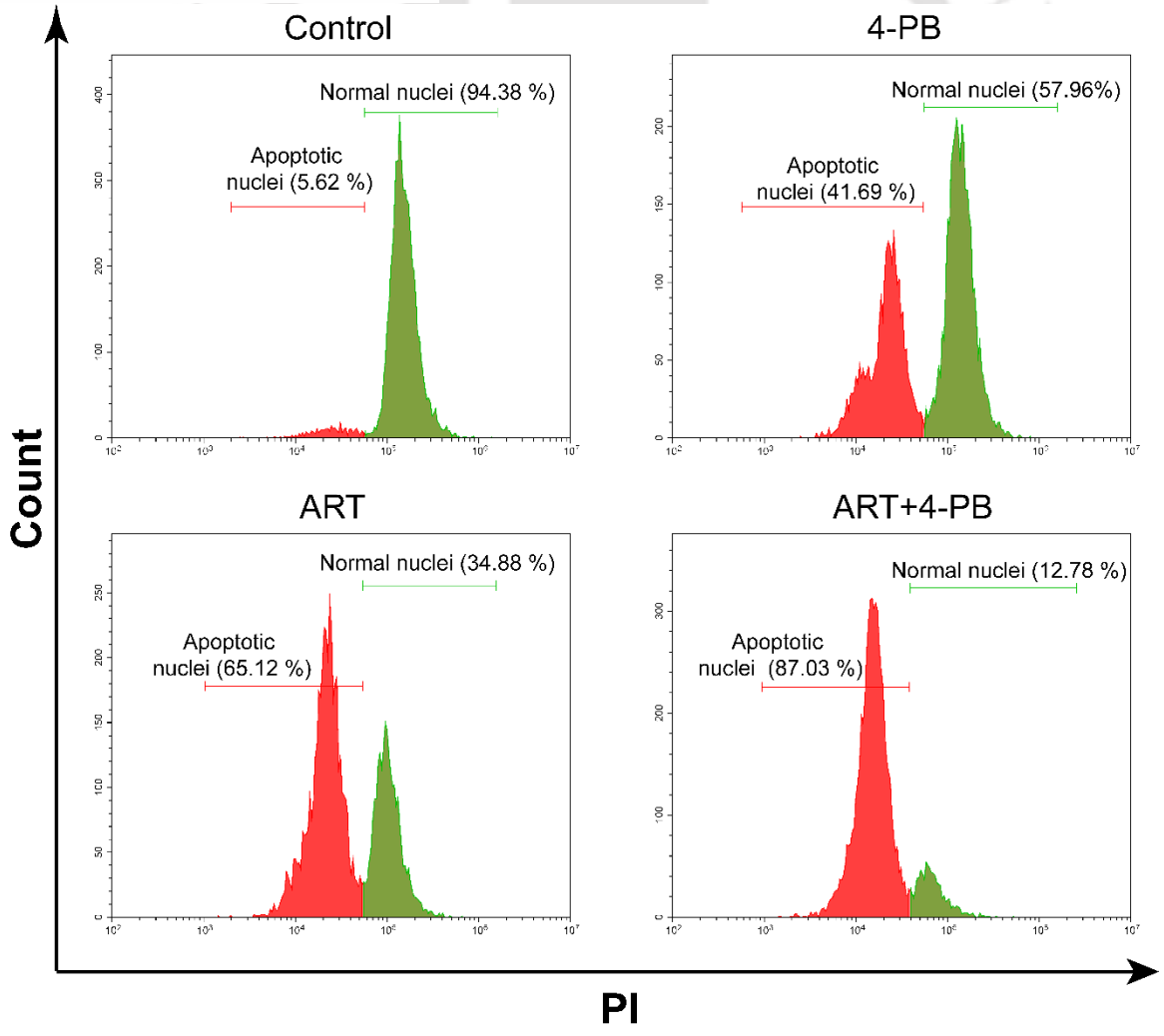

Figure 3.9. PI based apoptotic cell analysis using flow cytometer.

PI staining is a rapid, reliable and reproducible method for the separation of apoptotic cell population from the live cell population. In our analysis, the extent of apoptosis mediated by ART and/or 4-PB was assessed. After 48 h of treatment, 4-PB showed 41.69 % of apoptotic cell population and ART showed 65.12 % of apoptotic cell population. When MCF-7 cells was treated with the combination drug, the extent of apoptotic cell population increased drastically to 87.03 % **(Fig. 3.9)**.

To further validate the data generated by the PI apoptotic assay, PE Annexin V and 7-AAD flow cytometric assay **(Fig. 3.10)** was performed. After the end of the treatment duration, the cells were stained with PE Annexin V and 7-AAD. Flow cytometry data corroborated with the above finding that 4-PB enhanced the cytotoxic effect of ART. 23.21 % and 41.02 % of apoptotic cell population (early and late apoptotic combined) were found after treatment with 4-PB and ART, respectively. When the combination of both the drugs was used, the effect was enhanced by a considerate amount of 61.22 % of apoptotic cell population.

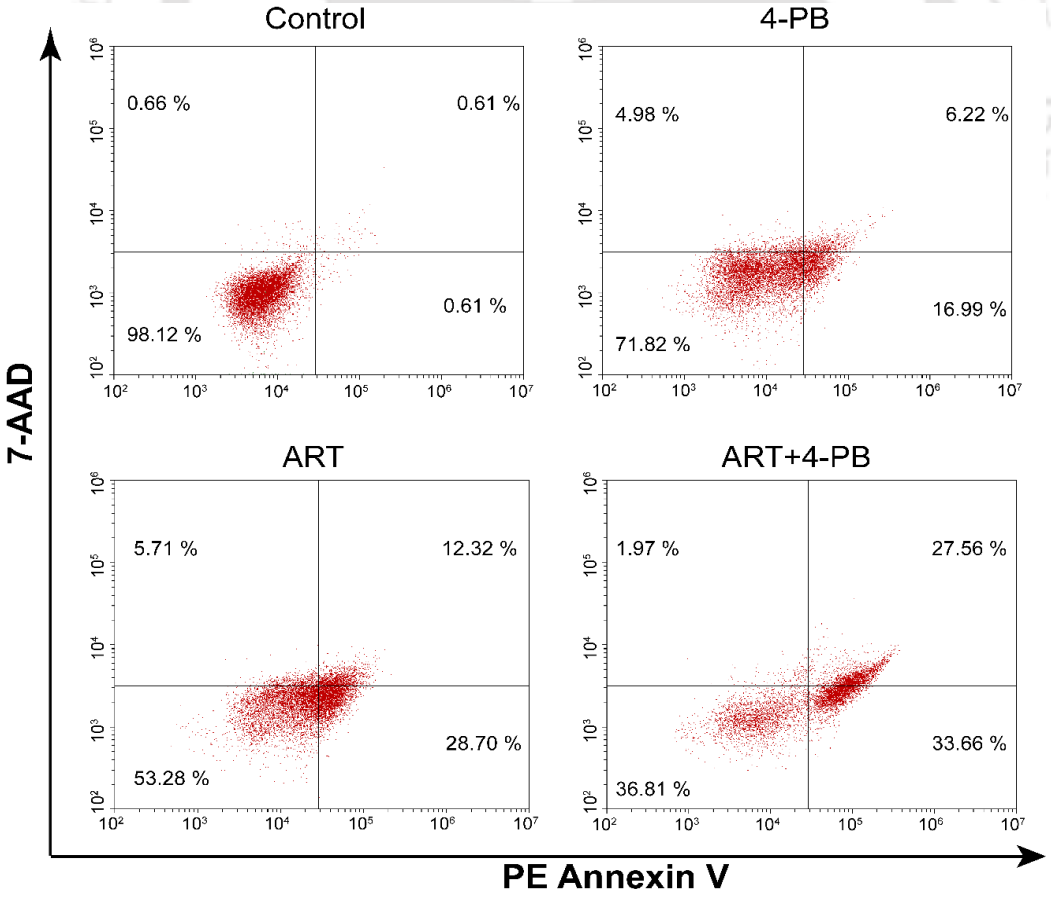

Figure 3.10. Assessment of early apoptotic, late apoptotic and necrotic cells was performed using PE Annexin V and 7-AAD based assay.

3.3.4 Isobologram depicted the interaction of 4-PB with ART is synergistic

When MCF-7 cells were treated with 4-PB and ART, each of the drugs alone was able to induce apoptosis. However, when treated with these two drugs combined, the effect was substantially more compared to that of the individual drug. This triggered our intrigue to find out the nature of the interaction between these two drugs by plotting isobologram which is based on Median-Effect Equation (Chou) and the Combination Index Theorem (Chou-Talalay). The combination index (CI) was used to express antagonism (CI > 1), additivity (CI = 1) or synergism (CI < 1). The CI was calculated using CompuSyn software.

For computing the nature of the interaction between 4-PB and ART, an experiment was designed keeping the concentration of 4-PB constant (i.e. 5-mM) while the concentration of ART was varied. Based on the available information about the mode of action of 4-PB and ART, it was assumed that the 4-PB does not preclude the effect of ART and *vice versa*, thus both can be treated/regarded as mutually non-exclusive. At the lowest concentration (4-PB + 10 µM ART), 23 % apoptosis was induced in MCF-7 cells, having a CI value of 1.3, indicating the interaction was close to

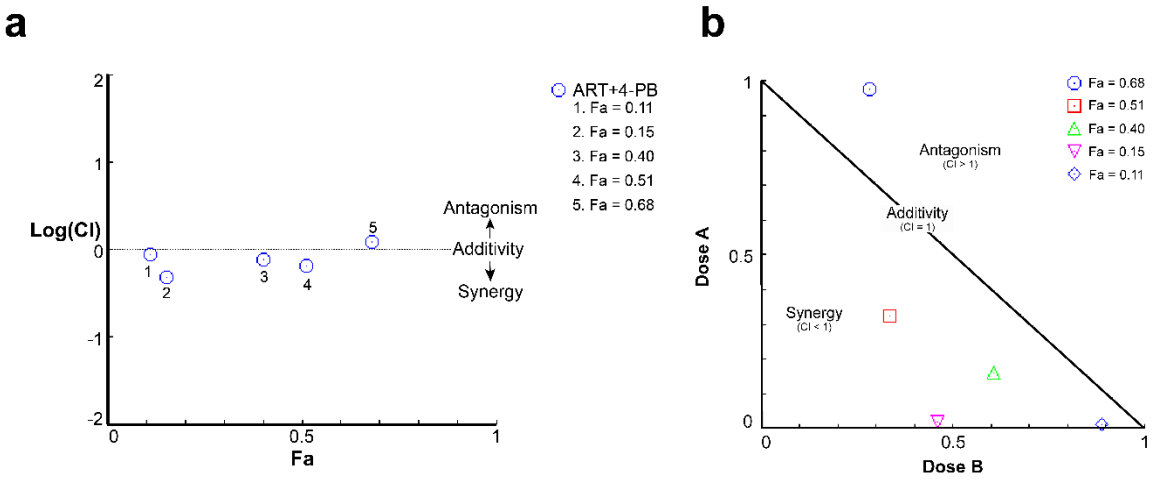

Figure 3.11. Nature of interaction between 4-PB and ART was analysed by using the Median-Effect Principle (Chou) and the Combination Index-Isobologram Theorem (Chou-Talalay). (a) CI plot showed substantial synergism at higher Fa values. (b) Isobologram showed visual, not quantitative determination of synergism or antagonism. Combination data points on the isobologram provided the nature of interaction with the combination treatment at different Fa.

additive. In contrast, when the concentration of ART was increased (20 µM, 50 µM, 100 µM, and 250 µM) the CI value was decreased to 0.66, 0.77, 0.48, and 0.9 (indicating synergism) with an apoptosis of 49 %, 60 %, 85 %, and 89 % of cells, respectively. Basically, it was observed that, when the concentration of 4-PB was kept constant and the concentration of ART was increased, the value of CI also decreased up to 250 µM concentration of ART, suggesting an increase in the synergism between two drugs **(Fig. 3.11a & b)**.

3.3.5 4-PB and ART increased oxidative stress in MCF7 cells

To investigate the mechanism of cell death induced by 4-PB and ART, the role of these drugs were examined in increasing the oxidative stress in the cells. The level of intracellular ROS generated was estimated using intracellular peroxide-dependent oxidation of DCFH-DA to form fluorescent DCF. Fluorescence of DCF increases proportionally with the increase in the intracellular ROS generation. To measure ROS,

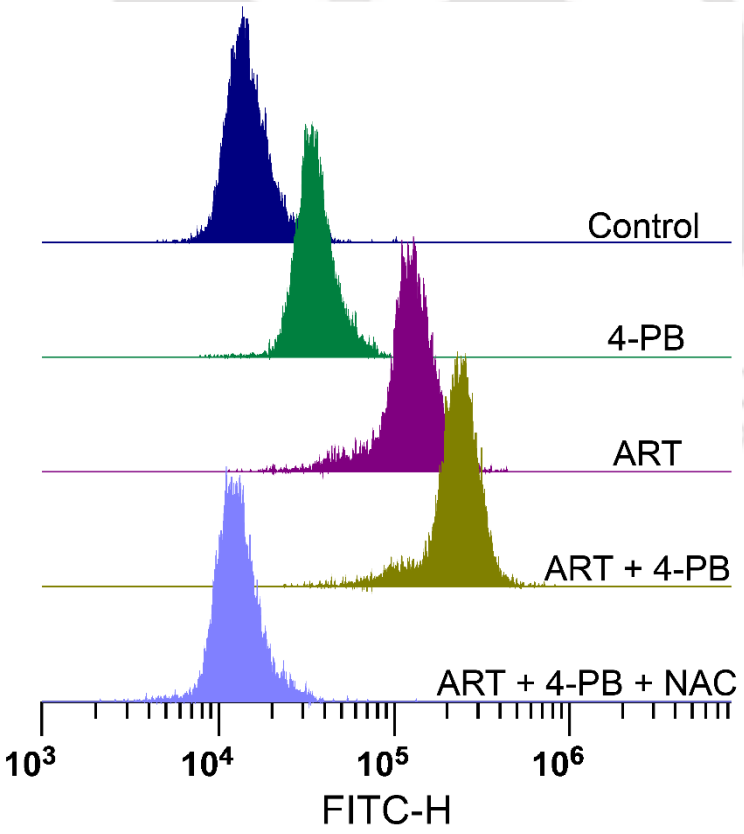

Figure 3.12. ROS generation in MCF-7 cells was examined by using DCFH-DA dye. The fluorescence level of DCF corresponds to the amount of ROS generated inside the cell.

the MCF-7 cells were treated with ART and/or 4-PB in the presence or absence of NAC for 8 h at 37º C. An increase in DCF fluorescence was noticed in the treated samples with 4-PB or ART **(Fig. 3.12)**, however, the fluorescence intensity was considerably more in case of ART-treated samples, suggesting an extensive ROS generation. Consequently, the fluorescence intensity increased sharply in samples treated with the combination of both the drugs. The addition of NAC to the medium of the treated samples attenuated the DCF fluorescence as of control fluorescence, implying that the increase in fluorescence was due to ROS generation.

3.3.4 Regulation of pro-apoptotic gene by 4-PB

To elucidate the mechanism by which 4-PB facilitate the enhancement of ART activity, the expression of anti-proliferative genes expression was initially checked. Initial investigation ascertained the expression of Skp2 in untreated MCF7 and treated MCF7 cells, and found that the treatment with 4-PB led to the downregulation of Skp2 protein **(Fig. 3.13)**. The downregulation of Skp2 further prevents the degradation of $p27^{Kip1}$ and $p21^{Cip1}$ proteins [20, 21]. Both $p27^{Kip1}$ and $p21^{Cip1}$ proteins are regarded as potent tumour suppressor proteins as their upregulation leads to the cell cycle regulation and cells become more responsive towards DNA damage response.

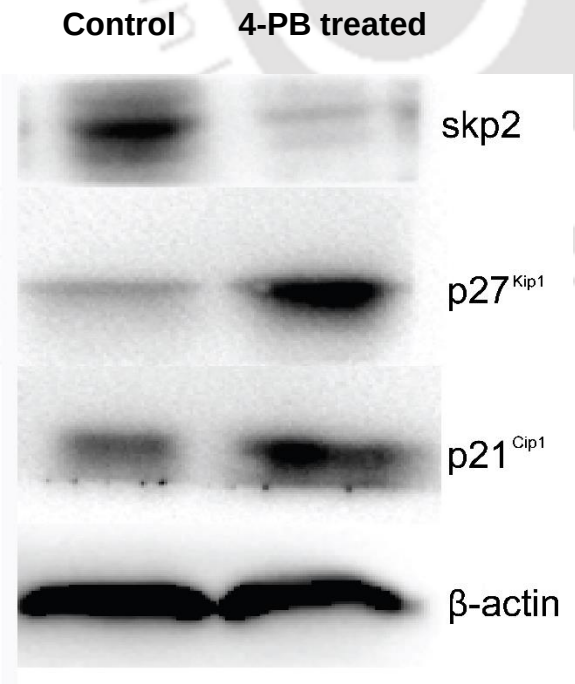

Figure 3.13. . Regulation of anti-tumour proteins Skp2, p27, and p21 were determined after 4-PB treatment in MCF7 cells.

3.3.6 Cell cycle perturbation after treatment with ART and/or 4-PB

Cytofluorimetric analysis of cells after synchronisation and treatment with ART and/or 4-PB showed the MCF-7 cells were progressively blocked in the G0/G1 phase of the cell cycle. However, after the treatment with the combination drugs, the percentage of cell population residing in the G0/G1 phase was considerably higher than the cells exposed to individual drug alone. When treated with 4-PB and ART alone the percentage of cells residing in theG0/G1 phase of the cell cycle were 69.38 % and 71.82 %, respectively. Besides, G0/G1 phase population achieved 83.84 % after treatment with both 4-PB + ART combined. The data suggested that 4-PB enhanced the G0/G1 arrest induced by ART treatment **(Fig. 3.14)**.

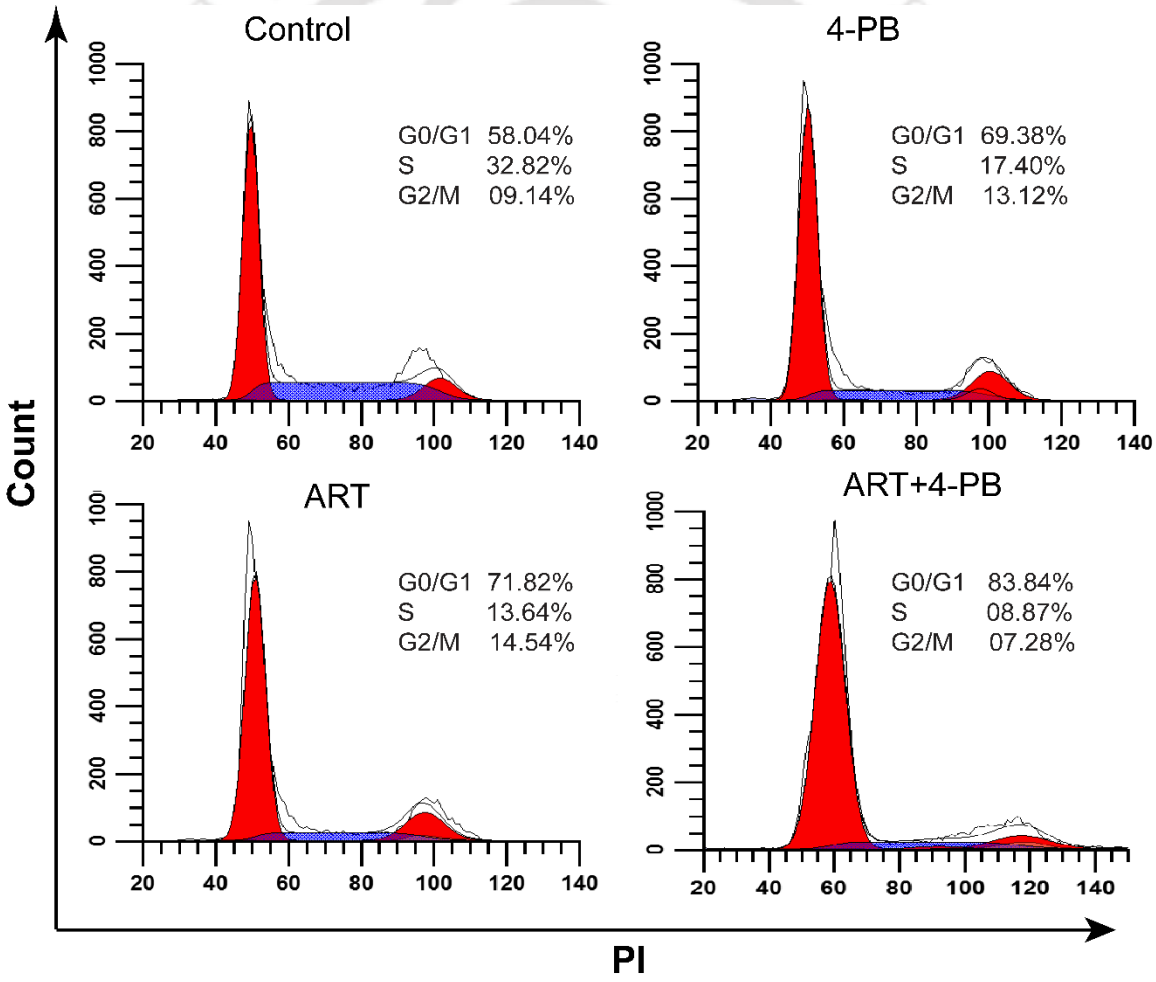

Figure 3.14. The synchronised MCF-7 cells were treated with ART and/or 4-PB. After the end of the treatment duration, the phases of cell cycle were evaluated using PI dye. The data were acquired in the flow cytometer and analysed using ModFit LT software.

3.3.7 Mechanism underlying 4-PB mediated enhanced ART DNA damaging effect

It has been well known that ART induces DNA damage by generating ample amount of ROS inside the cell [22], where evidence was provided that 4-PB enhanced the effect of ART in MCF-7 cells. This compelling evidence propelled us to find the underlying mechanism behind the synergism showed by 4-PB and ART.

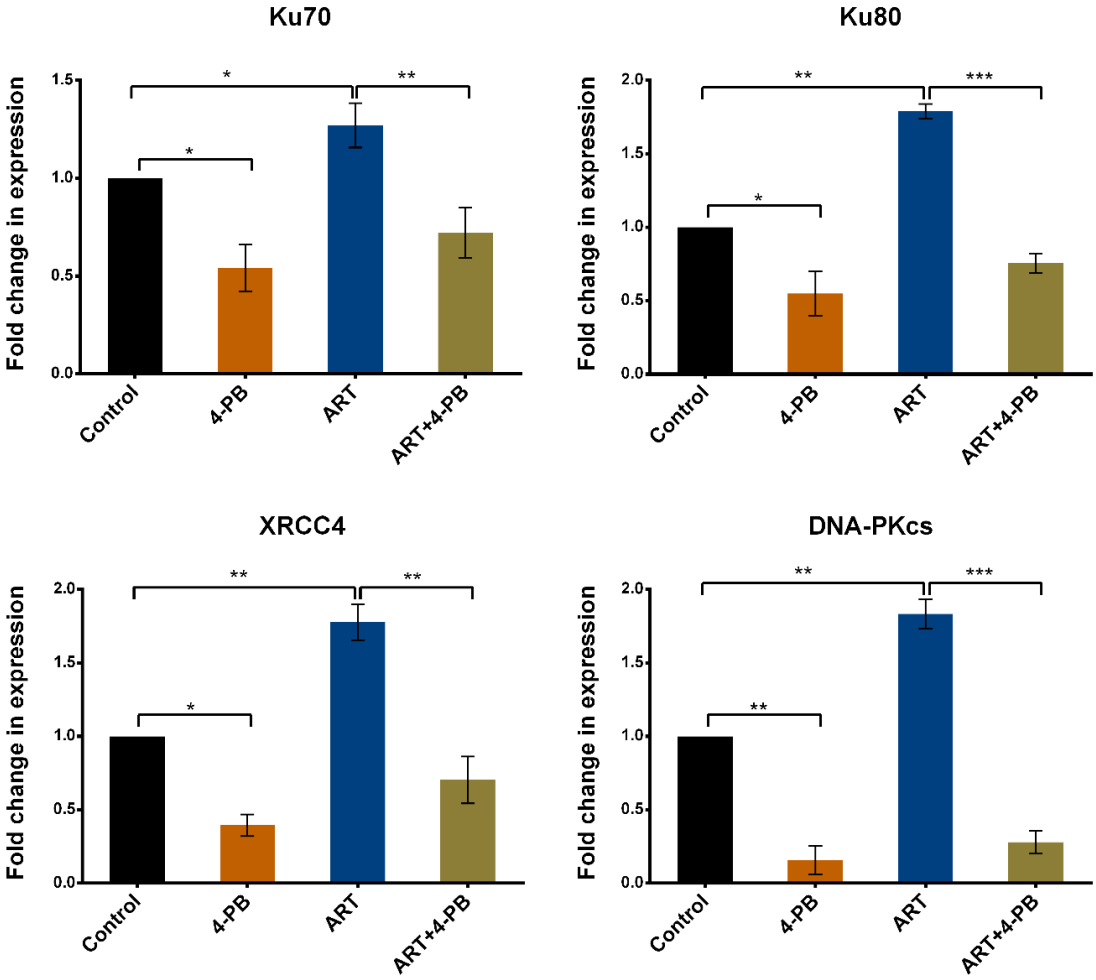

Figure 3.15. Expression analyses of DDR pathways. The mRNA expression levels of DDR elements of NHEJ pathway viz. Ku70, Ku80, XRCC4 and DNA-PKcs was assessed using qPCR (n = 3).

As an initial investigation into the underlying mechanism, the effect of 4-PB on the expression of well-known DDR proteins was examined, with or without the treatment involving ART. **Figure 3.15** showed real-time PCR analysis of the mRNA expression of Ku70, Ku80, XRCC4, and DNA-PKcs were performed on the MCF-7 cells after treatment with ART and/or 4-PB. The data showed a significant decrease in the

expression of all the four proteins at the mRNA level when treated with 4-PB alone. However, the expression of Ku70, Ku80, XRCC4, and DNA-PKcs increased significantly following treatment with ART. Further, when MCF-7 cells were exposed to both the drugs simultaneously, there was a decrease in the expression of DNA repair proteins was observed.

3.3.8 Therapeutic effectivity of combination drug in murine model

For the assessment of the potentiality of the drug combination, the mice were split into five groups (n = 10). Except in group 1, DLA was induced in all other groups. It took 8 days for the tumour to attain an appropriate volume for drug treatment (swelling of the peritoneum was due to the accumulation of ascitic fluid). Administration of the drug was started after the tumour was grown (from 8th day). On the 17th day, the cell viability assay was performed and the acquired data **(Table 3.1)** showed a significant decrease in the viable cell count after the treatment with the combination drug compared with the other treatment groups (4-PB or ART). Along with the cell viability, the reduction in the volume of the tumour also followed the same pattern where when 4-PB and ART administered simultaneously in DLA mice, the effectivity was more compared with the alone drug treatment **(Fig. 3.16 & 3.17)**. The above finding was also reflected in the lifespan of the mice **(Fig. 3.18)**. In the control group, all the DLA mice died at the end of the 18th day after the tumour inoculation, while for the 4-PB and ART treated mice were alive up to 59 days but eventually died at the end of the observation period. However, the group receiving the combination treatment was alive after the end of 40 days observation (animals were alive up to 50 days, death observed from day 51, 53, 55 & 59). Although, both the drugs individually showed an effective reduction in cell viability as well as shrinking of tumour volume, both failed to increase the lifespan of the mice however, the combination drug did successfully increased the lifespan of the mice.

DLA bearing mice were observed to have elevated levels of WBC and reduced levels of Hb and RBC count. Treatment with the combination drugs averted these conditions and restored the levels of WBC, RBC, and Hb counts to normal **(Table 3.2)**. A significant decline in the liver function enzyme (SGOT, SGPT & ALP) was observed, as compared to the control group **(Table 3.3)**. In **figure 3.19**, histopathological examination of liver and kidney tissues showed a remarkable recovery in the

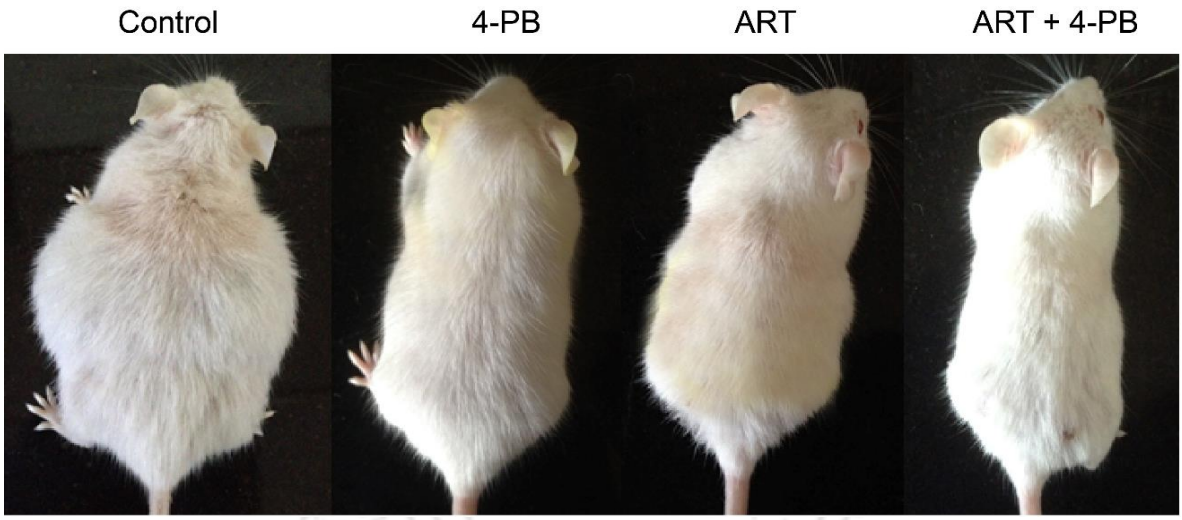

Figure 3.16. Reduction in the tumour volume was easily visualised in above image, taken after the respective drug treatment.

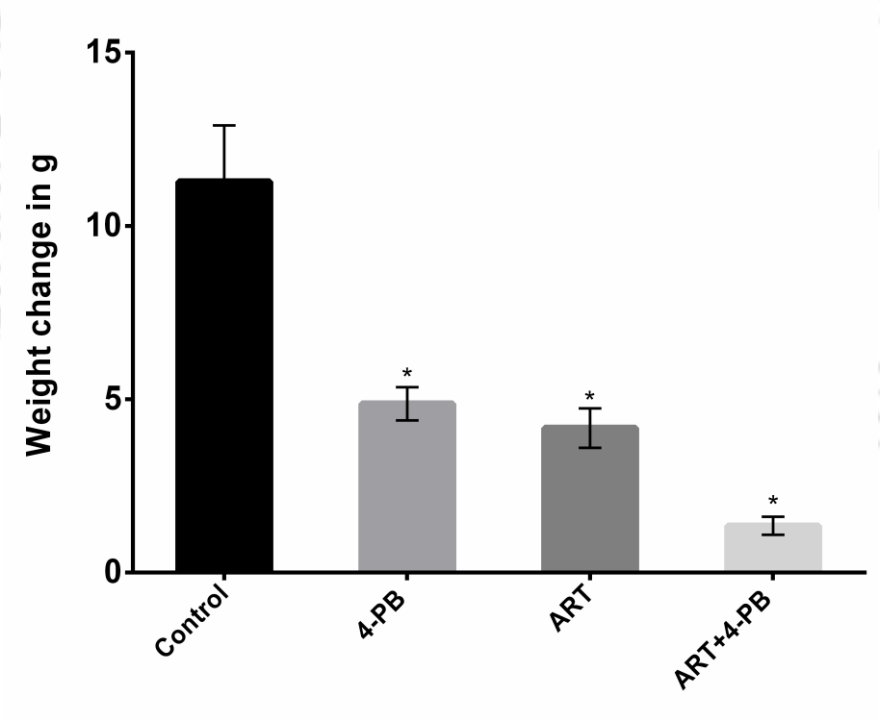

Figure 3.17. Reduction in the weight of the mice was the indicator of the reduction in the volume the tumour. The effect of the drugs on the tumour volume after 15 days of DLA induction and seven days of drug treatment were investigated by weighing mice at different time interval.

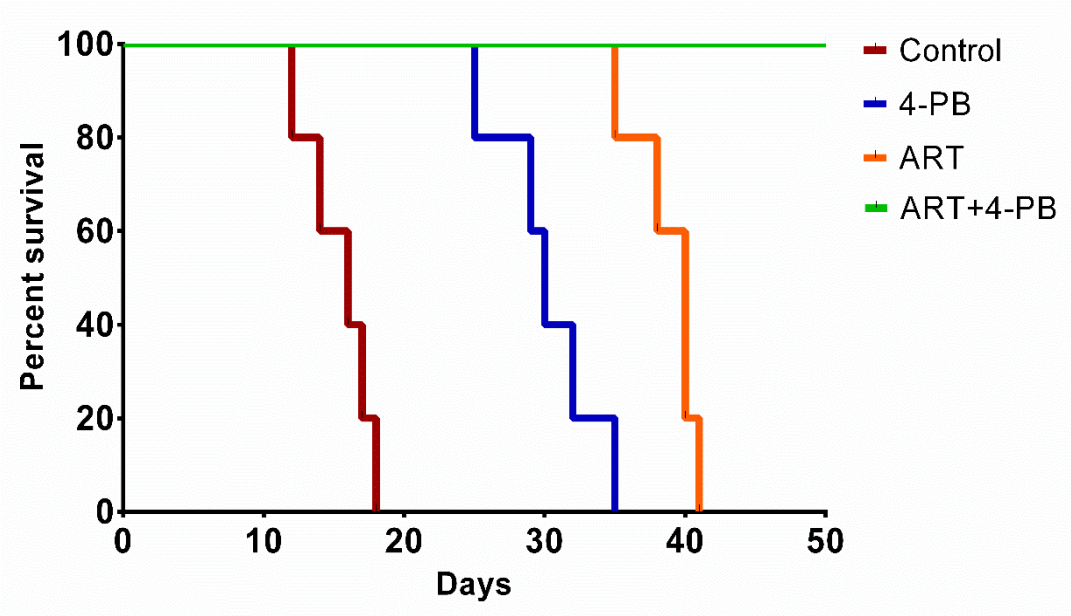

Figure 3.18. The changes in the lifespan of the mice was analysed after calculating the percent survival fraction of the mice after treatment. The percent survival curve was plotted using Kaplan-Meier curve.

conditions that changed due to the DLA induction. For instance, in kidney, glomerular atrophy, tubular congestion, infiltration of cells and deformed epithelial cells were seen, however, the conditions were reverted to normal with the decreased occurrence of tubular, glomerular and blood vessel congestion in the treated groups. In the liver examination, an abnormal arrangements of hepatocytes with polymorphic neutrophil infiltration, hepatic fibrillation, haemorrhage and perinuclear clumping of cytoplasm was observed in control group.

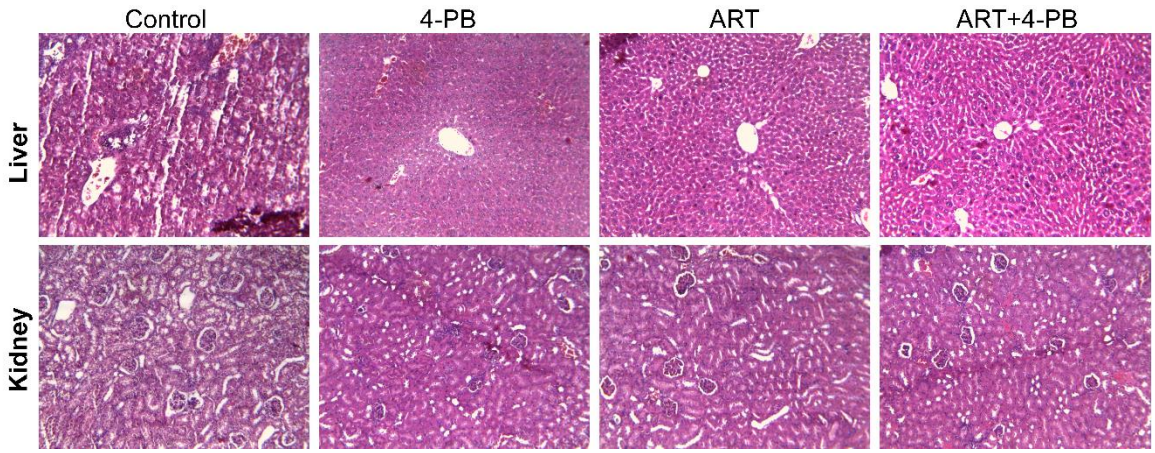

Figure 3.19. Histopathological analyses of liver and kidney tissues of mice.

Interestingly, in the treated group, reduction in the damages with normal cellular ultrastructures which were comparable to normal animals was observed. Overall, these changes were more profound in the combination drug treated group compared to the individual drug treatment regime.

Table 3.1. Effect of drug treatment on DLA cell viability in mice:

S. No	Treatment	Viable cell count (10^5 cells/ml)
1	DLA + Saline	418.4 ± 19.7
2	DLA + 4-PB	10.35 ± 1.5*
3	DLA + Artesunate	5.82 ± 1.4*
4	DLA + 4-PB + Artesunate	2.47 ± 0.8*

Table 3.2. Effect of drug treatment on hematological parameters:

S.No	Treatment	RBC (cells/ml X 10^6)	WBC (cells/ml X 10^3)	Hb g/dl
1	Normal animals	5.24 ± 0.43	10.14 ± 0.32	12.7 ± 0.53
2	DLA + Saline	2.73 ± 0.21$^{\$}$	20.35 ± 1.04$^{\$}$	6.6 ± 0.27$^{\$}$
4	DLA + 4-PB	4.5 ± 0.47*	14.46 ± 0.94*	8.9 ± 0.52*
4	DLA + Artesunate	3.58 ± 0.38*	16.62 ± 1.12*	8.4 ± 0.46*
7	DLA + 4-PB + Artesunate	4.91 ± 0.55*	13.18 ± 0.75*	11.1 ± 0.38*

Table 3.3. Effect of drug treatment on serum biochemical enzymes:

S. No	Treatment	SGOT	SGPT	ALP
1	Normal animals	46.3 ± 2.74	38.2 ± 2.43	114.6 ± 5.26
2	DLA + Saline	92.8 ± 4.26$	68.7 ± 3.64$	226.7 ± 9.42$
3	DLA + 4PB	57.6 ± 3.22*	50.3 ± 2.87*	142.4 ± 8.46*
4	DLA + Artesunate	67.2 ± 4.14*	59.4 ± 3.36*	157.2 ± 8.27*
5	DLA + 4-PB + Artesunate	48.6 ± 3.64*	39.1 ± 2.76*	118.8 ± 7.53*

All the results were expressed in mean ± S.D. $ $p < 0.05$ in comparison of saline treated DLA animals with normal animals. * $p < 0.05$ in comparison of drug treated DLA animals with untreated group DLA animals.

3.4 Discussion

In this study, it has been shown that, 4-PB enhanced the cytotoxicity of the traditional antiparasitic drug ART against the breast cancer cell line as well as DLA in mice. 4-PB synergistically ameliorated the effect of ART in dose-dependent manner by contributing enhancing the expression of anti-tumour proteins like Cx43, p21 and p27, which led to the G1 arrest of the cell cycle and increasing ROS production. Additionally, it can subjugate the DDR pathways in the MCF-7 cell, thus amplifying the DNA damage effect of ART.

ART is recognised as a remarkable new generation of antimalarial drugs with no noticeable side effects or obvious adverse reactions in humans [23, 24]. Recent experimental evidence suggested that ART may provide a therapeutic alternative in rapid disseminating cancers, without inducing drug-based resistance [14, 25]. Although, a few reports of cell lines and laboratory animals toxicities have raised concerns due to high doses and prolonged use of ART [16], these findings have not been reported in humans taking numerous doses of artemisinin till date. Keeping these in mind a novel combination therapy was designed involving ART and 4-PB, in which, 4-PB reduced the effective cytotoxic ART concentration synergistically when administered on MCF-7 cell line and in the murine model.

4-PB has been effectively used in patients with hyperammonemia and urea cycle disorders (UCDs) involving deficiencies of carbamyl phosphate synthetase (CPS), ornithine transcarbamylase (OTC), or argininosuccinic acid synthetase (AS) [26]. Although, two HDACi namely vorinostat (suberoylanilide hydroxamic acid, Zolinza) and depsipeptide (romidepsin, Istodax) have received approval from the US FDA for the treatment of cutaneous T-cell lymphoma in 2006 and 2009 [27], respectively, 4-PB's potentiality as an anti-cancer drug is still under evaluation in various clinical trials [28].

Initial objective of this study was to design an effective chemoprevention cocktail that would have less adverse effect and would be superior to individual drug therapy. In present study, it was revealed that, 4-PB alone was effective in reducing the cell viability of cultured MCF-7 cells. However, a high dose of 4-PB was required to accomplish a significant cell death. In contrast, when an intermediate dose of 4-PB

(5 mM) was used in conjunction with the dose-dependent cell viability of ART on MCF-7 cells, it showed a significant decrease in the IC_{50} of ART (55.32 ± 6.24 µM to 26.22 ± 3.17 µM). Further, the cell viability data was corroborated with two different flow cytometry based apoptotic assays, namely, PI apoptosis assay and PE Annexin V & 7-AAD assay by taking the near IC_{50} dose of ART (50 µM) and 5 mM of 4-PB. The analysis of live and dead nuclei using PI dye after treatment provided a clear insight on the enhancement of the ART effect in combination with 4-PB. When treated with 4-PB and ART, the MCF-7 cells showed 41.69 % and 65.12 % of apoptotic nuclei, respectively. The percentage of apoptotic nuclei was increased to 87.03 % when both the drugs were combined. A similar trend in the PE Annexin V & 7-AAD apoptotic assay was seen, where 4-PB and ART showed 23.21 % and 41.02 % of the apoptotic cell population (early + late apoptotic cells), respectively, while the combination of drug showed considerably large percent of apoptotic cell population of 61.22 %.

The above observations concluded the enhancement of the cytotoxity of ART when combined with 4-PB. Further investigation on the role of 4-PB in heightening the effect of ART by analysing the distribution of cells in several phases of the cell cycle was done. Increase in the expression of $p27^{Kip1}$ and $p21^{Cip1}$ proteins makes cell susceptible to G1 arrest [29, 30]. Based on these reports, analysis of the DNA content of the cell population for cell cycle analysis using PI was performed. Thus, when synchronised MCF-7 cells were treated with combination drug, they showed a substantial accumulation of cells in G1 phase. Basically, 4-PB amplified the G1 arrest after the treatment with ART. In a similar fashion, the enhancement in the ROS generation inside the cells after the combination treatment was also observed.

Above data imply that the 4-PB demonstrated strong synergism with ART in inducing a profound level of apoptosis in dose-dependent manner. Based on the CI values, it was deduced that the interaction between 4-PB and ART was synergistic rather than additive. To figure out the underlying pathway responsible for the said enhanced effect, expression levels of DDR elements after drug treatment was analysed. Till date, there has been no report of downregulation of DDR elements after the treatment with 4-PB in MCF-7 cells. The only notable exception is a report that demonstrated the role of 4-PB in attenuation of the expression of Bcl-XL, DNA-PK, Caveolin-1, and VEGF was behind the increase in the sensitivity towards radiation-

induced apoptosis in prostate cancer cells [31]. To elucidate the exact molecular mechanism by which 4-PB exerts synergistic effect with ART, analysis of the DNA repair processes was performed, as it has been reported earlier that ART induces DNA damage in cancer cells mediated by ROS [22, 32]. Based on these reports, an investigation was performed to find the expression levels of key proteins involved in the nonhomologous end joining pathway, namely Ku70, Ku86, XRCC4, and DNA-PKcs, which is crucial in DDR processes [33-35]. The qPCR analysis of the expression of these proteins showed downregulation at mRNA level after treatment with 4-PB. However, when treated with ART alone, the levels of these proteins increased significantly. Interestingly, the elevation in the expression of these proteins diminished when 4-PB was introduced with the ART in the medium. Thus, suggesting the involvement of attenuation of Ku70, Ku86, XRCC4, and DNA-PKcs by 4-PB in enhancing the effect of the combination drug. The downregulation of these effector proteins could be the reason of the synergistic action of 4-PB with ART.

To further examine the efficacy of our combination drug cocktail, initial investigation was performed in murine model. DLA bearing Swiss albino mice were initially tested for the tolerable doses of ART and/or 4-PB. Once done, the treatment of the DLA mice with ART and/or 4-PB as described in materials and methods section was started. The reduction in the volume of the tumour after treatment with ART and/or 4-PB, both visually and by weighing the mice was found. However, the reduction in tumour volume was more pronounced in the mice treated with the combination drug. Even the survival probability data corroborated with the above findings. Under the observation period of 40 days, mice treated with combination drug survived over 40 days while others died within the observation period. The histological parameters of the treated mice were improved drastically compared with the control DLA mice.

In summary, this study have presented a novel combination of the drugs which are already in use for the treatment of other diseases, as probable anti-cancer therapy. This drug combination holds an immense potential for further testing in the clinical trials. In this study, it has been shown that 4-PB synergistically enhanced the efficacy of ART and potentiated its cytotoxicity against MCF-7 cells. The underlying mechanism behind this revolves around the overall attenuation of the DDR elements

inside the cell. The combination therapy even showed its effectivity in DLA mice model. Overall, a comprehensive understanding of these findings required further studies. However, our observations reported here emphasise the need for persistent improvement of strategies for making human tumour cells susceptible to cancer therapies that kill cancer cells by inducing DNA damage.

3.5 References

[1] M. Esteller, J.G. Herman, Cancer as an epigenetic disease: DNA methylation and chromatin alterations in human tumours, The Journal of pathology 196(1) (2002) 1-7.

[2] T. Kouzarides, Histone acetylases and deacetylases in cell proliferation, Curr Opin Genet Dev 9(1) (1999) 40-48.

[3] W. Gu, R.G. Roeder, Activation of p53 sequence-specific DNA binding by acetylation of the p53 C-terminal domain, Cell 90(4) (1997) 595-606.

[4] Y.-H. Kim, J.-W. Park, J.-Y. Lee, T.K. Kwon, Sodium butyrate sensitizes TRAIL-mediated apoptosis by induction of transcription from the DR5 gene promoter through Sp1 sites in colon cancer cells, Carcinogenesis 25(10) (2004) 1813-1820.

[5] R. Feinman, K.O. Clarke, L.E. Harrison, Phenylbutyrate-induced apoptosis is associated with inactivation of NF-κB in HT-29 colon cancer cells, Cancer Chemother Pharmacol 49(1) (2002) 27-34.

[6] W.K. Kelly, O.A. O'Connor, P.A. Marks, Histone deacetylase inhibitors: from target to clinical trials, Expert Opin. Invest. Drugs 11(12) (2002) 1695-1713.

[7] S.W. Brusilow, J. Finkelstien, Restoration of nitrogen homeostasis in a man with ornithine transcarbamylase deficiency, Metabolism 42(10) (1993) 1336-1339.

[8] R.C. Rubenstein, P.L. Zeitlin, A Pilot Clinical Trial of Oral Sodium 4-Phenylbutyrate (Buphenyl) in Δ F508-Homozygous Cystic Fibrosis Patients: Partial Restoration of Nasal Epithelial CFTR Function, Am J Respir Crit Care Med 157(2) (1998) 484-490.

[9] A. Munshi, J.F. Kurland, T. Nishikawa, T. Tanaka, M.L. Hobbs, S.L. Tucker, S. Ismail, C. Stevens, R.E. Meyn, Histone deacetylase inhibitors radiosensitize human melanoma cells by suppressing DNA repair activity, Clinical cancer research : an official journal of the American Association for Cancer Research 11(13) (2005) 4912-4922.

[10] Z. Khan, M. Akhtar, T. Asklund, B. Juliusson, P.M. Almqvist, T.J. Ekström, HDAC inhibition amplifies gap junction communication in neural progenitors: potential for cell-mediated enzyme prodrug therapy, Exp Cell Res 313(13) (2007) 2958-2967.

[11] O. Ammerpohl, A. Trauzold, B. Schniewind, U. Griep, C. Pilarsky, R. Grutzmann, H.D.D. Saeger, O. Janssen, B. Sipos, G. Kloppel, H. Kalthoff, Complementary effects of HDAC inhibitor 4-PB on gap junction communication and cellular export mechanisms support restoration of chemosensitivity of PDAC cells, Br J Cancer 96(1) (2007) 73-81.

[12] T. Asklund, I.B. Appelskog, O. Ammerpohl, T.J. Ekström, P.M. Almqvist, Histone deacetylase inhibitor 4-phenylbutyrate modulates glial fibrillary acidic protein and connexin 43 expression, and enhances gap-junction communication, in human glioblastoma cells, European journal of cancer (Oxford, England : 1990) 40(7) (2004) 1073-1081.

[13] T. Hampton, Artesunate and Malaria, JAMA 304(23) (2010) 2582-2582.
[14] M.P. Crespo-Ortiz, M.Q. Wei, Antitumour Activity of Artemisinin and Its Derivatives: From a Well-Known Antimalarial Agent to a Potential Anticancer Drug, BioMed Research International 2012 (2011).
[15] N. Hosoya, K. Miyagawa, Targeting DNA damage response in cancer therapy, Cancer Sci 105(4) (2014) 370-388.
[16] T. Gordi, E.-I. Lepist, Artemisinin derivatives: toxic for laboratory animals, safe for humans?, Toxicol. Lett. 147(2) (2004) 99-107.
[17] A. Raza, V. Kohila, S.S. Ghosh, Redesigned Escherichia coli cytosine deaminase: a new facet of suicide gene therapy, The journal of gene medicine 17(6-7) (2015) 132-139.
[18] C. Riccardi, I. Nicoletti, Analysis of apoptosis by propidium iodide staining and flow cytometry, Nat. Protoc. 1(3) (2006) 1458-1461.
[19] S.D. Gore, M.A. Carducci, Modifying histones to tame cancer: clinical development of sodium phenylbutyrate and other histone deacetylase inhibitors, Expert Opin. Invest. Drugs 9(12) (2000) 2923-2934.
[20] Y.-W.W. Zhang, M. Kaneda, I. Morita, The gap junction-independent tumour-suppressing effect of connexin 43, The Journal of biological chemistry 278(45) (2003) 44852-44856.
[21] G. Bornstein, J. Bloom, D. Sitry-Shevah, K. Nakayama, M. Pagano, A. Hershko, Role of the SCFSkp2 ubiquitin ligase in the degradation of p21Cip1 in S phase, J Biol Chem 278(28) (2003) 25752-25757.
[22] N. Berdelle, T. Nikolova, S. Quiros, T. Efferth, B. Kaina, Artesunate induces oxidative DNA damage, sustained DNA double-strand breaks, and the ATM/ATR damage response in cancer cells, Mol Cancer Ther 10(12) (2011) 2224-2233.
[23] A. Benakis, M. Paris, L. Loutan, C.T. Plessas, S.T. Plessas, Pharmacokinetics of artemisinin and artesunate after oral administration in healthy volunteers, Am J Trop Med Hyg 56(1) (1997) 17-23.
[24] J. Fishwick, W.G. McLean, G. Edwards, S.A. Ward, The toxicity of artemisinin and related compounds on neuronal and glial cells in culture, Chem-Biol Interact 96(3) (1995) 263-271.
[25] T. Efferth, H. Dunstan, A. Sauerbrey, H. Miyachi, C. Chitambar, The anti-malarial artesunate is also active against cancer, Int J Oncol 18(4) (2001) 767-773.
[26] M.L. Batshaw, R.B. MacArthur, M. Tuchman, Alternative pathway therapy for urea cycle disorders: twenty years later, The Journal of pediatrics 138(1) (2001) S46-S55.
[27] K. Ververis, A. Hiong, T.C. Karagiannis, P.V. Licciardi, Histone deacetylase inhibitors (HDACIs): multitargeted anticancer agents, Biologics : targets & therapy 7 (2013) 47-60.
[28] K.T. Smith, J.L. Workman, Histone deacetylase inhibitors: Anticancer compounds, The International Journal of Biochemistry & Cell Biology 41(1) (2009) 21-25.

[29] S. Bates, K.M. Ryan, A.C. Phillips, K.H. Vousden, Cell cycle arrest and DNA endoreduplication following p21Waf1/Cip1 expression, Oncogene 17(13) (1998) 1691-1703.

[30] H. Toyoshima, T. Hunter, p27, a novel inhibitor of G1 cyclin-Cdk protein kinase activity, is related to p21, Cell 78(1) (1994) 67-74.

[31] M. Goh, F. Chen, M.T. Paulsen, A.M. Yeager, E.S. Dyer, M. Ljungman, Phenylbutyrate attenuates the expression of Bcl-X(L), DNA-PK, caveolin-1, and VEGF in prostate cancer cells, Neoplasia (New York, N.Y.) 3(4) (2001) 331-338.

[32] P.C. Li, E. Lam, W.P. Roos, M.Z. Zdzienicka, B. Kaina, T. Efferth, Artesunate derived from traditional Chinese medicine induces DNA damage and repair, Cancer Res 68(11) (2008) 4347-4351.

[33] J.E. Haber, Partners and pathways: repairing a double-strand break, Trends Genet 16(6) (2000) 259-264.

[34] P. Jeggo, Identification of genes involved in repair of DNA double-strand breaks in mammalian cells, Radiat Res 150(5s) (1998) S80-S91.

[35] K.K. Khanna, S.P. Jackson, DNA double-strand breaks: signaling, repair and the cancer connection, Nat Genet 27(3) (2001) 247-254.

Chapter 4

Expression of Connexin 43 potentiated the redesigned cytosine deaminase activity and enhanced suicide gene therapy

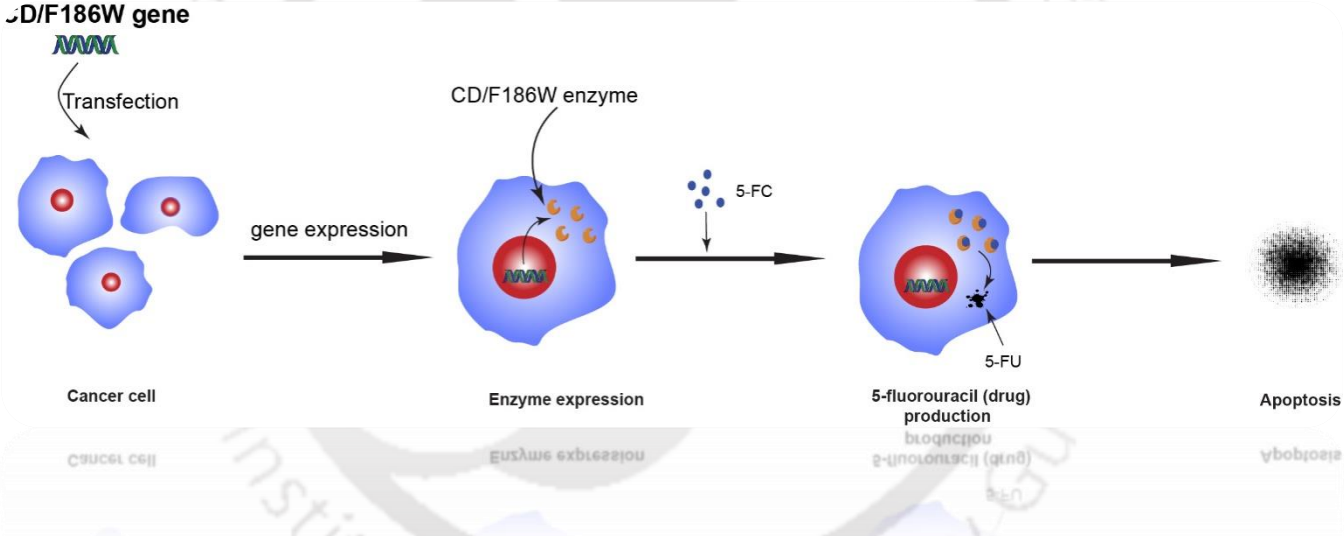

Chapter 4

Expression of Connexin 43 potentiated the redesigned cytosine deaminase activity and enhanced suicide gene therapy

4.1 Introduction

Gene therapy currently has a great impact on the treatment options of various diseases including cancer. As suicide gene therapy (SGT) entered various clinical trials, the factors limiting its potency cannot be overlooked. Gene-directed enzyme prodrug therapy (GDEPT) based on the principles of SGT incorporates the intratumoural delivery of genes encoding enzymes, which activates prodrug [1]. GDEPT has potential to overcome the limitations of conventional cancer therapeutics as the former has the advantage of bystander effect as well as targeted therapy [2-4]. Two combinations of enzymes and prodrugs have been widely studied: the *Escherichia coli* cytosine deaminase (CD; EC 3.5.4.1) with antifungal drug 5-fluorocytosine (CD/5-FC) and the herpes simplex virus thymidine kinase (HSVtk) with the anti-herpetic ganciclovir (GCV) [5-10]. HSVtk/GCV therapy exhibits more cytotoxicity towards cancer cells due to its gap junction dependent bystander effect [5]. Since the triphosphate GCV cannot diffuse through the cell membrane, its efficacy is limited towards gap junction deficient cancer cells [11]. However, the CD/5-FC system does not rely on gap junction as the toxic product 5-fluorouracil (5-FU) can freely diffuse across the cell membrane, overcoming the limitations of the HSVtk/GCV system [12].

The CD enzyme catalyzes the hydrolytic deamination of cytosine into uracil. It can also convert the inert prodrug 5-FC into highly toxic chemotherapeutic drug 5-FU, which is then further converted into potent antimetabolites (5-FdUMP, 5-FdUTP, 5-FUTP) by cellular enzymes. Thus, the series of events viz. irreversible inhibition of thymidylate synthase and formation of (5-FU) RNA and (5-FU) DNA, results in cell death [13, 14]. This enzyme is found in several bacteria and fungi, but not in

mammalian cells [15]. Thus, drug resistant mammalian cells become sensitive towards 5-FC when transfected with CD.

Although, the CD/5-FC system has shown its efficacy in a number of clinical trials, its application in therapy has been limited [16-18]. Despite having various contrasting features, bacterial CD (bCD) still faces setbacks due to its low specificity towards prodrug, 5-FC,thus limiting the overall therapeutic response [19]. It has been shown that yeast cytosine deaminase (yCD) has better affinity towards 5-FC, when compared with bCD. However, it is less thermostable than bCD, making bCD a better choice for GDEPT applications. The attempt has been made to create a stable mutant of bCD by random mutagenesis, having marginally improved affinity towards prodrug, 5-FC [20].

During a previous study, computational as well as genetic engineering approaches were exploited to design bCD mutants with improved specificity towards prodrug, 5-FC, to overcome the limitation of bCD [21]. Unlike earlier reports on designing mutants by random mutagenesis [22], in this study site directed mutagenesis (SDM) was performed to alter substrate specificity of bCD, both *in silico* as well as *in vitro*. Out of these promising mutants, F186W was chosen based on kinetic values **(Table 4.1)** and investigated its potentiality and application by two different ways.

Table 4.1. Relative specificity of wtCD and F186W enzymes [21].

Enzyme	Specificity with respect to 5-FC	Relative to wtCD
wtCD	0.094	1.0
F186W	0.556	5.95

First, the activity of the mutant F186W/5-FC on lung cancer cells and its potency in comparison to wild type bCD (wtCD or CD) was investigated. The results demonstrated that this mutant significantly enhanced the therapeutic efficacy of CD/5-FC mediated suicide gene therapy on A549 cells and has the potential to emerge as a substitute to wtCD.

In other set of experiments, a co-transfection system has been designed in which MCF-7 cells were co-transfected with Cx43 and wtCD/F186W gene. After the

transfection, the effect of Cx43 expression was studied in conjunction with suicide gene therapy mediated by wtCD or F186W mutant.

4.2 Materials and Methods

4.2.1 Cell line and culture conditions

Adenocarcinomic human alveolar basal epithelial cell line (A549) and human breast adenocarcinoma (MCF-7) cells were procured from the National Centre for Cell Science (NCCS), Pune, India. The cells were maintained in Dulbecco's modified Eagle's medium (DMEM high glucose), supplemented with 10% fetal bovine serum (FBS), 1% penicillin/streptomycin (100 U/ml; all from Sigma-Aldrich), at 37°C in humidified air containing 5% CO2. Treatments with drug 5-FC were performed (usually 72 h) at various concentrations.

4.2.2 Construction of mammalian expression vector

The wtCD and F186W mutants were sub-cloned from pGEX-4T2 (Amersham) containing wtCD and F186W in to the mammalian expression vector, pVITRO2-hygro-GFP/LacZ (Invivogen, USA). The wtCD and F186W genes were amplified from their corresponding bacterial expression vectors viz. pGEX-wtCD and pGEX-F186W, respectively. The pVITRO2-GFP/wtCD and pVITRO2-GFP/F186W were constructed by replacing the LacZ gene with wtCD and F186W, respectively, by using forward primer 5'CGTCCATGGGAATGGTGTCGAATAACGC3' and reverse primer 5'CCTTGCTA-GCTTAGCTCCGCTGATACGTTT3' with NcoI and NheI restriction sites. Further, the constructs were confirmed by the restriction enzyme digestion using NcoI and NheI. The previously designed Cx43-pEGFP-N1 mammalian expression was used in this study.

4.2.3 Transfection and detection of Cx43 and wtCD/F186W expression

Cells were transfected using Lipofectamine 3000 reagent (Invitrogen) as per the manufacturer's protocol. The concentration of DNA and Lipofectamine were kept constant throughout the experiments. After 6 h of transfection, cells were further treated with prodrug. For confirmation of the Cx43, wtCD and F186W expressions, the total RNA of the transfected cells was isolated using GenElute Mammalian Total RNA Miniprep Kit (Sigma-Aldrich). Further, 1 μg of RNA was used for the generation

of cDNA with the help of Verso cDNA Kit (Thermo Scientific). Semi-quantitative PCR was performed using Cx43 and CD primers taking cDNA of the transfected cells as template. The β-actin gene expression was used as internal control. The PCR products were ran on 1.2% agarose gel and stained with ethidium bromide. As the wtCD and F186W genes were inserted in a GFP expressing vector, the extent of transfection was visualized in fluorescence microscope after 6 h of transfection.

4.2.4 Assessment of cell viability by MTT assay

The initial comparative analysis between parental, wtCD and F186W transfected A549 cells were performed by assessing cell viability after 5-FC exposure. Thereafter, the wtCD and F186W mutant were transfected in Cx43 transfected MCF-7 cells. The cells were then treated with 5-FC and cell viability was assessed as following. Cells were seeded in 96-well plates at a density of 7,000 cells/well in DMEM medium supplemented with 10% FBS. The cells were allowed to adhere overnight and transfection was performed in serum-free medium. After 6 h of transfection the serum free medium was replaced with experimental medium. The cells were exposed to various concentrations of 5-FC (0.05, 0.1, 0.5, 1 & 5 mM) or PBS (control) for 72 h. After the indicated time, the anti-cell proliferative activity of wtCD and F186W was assessed by 3-(4,5-dimethylthiazol-2-yl)-2,5-diphenyltetrazolium-bromide (MTT) assay (HiMedia) [23]. Fractional cell survival at each drug concentration was calculated by measuring absorbance at 550nm (Bio-Rad) and subtracting the background measurement at 650nm. Cell viability (%) was calculated relative to untreated viable cells. Each experiment was performed in triplicates and at least twice. The proliferation of control group was set as 100%.

4.2.5 Trypan blue dye exclusion assay

Cells at a density of 1x105 were seeded in 6-well plate. After transfected cells were exposed to 5-FC (0.01 & 1 mM) for 72 h, the cells were harvested and mixed with equal volume of 0.4% trypan blue dye (Invitrogen). Cells were loaded over the counting chamber. Live and healthy cells were unstained or excluded from dye, while dead or membrane compromised cells appeared to retain the dye and appeared blue. The viable cells (%) were counted using Countess-automated cell counter (Invitrogen).

4.2.6 Acridine Orange/Ethidium Bromide Dual Staining

Morphological identification of live, apoptotic and necrotic cells were performed by dual staining with acridine orange (AO)/ethidium bromide (EtBr) (Sigma-Aldrich). Cells were grown to 70-80% confluency in 12-well plate. After transfection with wtCD and F186W, cells were treated with 1mM 5-FC for 74 h. After the indicated time, the media were removed and washed with cold PBS. Fresh PBS containing 2 µg/ml AO and 6 µg/ml EtBr was added to the cells and kept in the dark for 10 min. The cells were then washed thoroughly with fresh PBS and visualized under the fluorescence microscope (Nikon Eclipse Ti-U, Japan; excitation filter of 480/15 nm for AO and 540/25 nm for EtBr, respectively).

4.2.7 Cell cycle analysis

The proportions of cells in different cell cycle phases were determined by flow cytometric analysis of their DNA content. Cells were seeded at a density of 1x105 in 6-well plate and left overnight for attachment. The cells maintained in serum containing media were replaced with serum-free media and left for cell synchronization for 48 h. Subsequently, cells were transfected with wtCD and F186W, and then exposed to 1mM of 5-FC for 48 h. At the end of the treatment period, cells were harvested and fixed in 70% alcohol solution for 15 min in ice. The fixed cells were collected by centrifugation and stained with propidium iodide (PI; Sigma-Aldrich) staining solution (50 µg/ml PI, 0.1 mg/ml RNase A, and 0.05% triton X-100) at 37° C for 30 min in the dark. Further the stained cells were analyzed by flow cytometer (FacsCalibur, BD Biosciences, NJ) at 10,000 events each. The various phases of cell cycle were then assessed by CellQuest and ModFit LT software (Verity House Software,ME). A similar protocol was used to investigate the cell cycle profile of wtCD/F186W gene transfected Cx43-MCF& cells after treatment.

4.2.8 Caspase-3 assay for apoptosis detection

For assessing apoptotic cell population, phycoerythrin (PE) conjugated caspase-3 antibody (BD Biosciences, NJ) was used. Cells were grown in 6-well plate at 70-80% confluency. After treatment for 62 h, as described above, cells were harvested with trypsin-EDTA. The detached cells were fixed with 0.1% formaldehyde in PBS at 370 C for 10 min. Fixed cells were centrifuged at 450xg for 6 min at 40C and washed with

cold PBS. Then, the cells were permealized with 0.5% tween-20 in PBS for 10 min. Further, the cells were washed with PBS for two times, 20 µl of caspase-3 conjugated with PE antibody (as per the manufacturer's protocol) was added to each sample, before incubation in the dark for 30 min. The samples were then analyzed with flow cytometer (FacsCalibur, BD Biosciences, NJ) at 10,000 events each. The data were analyzed by Cell Quest Pro software in the same instrument.

4.2.9 Fluoremetric analyses of apoptotic cells using PI and PE Annexin V/7-AAD

The apoptotic population of the cells were analysed using the protocol described earlier [23]. MCF-7 cells were treated with 5-FC for 72 h. After the completion of the treatment duration, the cells were collected, fixed in 70 % ethanol and processed following the protocol mentioned above. The cells were then analysed by using CytoFLEX flow cytometer (Beckman Coulter) using 488 nm laser line for excitation. Red fluorescence of PI was measured in PE-A channel.

The different apoptotic cell populations were quantified using PE (phycoerythrin) Annexin V and 7-AAD (7-aminoactinomycin D), following treatment with 5-FC. In brief, cells were grown and treated with 1mM of 5-FC for 72 h. After the end of the treatment duration, the cells were collected by trypsinization and stained with PE Annexin V and 7-AAD, following the manufacturer's protocol (BD Biosciences). Further, the extent of apoptosis in the cells were analysed using flow cytometer (CytoFLEX, Beckman Coulter).

4.2.10 Statistical analysis

The IC_{50} dose was calculated using non-linear curve regression analysis and the level of significance were calculated using unpaired two-tailed t-test. Data points were expressed as the mean ± SD (SD = standard deviation) and experiments were performed at least thrice in triplicates. To assess the statistical significance of differences, the one- and two-way analysis of variance (ANOVA) and Tukey's post hoc test were used for pairwise comparisons. Data were analysed using Prism, version 6.01 (GraphPad Software Inc., San Diego, CA, USA). Statistically significant values (p-value) for unpaired two-tailed t-test were provided in the result section while for one- and two-way analysis of variance (ANOVA) the p-value corresponds to *p< 0.05, **p< 0.01, ***p< 0.001 and ****p< 0.0001.

4.3 Results and Discussion

4.3.1 Sub-cloning and characterization of wtCD and F186W genes

A 1,298 bp fragment of each of wtCD and F186W genes, having *NcoI* and *NheI* overhangs, was amplified from their respective pGEX-4T2 bacterial expression vector. The genes were further sub-cloned into the mammalian expression vector, pVITRO2-hygro-GFP/LacZ, replacing LacZ gene. The clones were confirmed by performing restriction digestion with the enzymes, *NcoI* and *NheI* **(Fig. 4.1)**.

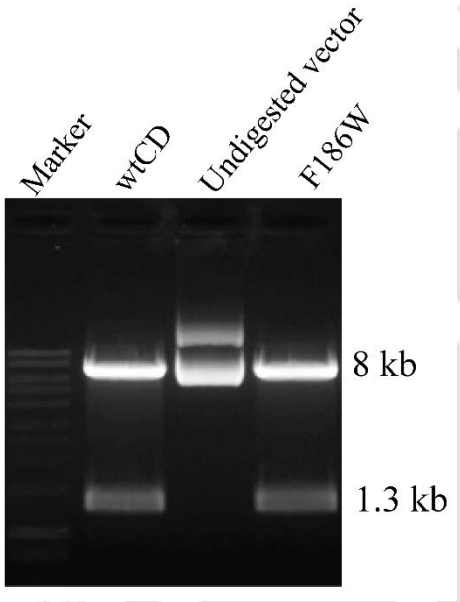

Figure 4.1. Agarose gel electrophoresis depicted clone confirmation by restriction digestion of wtCD and F186W genes (~1.3 kb) containing vector, using NcoI/NheI restriction enzymes. The undigested vector having size of ~8 kb was taken as control.

4.3.2 Transient transfection and expression analysis

Mammalian expression vectors containing genes, pVITRO2-GFP/CD and pVITRO2-GFP/F186W respectively, were then transfected in A549 cancer cell lines. Transfection efficiencies were initially assessed by visualized in fluorescence microscope for GFP expression **(Fig. 4.2)**. Furthermore, to examine the expression of wtCD and F186W, the whole RNA from the transfected A549 cells were isolated and cDNA was prepared. Using CD gene specific primers, expression of wtCD and F186W gene were analyzed by semi-quantitative PCR **(Fig. 4.3)**. The transfected cell lines showed a distinct band at 1.3 kb, which coincided with the position of CD gene amplified from vector alone, while in untransfected cell line the band was absent.

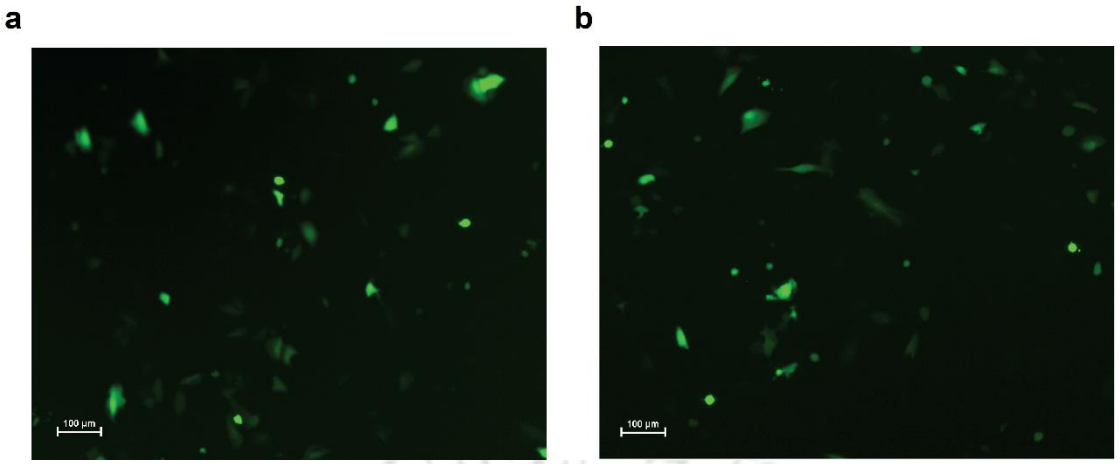

Figure 4.2. After 6 h of transfection, the expression of GFP was visualized under fluorescence microscope (scale bar 100 µm). The GFP expressions of wtCD and F186W were shown in figure (a) & (b), respectively.

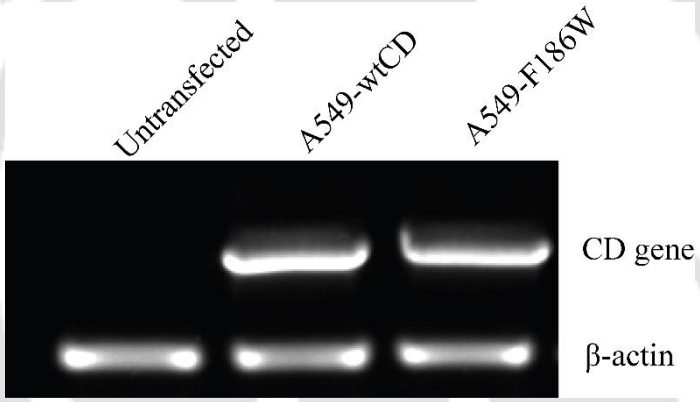

Figure 4.3. Expression of wtCD and F186W genes were evaluated by reverse transcriptase-PCR (RT-PCR) after transfection. β-actin gene was taken as control.

4.3.3 Comparative analysis of wtCD and F186W by cell viability assays

To address whether the mutant F186W is more efficient than wtCD, initial analysis was performed by assessing cell viability assay of wtCD and F186W transfected cell lines, after being exposed to different concentrations of 5-FC. **Figure 4.4** showed the comparative analysis of wtCD and F186W transfected A549 cells, treated with the different concentrations of the prodrug 5-FC. After 72 h treatment, the data obtained clearly indicated that the F186W was much more effective than wtCD, whereas the parental cells remained unresponsive towards 5-FC exposure. Therefore, it was observed that the F186W had better 5-FC utilization activity than wtCD. The IC_{50} value of wtCD was found to be at 1mM 5-FC concentration, while for F186W it was 0.3mM

5-FC which was far less **(Fig. 4.6)**. Hence, 1mM (~IC_{50} of wtCD) of 5-FC was chosen for further experimental analysis and comparisons.

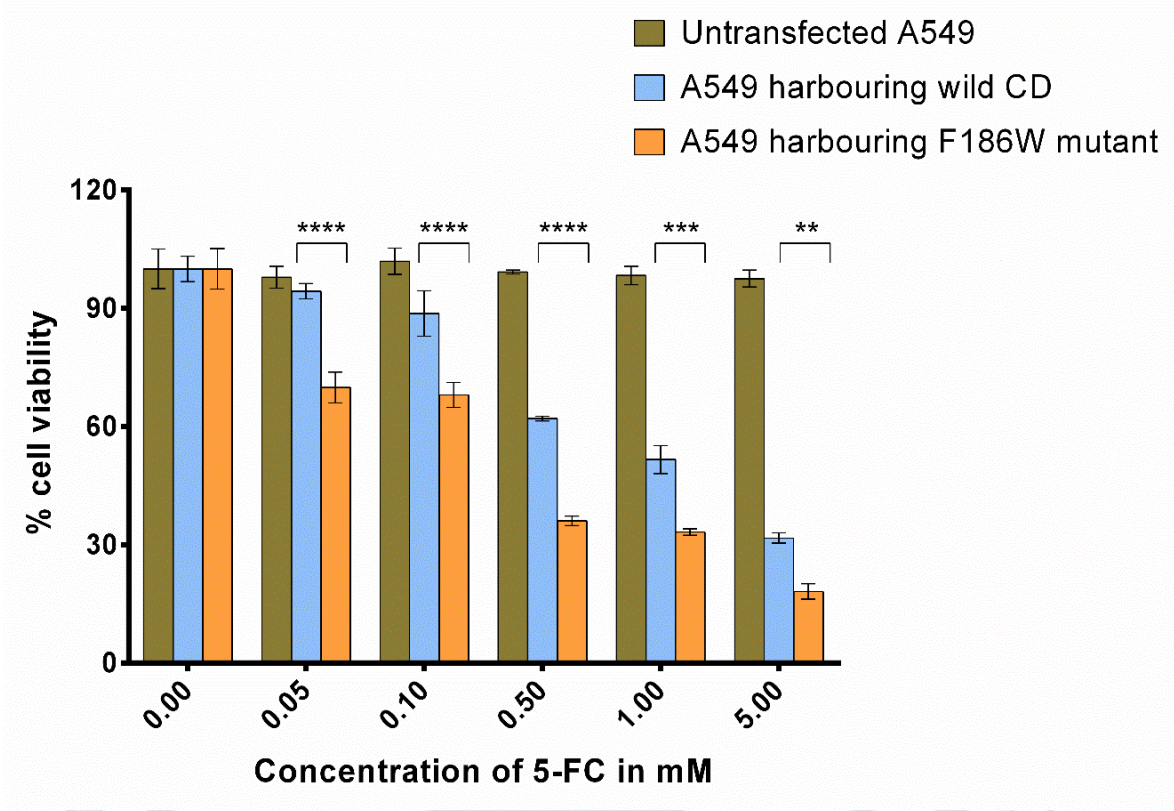

Figure 4.4. Cell viability assay. Cell viability assay (MTT assay) was performed for initial comparative analysis between wtCD and F186W expressing A549 cells. The data showed a significant advantage of F186W over wtCD. Herein, after 72 h of treatment with the increasing doses of 5-FC, the resulting data suggested that the F186W reached its IC50 at far less concentration than wtCD. Statistically significant values were denoted by * ($p<0.05$), ** ($p<0.01$), *** ($p<0.001$) and **** ($p<0.0001$).

Further, the trypan blue dye exclusion assay supported the results obtained from the MTT assay **(Fig. 4.5)**. The trypan blue dye exclusion assay provided a direct identification and calculation of live (unstained; excluded from trypan blue) and membrane compromised or dead cells (blue, stained) in treated cell population.

4.3.4 Assessment of mode of cell death by dual staining with AO/EtBr

To gain further insight into the fashion of cell death, the treated cells were stained with fluorescent DNA intercalating dye namely AO/EtBr and observed under fluorescence microscope. In **figure 4.7**, it is evident that untreated transfected cells had uniformly stained green nuclei indicating healthy viable cells. When both wtCD

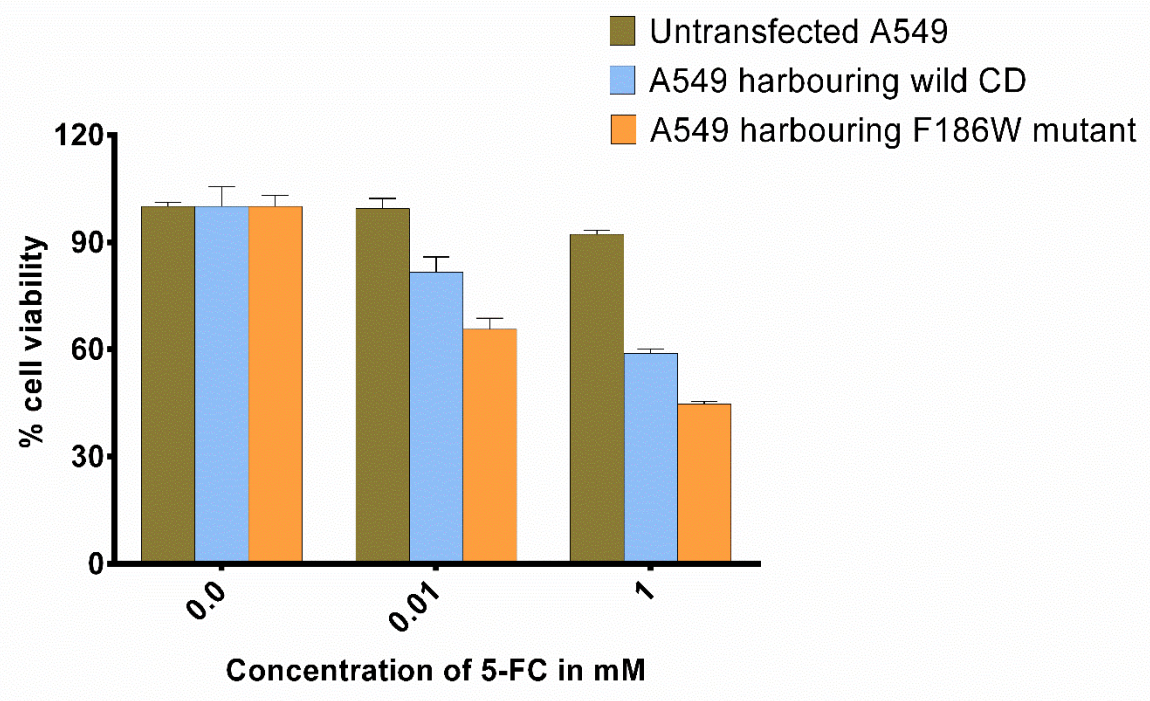

Figure 4.5. Further to support the experimental data of MTT assay, trypan blue dye exclusion assay was performed.

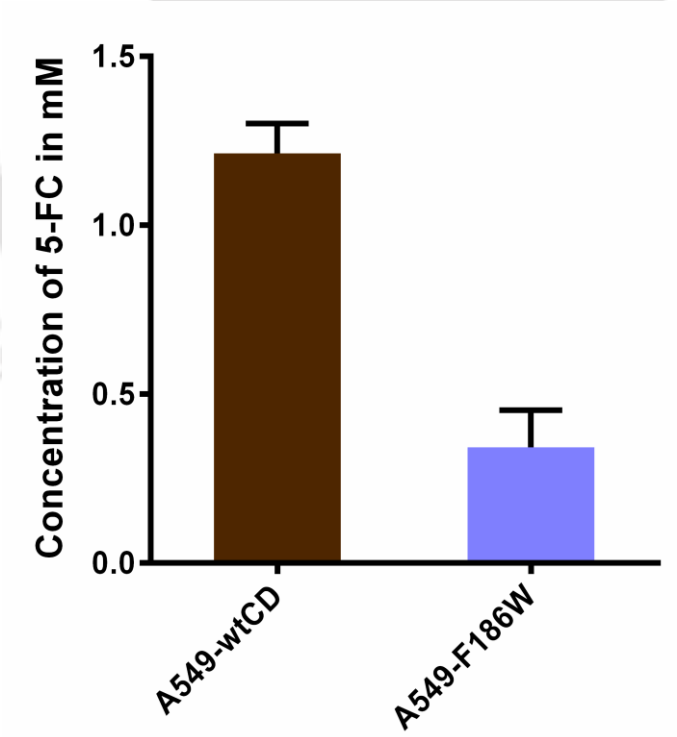

Figure 4.6. IC50 value of wtCD and F186W expressing A549 cells when treated with 5-FC was calculated using non-linear curve regression analysis.

and F186W tansfected cells were treated with IC_{50} dose of wtCD, it showed green, orange and red nuclei implying the presence of live, early and late apoptotic cells. However, by analyzing the cell population microscopically, it could be inferred that the F186W containing cell lines had much more apoptotic cells than wtCD harbouring cells. Thus, AO/EB staining results illustrated possible induction of apoptosis was more in F186W cell lines.

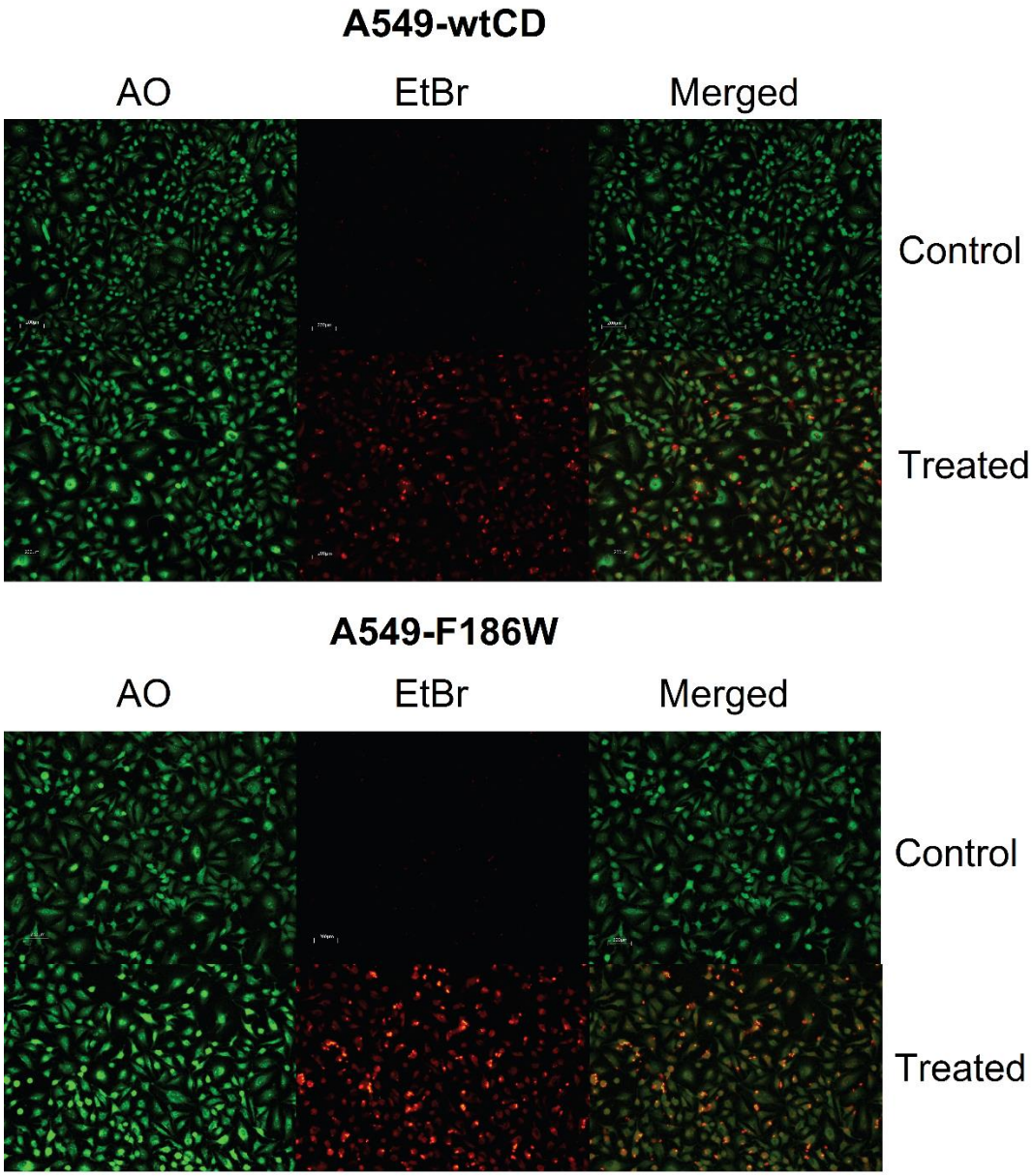

Figure 4.7. Representative image of AO/EtBR dual staining: the transfected cells were treated with 1 mM of 5-FC for 72 h. At the end of the treatment duration, the cells were stained with AO/EtBr. The AO and EtBr stained cells image were merged to distinguish between live (green), early apoptotic (orange) and dead (red) cells.

4.3.5 5-FC induced G1 arrest in CD transfected cells

5-FU induced G1 arrest in cells was reported previously [24]. CD catalysed 5-FC conversion to 5-FU may also attribute the same. The flow cytometric analysis of DNA content of wtCD and the F186W transfected cells, after 5-FC treatment, showed G1 arrest. Cells were serum deprived for 48 h resulting in G1 arrest of cells. Replacement of serum enriched media led to synchronized progression of cells into S-phase of the cell cycle. Exposure of parental cells towards 5-FC resulted no significant cell cycle arrest. wtCD and F186W transfected cells, when treated with 5-FC, remarkably increased the G1 population of cells **(Fig. 4.8)**. However the percentage of cells in F186W transfected cells were much more pronounced than the wtCD one. Thus, it could be concluded that the conversion of 5-FC to 5-FU by F186W mutant was more compelling than wtCD, supporting previously reported in vitro data [21]. The apoptotic cell population was excluded while analysing treated cells using ModFit LT software. Further, for analysis of apoptotic cells, caspase 3 assay was performed.

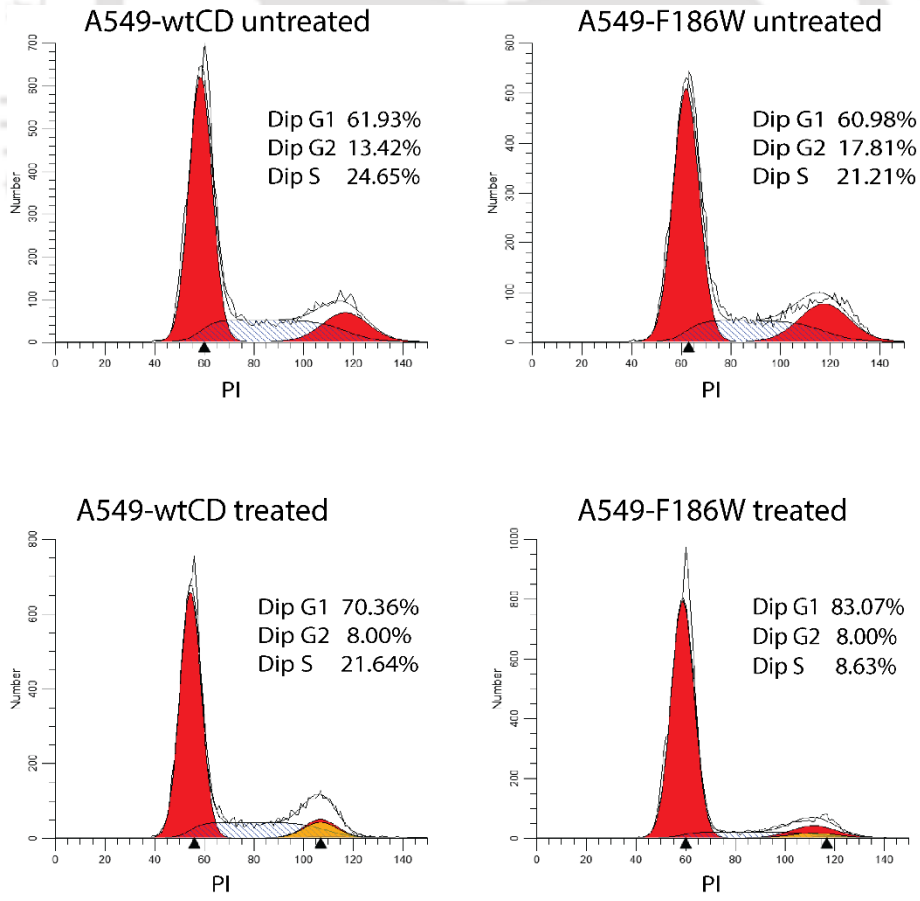

Figure 4.8. Cell cycle analysis using PI. The synchronized A549 cells were transfected and treated with 1 mM of 5-FC for 48 h.

4.3.6 Csapase 3 activity was more pronounced in F186W expressing cells than wtCD expressing cells

Caspase 3 cleavage is a crucial evidence for the progression and execution of apoptosis [25]. F186W transfected cells, when exposed to 5-FC, showed 44.87% caspase 3 activity compared to the parental cell line. On the other hand, the wtCD transfected cells depicted only 28.99% of caspase 3 activity **(Fig. 4.9)** under similar conditions. Thus, our experimental data provided a clear insight in to the mode of cell death and the comparative analysis of the activity of wtCD and F186W. Caspase 3 activity in F186W-A549 cells was increased approximately 1.5 fold as compared to wtCD-A549 cells. It was previously established that 5-FU, generated from 5-FC by CD, substantially mediates bystander effects irrespective of gap junction [26]. As F186W-A549 achieved IC50 value with much lower concentration of 5-FU, it may be inferred that bystander effect is much more prominent in mutant than wtCD-A549, while minimizing the side effects of high concentration of 5-FC [27].

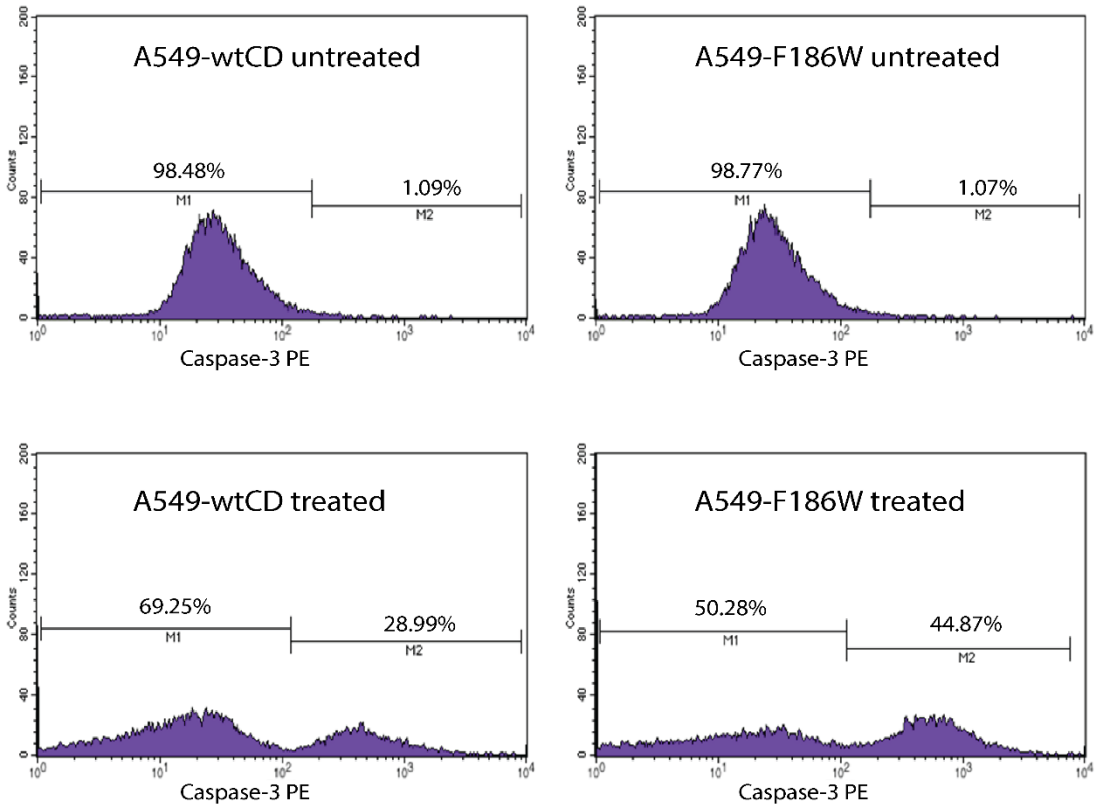

Figure 4.9. Caspase 3 assay for the progression and execution of apoptosis. Herein, the wtCD and F186W transfected A549 cells were treated with 1 mM of 5-FC for 72 h.

4.3.7 Expression of Cx43 in MCF-7 cells and co-transfection of Cx43 with wtCD/F186W gene

The pEFGP-N1-Cx43 construct was stably transfected into MCF7 cells. RT-PCR of cDNA library of Cx43-MCF7 lysate using Cx43 specific primers, amplified a gene having a size of 1.2 kb, which corresponds to the Cx43 gene **(Fig. 4.10)**. The relative expression analysis of Cx43 in MCF7 and Cx43-MCF7 cells showed the 157-fold increase in the expression of Cx43 in Cx43-MCF7 cells relative to the Cx43 expression in MCF-7. The above PCR-based analysis confirmed the transfection and expression of Cx43 gene with the formation of Cx43 mRNA. Further, wtCD or F186W gene containing pVITRO2 mammalian expression vector was then stably transfected in Cx43-MCF7 cells.

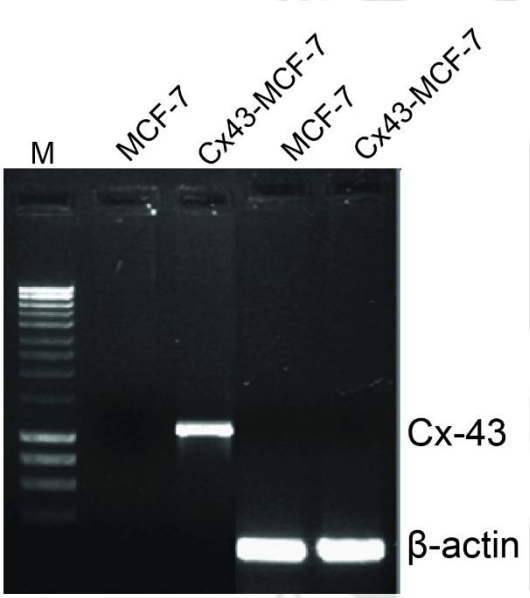

Figure 4.10. Expression level of Cx43 gene was initially examined by semi-quantitative PCR using cDNA library of MCF7 and Cx43 transfected MCF7 cells. β-actin was used as endogenous control.

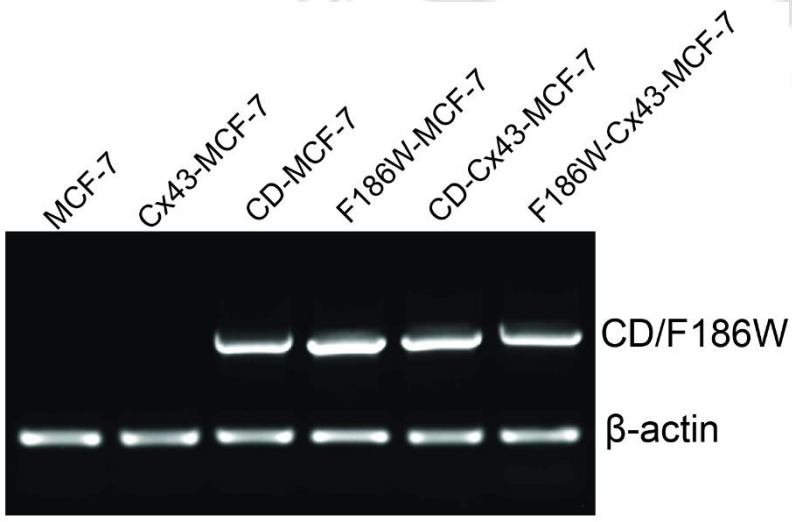

Figure 4.11. Expression level of CD and F186W gene was examined by semi-quantitative PCR after transfection. The CD/F186W gene band has been cropped and merged on top of the β-actin.

After the stable cell line was generated having both Cx43 and wtCD/F186W gene, they are screened for the mRNA expression. The transfected cell lines showed a distinct band at 1.3 kb **(Fig. 4.11)**, which coincided with the position of CD gene amplified from vector alone, while in untransfected cell line the band was absent.

4.3.7 Expression of Cx43 enhanced the suicide gene activity of wtCD/F186W gene

To probe into the effect of Cx43 expression in MCF-7 cells on the activity of CD and F186W mutant, MTT based cell viability assay was performed. Initially, the effect of the prodrug 5-FC was assessed on the MCF-7 and Cx43-MCF-7 cells and it was found that the 5-FC was having no cytotoxic effect on these cells at clinically relevant concentration **(Fig. 4.12)**.

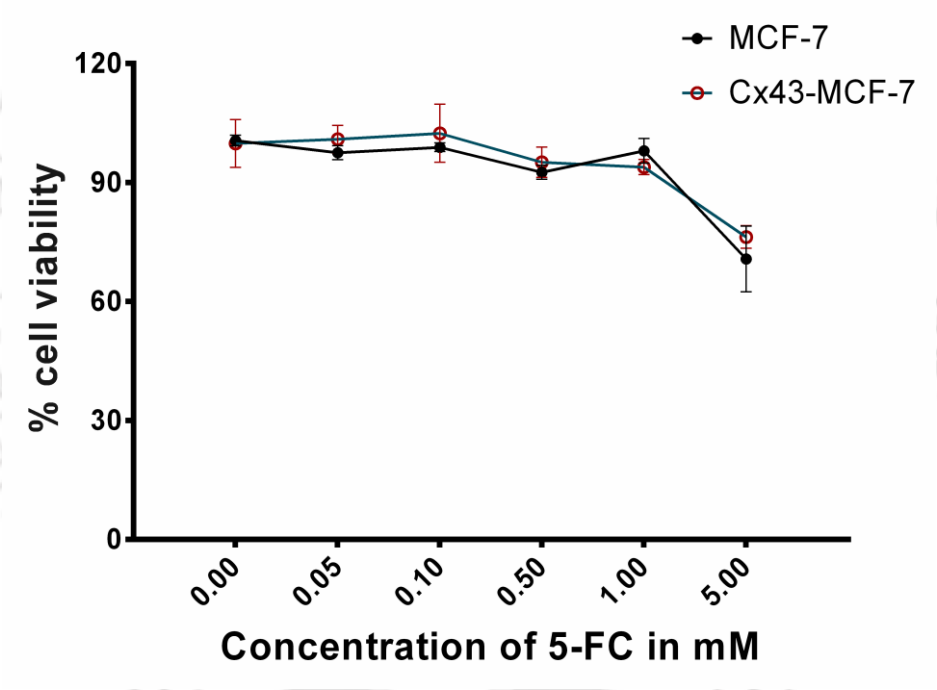

Figure 4.12. Reduction in cell viability was assessed after treating MCF-7 cells and Cx43-MCF-7 cells with different concentrations of 5-FC.

When MCF-7 and Cx43-MCF-7 cells transfected with CD gene were subjected to 5-FC treatment, a dose dependent decrease in cell viability was observed **(Fig. 4.13)**. The CD enzyme formed inside the CD gene transfected cells converted prodrug 5-FC into cytotoxic drug 5-FU resulting in the decrease in cell viability. However, the dose dependent cytotoxicity was more pronounced in the CD-Cx43-MCF-7cells when compared with CD-MCF-7 cells alone. A similar trend was observed in case of F186W mutant. The F186W-Cx43-MCF-7 mutant showed more sensitivity towards 5-FC

treatment as compared to F186W-MCF-7 cells. However, the F186W-Cx43-MCF-7 cells showed remarkable sensitivity towards 5-FC when compared with CD-Cx43-MCF-7 cells **(Fig. 4.14)**.

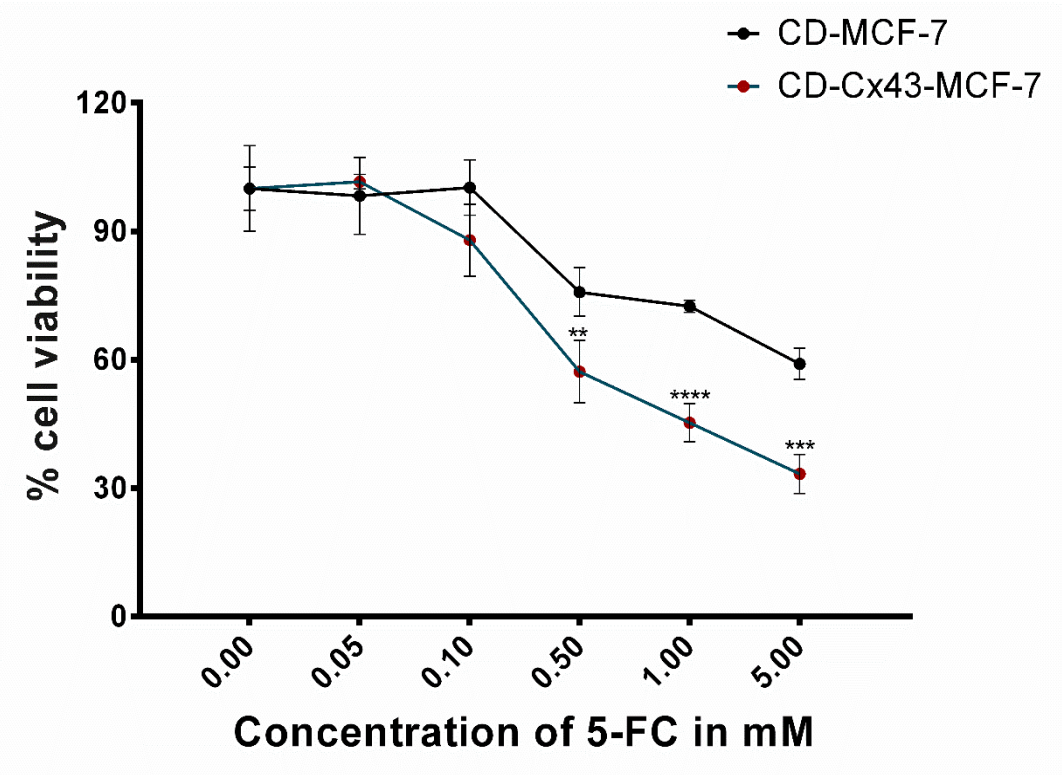

Figure 4.13. Effect of 5-FC in terms of reduction in percentage of viable cells as demonstrated by MTT assay.

In particular, the toxicity level (measured as IC_{50}) induced by 5-FC was much higher for MCF-7 transfected with CD than Cx43-MCF-7 transfected with CD. Similarly, a less dose of 5-FC was required to reach IC_{50} for F186W-Cx43-MCF-7 when compared with F186W-MCF-7. The cell viability based data showed that the Cx43 transfected MCF-7 cells respond more effectively towards the 5-FC after co-transfecting it with CD/F186W gene compared to MCF-7 cells transfected with CD/F186W. Thus, it can inferred that Cx43 expression in MCF-7 cells make it more sensitive towards suicide gene therapy.

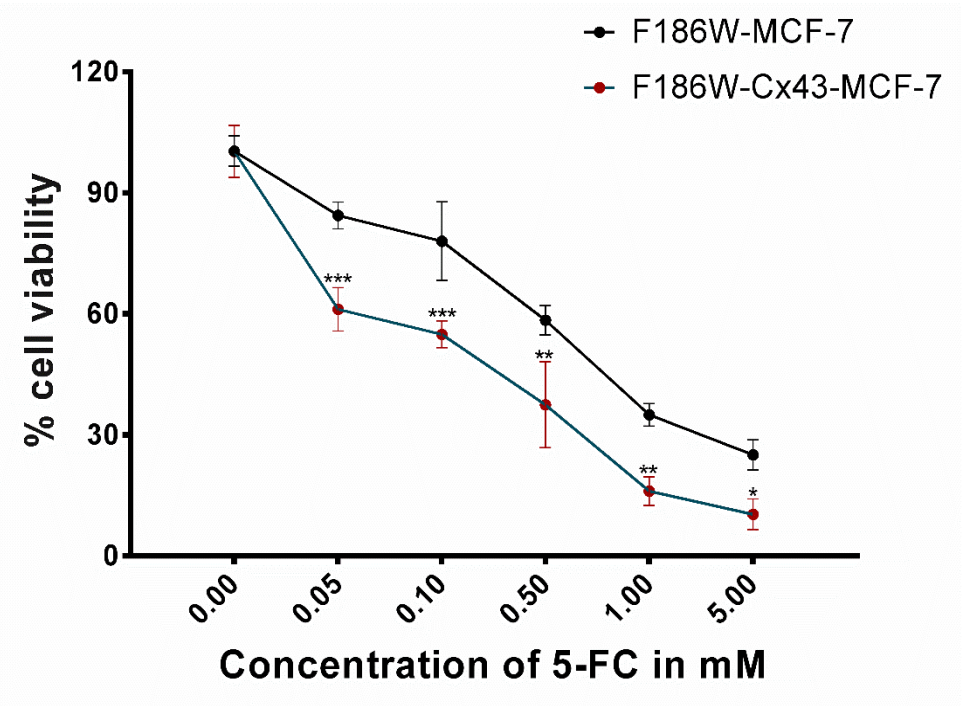

Figure 4.14. Dose dependent decrease in cell viability was observed after 5-FC treatment by MTT assay.

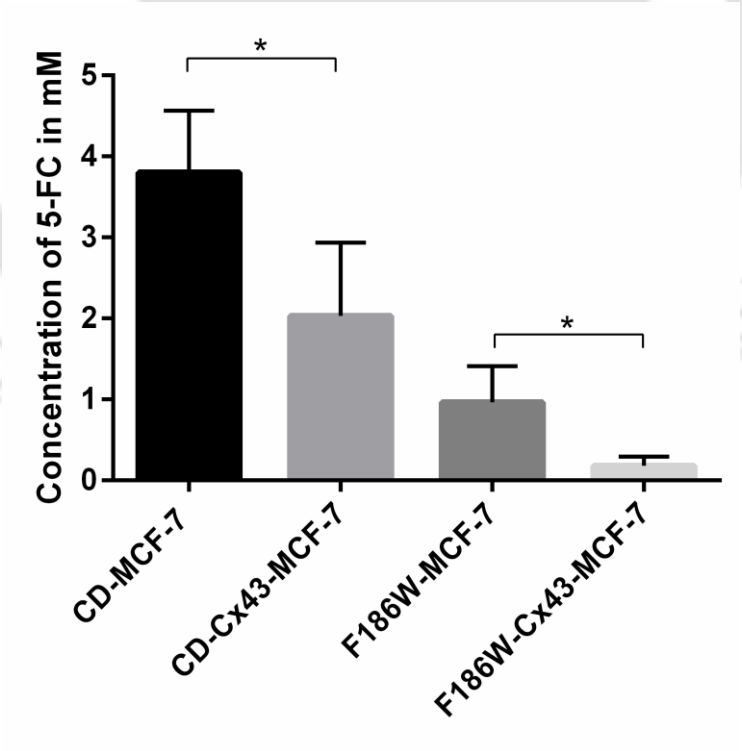

Figure 4.15. IC_{50} value of MCF-7 and Cx43-MCF-7 transfected with CD/F186W mutant was calculated using non-linear curve regression analysis and the level of significance were calculated using unpaired two tailed t-test (n = 3, p = 0.0020).

4.3.8 Expression of Cx43 enhanced the induction of apoptosis by 5-FC in co-transfected CD/F186W gene in MCF-7 cells

In order to establish that 5-FC treated co-transfected MCF-7 cells were undergoing apoptosis, two different sets of flow cytometry based experiments have been performed. First, the analysis of apoptotic nuclei was done using PI dye and second, the early apoptotic, late apoptotic and necrotic cells were differentiated using PE Annexin V and 7-AAD assay.

PI staining is a rapid, reliable and reproducible method for the separation of apoptotic cell population from the live cell population cell population from the live cell population. In our analysis, the extent of apoptosis mediated by 5-FC on CD/F186W transfected MCF7 or Cx43-MCF-7 cells were assessed. After 72 h of treatment, CD-MCF-7 showed 26.95 % of apoptotic cell population and CD-Cx43-MCF-7 cells showed 31.79 % of apoptotic cell population. Whereas, F186W-MCF-7 showed 39.05 % of apoptotic cell population and F186W-Cx43-MCF-7 cells showed 52.02 % of apoptotic cell population. **(Fig. 4.16)**.

To further validate the data generated by the PI apoptotic assay, PE Annexin V and 7-AAD flow cytometric assay **(Fig. 4.17)** was performed. After the end of the treatment duration, the cells were stained with PE Annexin V and 7-AAD. Flow cytometry data corroborated with the above finding that Cx43 enhanced the cytotoxic effect of CD and F186W. 25.58 % and 62.05 % of apoptotic cell population (early and late apoptotic combined) were found after treatment with 5-FC on CD-MCF-7 and CD-Cx43-MCF-7 cells, respectively. When F186W mutant was used in place of CD, the apoptotic population of treated F186W-MCF-7 and F186W-Cx43-MCF-7 cells was enhanced to 35.7 % and 76.07 %, respectively.

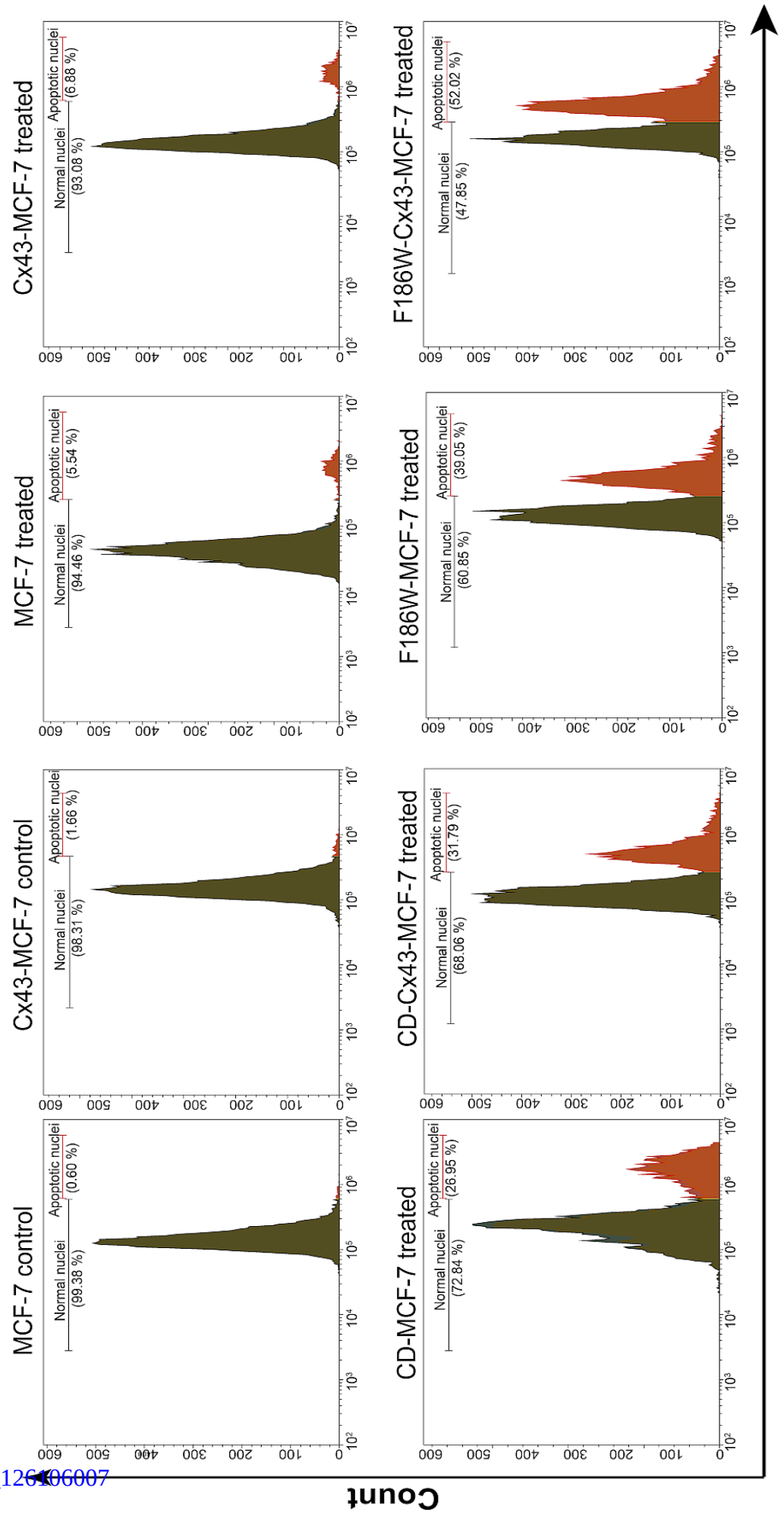

Figure 4.16. PI based apoptotic cell analysis using flow cytometer.

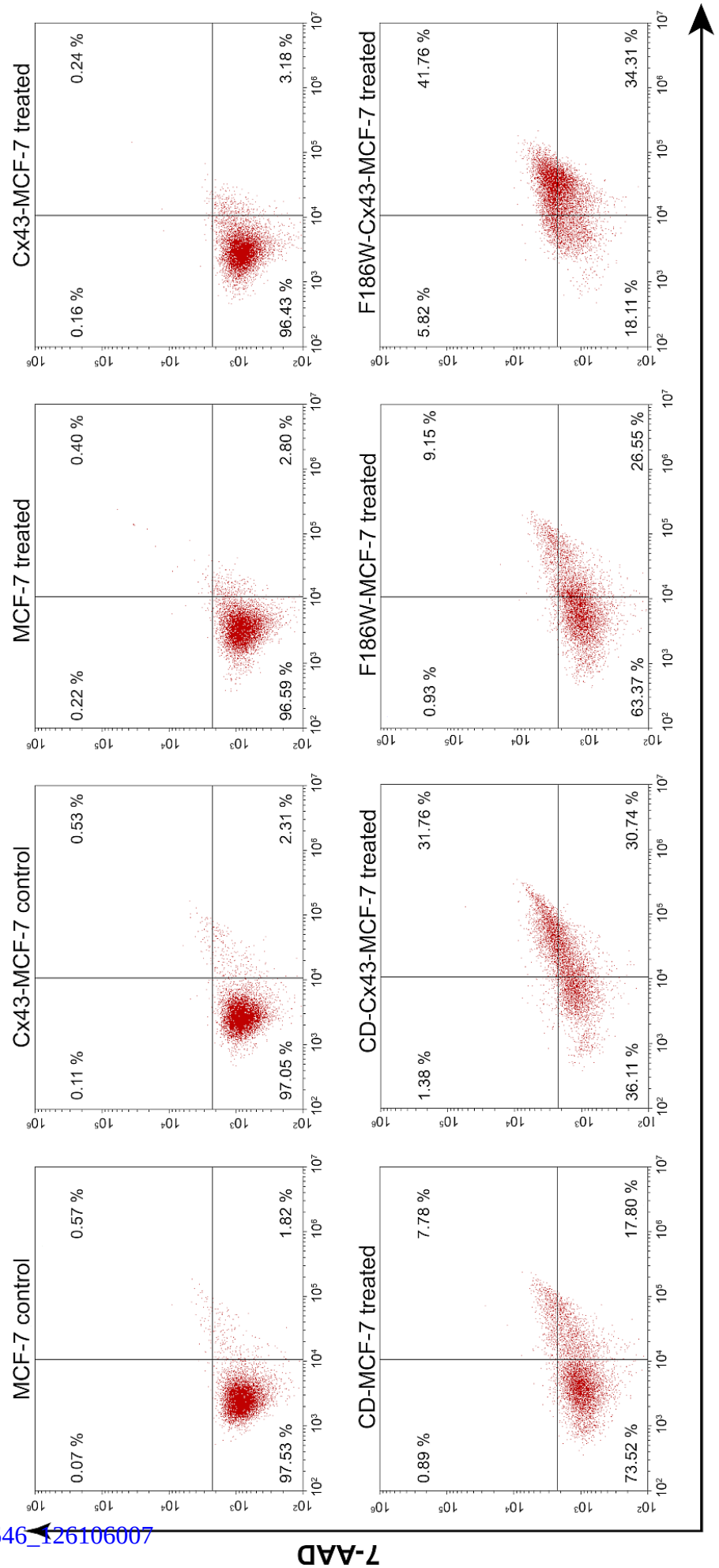

Figure 4.17. Assessment of early apoptotic, late apoptotic and necrotic cells was performed using PE Annexin V and 7-AAD based assay.

4.3.8 Expression of Cx43 induced G1 arrest after treatment with 5-FC in co-transfected CD/F186W gene in MCF-7 cells

Analysis of the DNA content of the cell population for cell cycle analysis using PI was performed. **Figure 4.18** showed the flow cytometry data analysed in ModFit LT software, revealing a considerate amount of cell population present in G1 phase of the cell cycle when treated with 5-FC, as reported earlier [24]. The CD-Cx43-MCF-7 cells when treated with 5-FC showed 79.53 % of G1 population, while for CD-MCF-7, it was just 56.37 %. Cx43 helped in the G1 arrest of the MCF-7 cell population mediated by 5-FU, which was formed from 5-FC after conversion with the help of CD enzyme. In a similar manner, F186W when co-transfected with Cx43 in MCF-7 cells, it causes substantial increase in the G1 arrest population i.e 90.11 % as compared to 74.31 % for F186W-MCF-7. Overall, F186W mutant was much more effective in arresting cell population in G1 phase relative to CD and its effectivity increased drastically when it was co-transfected with Cx43 gene.

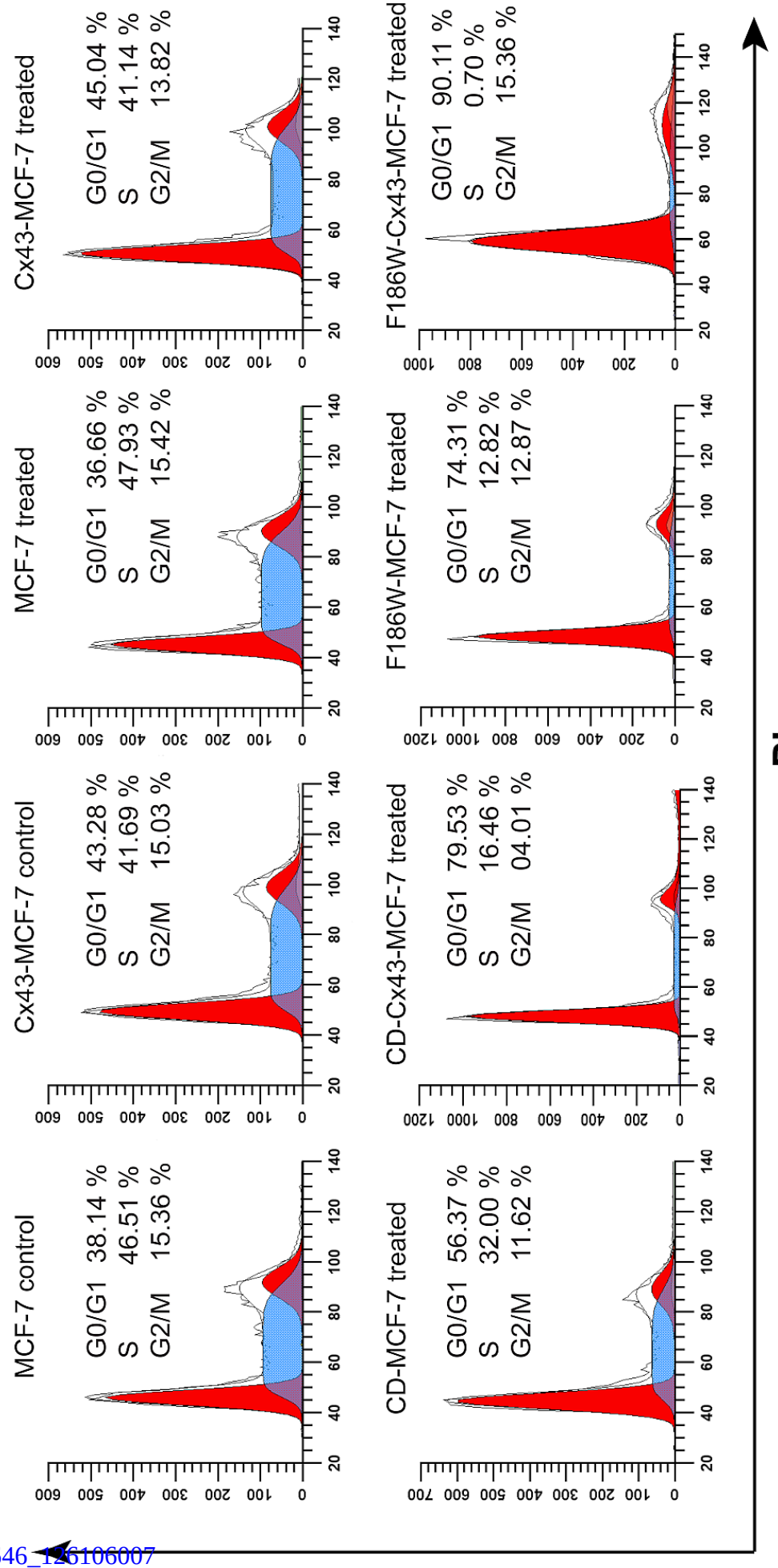

Figure 4.18. The synchronised MCF-7 cells were treated with 5-FC and after the end of the treatment duration, the phases of cell cycle were evaluated using PI dye. The data were acquired in the flow cytometer and analysed using ModFit LT software.

3.4 Conclusion

In summary, a simple transfection based experiment has established that the redesigned F186W mutant has superior therapeutic potency than the wtCD. Our experimental results suggest that the F186W is significantly more efficient in utilizing prodrug 5-FC for converting it in to toxic metabolite 5-FU when expressed in mammalian cancer cell line. As higher 5-FC drug dose leads to the systemic side effect by conversion of 5-FC into 5-FU by intestinal microflora [24], our study provides an alternate mutant, which has high affinity towards 5-FC thus, require very less dose of 5-FC to achieve IC_{50}. Our experimental analysis on computationally designed mutant F186W has established the mutant enzyme as superior candidate in cancer therapeutics. Hence, F186W mutant will be more suitable than wtCD for further gene therapy applications.

In further investigation, the potentiality of the F186W mutant was increased when it was co-transfected with the Cx43 gene. Cx43 expression led to the enhancement in the efficacy of both CD and F186W gene, however, it was more pronounced in case of mutant as the later was more effective towards 5-FC treatment. Since it was delineated in chapter 2 that the overexpression of Cx43 in MCF7 cells enhanced the sensitivity of MCF-7 cells towards chemotherapeutic drugs, the activation of underlying mechanism associated with it was also delineated. The substantial decrease in the expression of Skp2 protein, while the increased expression of both $p27^{Kip1}$ and $p21^{Cip1}$, an inhibitor of cyclin-dependent kinases, was the anti-tumour proteins responsible for increasing sensitivity of Cx43-MCF-7 cells towards drugs.

4.6 References

[1] C.J. Springer, I. Niculescu-Duvaz, Prodrug-activating systems in suicide gene therapy, J. Clin. Invest. 105(9) (2000) 1161-1167.

[2] M. Matuskova, K. Hlubinova, A. Pastorakova, L. Hunakova, V. Altanerova, C. Altaner, L. Kucerova, HSV-tk expressing mesenchymal stem cells exert bystander effect on human glioblastoma cells, Cancer Lett 290(1) (2010) 58-67.

[3] W. Li Bi, L.M. Parysek, R. Warnick, P.J. Stambrook, In Vitro Evidence That Metabolic Cooperation Is Responsible for the Bystander Effect Observed with HSV tk Retroviral Gene Therapy, Hum. Gene Ther. 4(6) (1993) 725-731.

[4] T. Asklund, I.B. Appelskog, O. Ammerpohl, I.A. Langmoen, M.S. Dilber, A. Aints, T.J. Ekström, P.M. Almqvist, Gap junction-mediated bystander effect in primary cultures of human malignant gliomas with recombinant expression of the HSVtk gene, Exp Cell Res 284(2) (2003) 183-193.

[5] M. Mesnil, C. Piccoli, G. Tiraby, K. Willecke, H. Yamasaki, Bystander killing of cancer cells by herpes simplex virus thymidine kinase gene is mediated by connexins, Proc Natl Acad Sci U S A 93(5) (1996) 1831-1835.

[6] Q.T. Trinh, E.A. Austin, D.M. Murray, V.C. Knick, B.E. Huber, Enzyme/Prodrug Gene Therapy: Comparison of Cytosine Deaminase/5-Fluorocytosine Versus Thymidine Kinase/Ganciclovir Enzyme/Prodrug Systems in a Human Colorectal Carcinoma Cell Line, Cancer Res 55(21) (1995) 4808-4812.

[7] M. Motohiro, S. Toshiya, M. Shusuke, C.G. Joseph, B. Masami, In vitro thymidine kinase/ganciclovir-based suicide gene therapy using replication defective herpes simplex virus-1 against leukemic B-cell malignancies (MCL, HCL, B-CLL), Leuk Res 27(8) (2003) 695699.

[8] C. Soubrane, R. Mouawad, O. Rixe, V. Calvez, A. Ghoumari, O. Verola, M. Weil, D. Khayat, Direct gene transfer of a plasmid carrying the Herpes Simplex Virus-thymidine kinase gene (HSV-TK) in transplanted murine melanoma: In vivo study, Eur J Cancer 32A(4) (1996) 691-695.

[9] S.-Q.Q. Lv, K.-B.B. Zhang, E.E. Zhang, F.-Y.Y. Gao, C.-L.L. Yin, C.-J.J. Huang, J.-Q.Q. He, H. Yang, Antitumour efficiency of the cytosine deaminase/5-fluorocytosine suicide gene therapy system on malignant gliomas: an in vivo study, Medical science monitor : international medical journal of experimental and clinical research 15(1) (2009) 20.

[10] C.A. Mullen, M. Kilstrup, R.M. Blaese, Transfer of the bacterial gene for cytosine deaminase to mammalian cells confers lethal sensitivity to 5-fluorocytosine: a negative selection system, Proc Natl Acad Sci U S A 89(1) (1992) 33-37.

[11] R.A. McMasters, R.L. Saylors, K.E. Jones, M.E. Hendrix, M.P. Moyer, R.R. Drake, Lack of bystander killing in herpes simplex virus thymidine kinase-transduced colon cell lines due to deficient connexin43 gap junction formation, Hum. Gene Ther. 9(15) (1998) 2253-2261.

[12] S. Kuriyama, K. Masui, T. Sakamoto, T. Nakatani, K. Tominaga, H. Fukui, K. Ikenaka, C.A. Mullen, T. Tsujii, Bacterial cytosine deaminase suicide gene transduction renders hepatocellular carcinoma sensitive to the prodrug 5-fluorocytosine, International Hepatology Communications 4(2) (1995) 72-79.

[13] C.J. Springer, I. Niculescu-Duvaz, Gene-directed enzyme prodrug therapy (GDEPT): choice of prodrugs, Adv. Drug Delivery Rev. 22(3) (1996) 351-364.

[14] F.L. Moolten, Drug sensitivity ("suicide") genes for selective cancer chemotherapy, Cancer Gene Ther 1(4) (1994) 279-287.

[15] G.C. Ireton, G. McDermott, M.E. Black, B.L. Stoddard, The structure of Escherichia coli cytosine deaminase, J. Mol. Biol. 315(4) (2002) 687-697.

[16] R.G. Crystal, E. Hirschowitz, M. Lieberman, J. Daly, E. Kazam, C. Henschke, D. Yankelevitz, N. Kemeny, R. Silverstein, A. Ohwada, T. Russi, A. Mastrangeli, A. Sanders, J. Cooke, B.-G. Harvey, Phase I Study of Direct Administration of a Replication Deficient Adenovirus Vector Containing the E. coli Cytosine Deaminase Gene to Metastatic Colon Carcinoma of the Liver in Association with the Oral Administration of the Pro-Drug 5-Fluorocytosine. The New York Hospital-Cornell Medical Center, New York, NY, Hum. Gene Ther. 8(8) (1997) 985-1001.

[17] J. Nemunaitis, C. Cunningham, N. Senzer, J. Kuhn, J. Cramm, C. Litz, R. Cavagnolo, A. Cahill, C. Clairmont, M. Sznol, Pilot trial of genetically modified, attenuated Salmonella expressing the E. coli cytosine deaminase gene in refractory cancer patients, Cancer Gene Ther 10(10) (0000) 737-744.

[18] H.S. Pandha, L.-A. Martin, A. Rigg, H.C. Hurst, G.W.H. Stamp, K. Sikora, N.R. Lemoine, Genetic Prodrug Activation Therapy for Breast Cancer: A Phase I Clinical Trial of erbB-2–Directed Suicide Gene Expression, J. Clin. Oncol. 17(7) (1999) 2180.

[19] E. Kievit, E. Bershad, E. Ng, P. Sethna, I. Dev, T.S. Lawrence, A. Rehemtulla, Superiority of Yeast over Bacterial Cytosine Deaminase for Enzyme/Prodrug Gene Therapy in Colon Cancer Xenografts, Cancer Res 59(7) (1999) 1417-1421.

[20] S.D. Mahan, G.C. Ireton, C. Knoeber, B.L. Stoddard, M.E. Black, Random mutagenesis and selection of Escherichia coli cytosine deaminase for cancer gene therapy, Protein Engineering Design and Selection 17(8) (2004) 625-633.

[21] V. Kohila, A. Jaiswal, S.S. Ghosh, Rationally designed Escherichia coli cytosine deaminase mutants with improved specificity towards the prodrug 5-fluorocytosine for potential gene therapy applications, MedChemComm 3(10) (2012) 1316-1322.

[22] M. Fuchita, A. Ardiani, L. Zhao, K. Serve, B.L. Stoddard, M.E. Black, Bacterial Cytosine Deaminase Mutants Created by Molecular Engineering Demonstrate Improved 5FC-Mediated Cell Killing In Vitro and In Vivo, Cancer Res 69(11) (2009) 4791-4799.

[23] C. Riccardi, I. Nicoletti, Analysis of apoptosis by propidium iodide staining and flow cytometry, Nat. Protoc. 1(3) (2006) 1458-1461.

[24] B.E. Harris, B.W. Manning, T. Federle, R.B. Diasio, Conversion of 5-fluorocytosine to 5-fluorouracil by human intestinal microflora, Antimicrob Agents Chemother 29(1) (1986) 44-48.

Chapter 5

Silver nanocluster based nanocarrier enhances the activity of 4-phenylbutyrate in spheroids

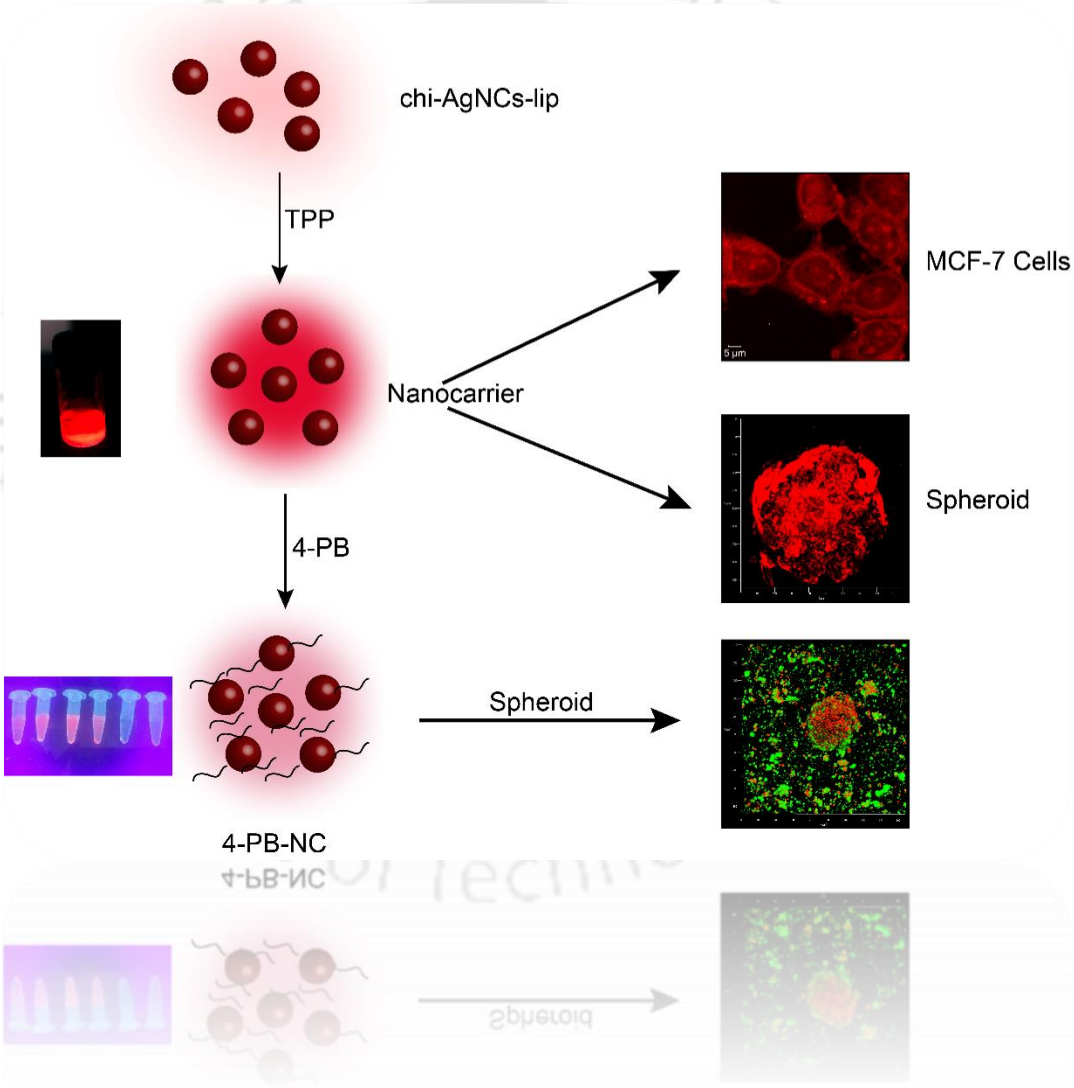

Chapter 5

Silver nanocluster based nanocarrier enhances the activity of 4-phenylbutyrate in spheroids

5.1 Introduction

Emergence of 'theranostics' provided a major breakthrough in the fields of electronics, biology and nanotechnology, which is having potential to contribute in medical diagnosis and therapy. Site specific delivery of therapeutic agents at the tumour sites while avoiding their non-specific accumulation inside the body i.e. "spatial drug delivery" is a matter of grave importance to check the amount and subsequent side effects of drugs are now under consideration[1-3]. In this aspect, nanocarriers (NCs) mediated drug delivery offers potential tool, as it exhibits high efficacy due to its small size and tunable physicochemical properties. However, the major hurdles faced by any conventional drug therapy is to access tumour site, mainly due to complex cellular organization inside the body. In such case, NPs mediated drug delivery increases its circulation in blood, half-life and bioavailability of the drugs within a therapeutic frame and consequently, avoid immediate dose and frequency escalation, thus mediating a controlled release of drug [4].

Composite NCs were synthesized by a novel method to accommodate the size and surface charge required for this study. The extraordinary photoluminescence of silver nanoclusters (AgNCs) was conveniently utilized for binding, imaging, and uptake analyses. Recently, both gold (Au) and AgNCs have attracted tremendous attention of researcher, due to cytotoxicity of Ag, AgNCs hold the extra potential of being an anti-cell proliferative agent. Ag can induce the production of ROS inside the cell at low doses and due to minimal expression of anti-oxidant enzyme in cancer cells, Ag has been established to exert maximum toxic effects to cancer cells and minimal effect to normal cells, as evidenced by its applicability in the biological system [5]. AgNCs have displayed immense potential in theranostics by virtue of their unique photophysical properties, arising due to their quantum confinement.

In this study, Ag based NCs has been used to stably deliver 4-PB in the cells and in the spheroid model. Spheroid is an artificially-created environment in which biological cells are permitted to grow or interact with their surroundings in all three dimension. 3D microenvironments with intricate cell-cell and cell-matrix interactions and complex transport dynamics for nutrients and cells. 3D spheroids more closely resemble *in vivo* tissue in terms of cellular communication and the development of extracellular matrices. Moreover, most of the cancer cells are devoid of GJIC, making it difficult for the chemotherapeutics drug to reach to the core of the tumour. 4-PB has known to increase Cx43 expression in cancer cells as discussed in chapter 3. In this study, an attempt has been made to assess the effect of 4-PB on tumour like spheroid model, Further, it has been previously reported that 4-PB suffered from few drawbacks which includes short half-life and even at the maximally tolerated dose the biologically active plasma concentrations were maintained for ~ 3.9 h. Thus, a NCs was designed using chitosan, AgNCs and lipoic acid (chi-AgNCs-lip), which helped in making it more stable, increases bioavailability, assist in delivery, minimize the drug dose and provided means for cancer cell imaging.

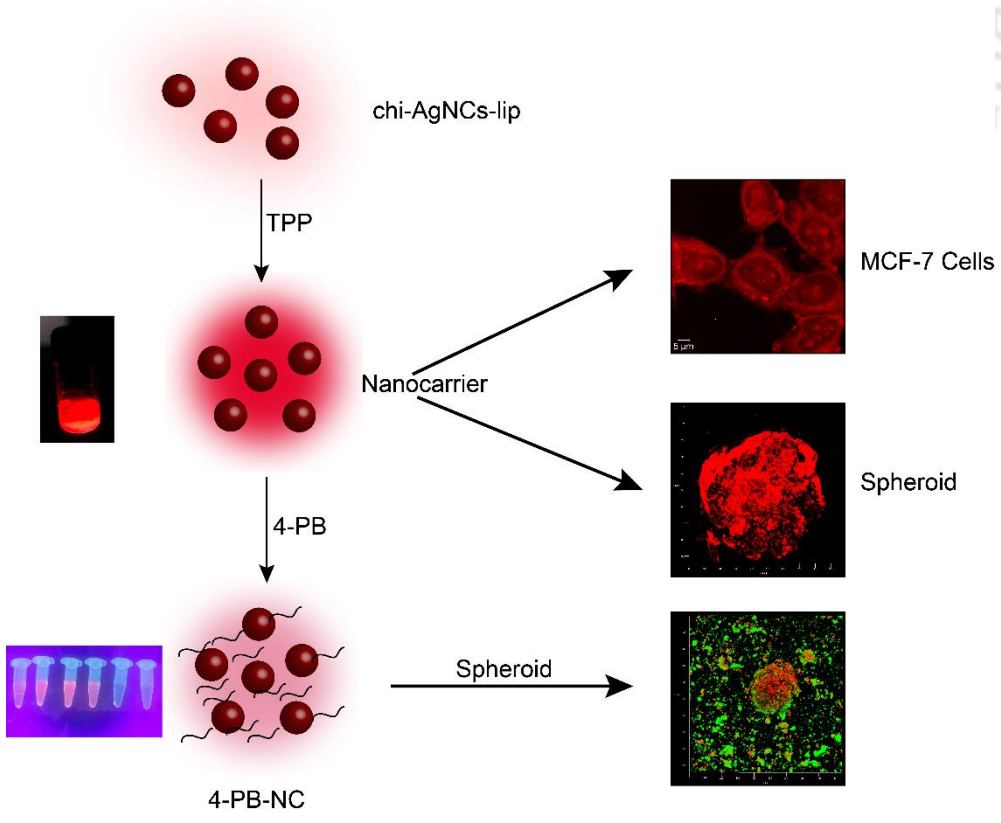

Figure 5.1. This illustration demonstrates the concept of the present study.

5.2 Materials and Methods

5.2.1 Chemicals

All items were purchased from Sigma-Aldrich, unless mentioned otherwise.

5.2.2 Synthesis of chitosan-lipoic acid-AgNCs (NCs)

The AgNCs were formulated based on previous report, with slight modifications [6]. The composite NCs was synthesised using novel synthesis methods. Briefly, 400 µl of 0.5% chitosan was dissolved in 4 ml Milli-Q water, to which 0.2 mg/ml Sodium tri-polyphosphate (TPP), 5 mg of sodium borohydride and 5.26 mg of lipoic acid were added. The solution was stirred for 45 min, by the end of which, the solution turned brown and the luminescence was observed under UV irradiation. Finally synthesized NCs were centrifuged to remove free clusters.

5.2.3 Characterization of NCs

The characterization of NCs was performed using UV-vis spectrophotometer (Perkin Elmer, Lambda 750) and fluorescence spectro-photometer (Fluoromax -4). Surface charge analyses and particle size distribution were performed by zeta potential and DLS measurements, respectively, using Malvern Zetasizer Nano ZS.

For imaging the AgNC, samples were drop-casted on carbon-coated copper grids and analysed with TEM (JEM 2100) at an accelerating voltage of 200 kV. Following formula was used to calculate quantum yield an established one-step method [7]:

$$Q = Q_R \frac{I\ OD^R\ n^2}{I^R\ OD\ n_R^2}$$

Here, Q stands for quantum yield, I denotes integrated luminescent intensity, OD connotes optical density (absorption), n is the refractive index, and R represents fluorescein, which is the reference dye used here.

5.2.4 Binding study of 4-PB with NCs

Binding of fixed amount of NCs and increasing concentrations of 4-PB was done for 1 h at 37 ºC. At the end of it, samples were centrifuged and pellet was redispersed in water. Luminescence of NPs was probed using fluorescence spectrophotometer LS55 PerkinElmer, at excitation and emission wavelengths of 425 nm and 650 nm, respectively. Binding percentage was calculated by the formula:

$$\text{Binding efficiency (\%)} = \frac{\text{Intensity}_{NCs} - \text{Intensity}_{NCs-4-PB}}{\text{Intensity}_{NCs}} \text{ X } 100$$

5.2.5 Cell culture and spheroid formation

Human breast adenocarcinoma (MCF-7) cells was procured from the National Centre for Cell Science (NCCS), Pune, India. The cells were maintained in Dulbecco's modified Eagle's medium (DMEM high glucose), supplemented with 10% fetal bovine serum (FBS), 1% penicillin/streptomycin (100 U/ml; all from Sigma-Aldrich), at 37°C in humidified air containing 5% CO2. Tumour spheroid model was generated based on the previously published report [8]. In each well, 1×10^4 MCF-7 cells were added, spun for 10 min at 400 x g and left to settle and aggregate for 96 h to form the desired tumour spheroids.

5.2.6 Assessment of cell viability by MTT assay

MCF-7 cells were seeded in 96-well plates at a density of 7,000 cells/well in DMEM medium supplemented with 10% FBS. The cells were allowed to adhere overnight. The cells were exposed to various concentrations of NCs or 4-PB-NCs or PBS (control) for 48 h. After the indicated time, the anti-cell proliferative activity was assessed by 3-(4,5-dimethylthiazol-2-yl)-2,5-diphenyltetrazolium-bromide (MTT) assay (HiMedia) [23]. Fractional cell survival at each drug concentration was calculated by measuring absorbance at 550nm (Infinite® 200 PRO, Tecan, Switzerland) and subtracting the background measurement at 650nm. Cell viability (%) was calculated relative to untreated viable cells. Each experiment was performed in triplicates and at least thrice. The proliferation of control group was set as 100%.

The cell viability of tumour spheroids were investigated by using alamar blue. Thereafter, the tumour spheroids were treated with 4-PB and 4-PB-NCs for 48 h. At

the end of treatment time, the tumour spheroids were collected, washed, and re-dispersed with the help of trypsin-EDTA. The dispersed cells then were collected and stained with Alamar blue. The cell viability was detected using plate reader (Infinite® 200 PRO, Tecan, Switzerland).

5.2.7 Trypan blue dye exclusion assay

Cells at a density of $1x10^5$ were seeded in 6-well plate. Cells were exposed to 4-PB and 4-PB-NCs for 48 h, the cells were harvested and mixed with equal volume of 0.4% trypan blue dye (Invitrogen). Cells were loaded over the counting chamber. Live and healthy cells were unstained or excluded from dye, while dead or membrane compromised cells appeared to retain the dye and appeared blue. The viable cells (%) were counted using Countess-automated cell counter (Invitrogen).

5.2.8 Calcein AM/PI Dual Staining

Morphological identification of live, apoptotic and necrotic cells present in spheroids were performed by dual staining with Calcein AM/PI (Sigma-Aldrich). Spheroids were grown for 96 h in 12-well plate. Cells were treated with 4-PB and 4-PB-NCs for 48 h. After the indicated time, the media were removed and washed with cold PBS. Fresh PBS containing 1 µM calcein AM and 5 µM PI was added to the cells and kept in the dark for 10 min. The cells were then washed thoroughly with fresh PBS and visualized under the confocal microscope (Zeiss, LSM 880).

5.2.9 Estimation of cellular uptake of NCs

To examine the uptake of luminescent AgNCs embedded NCs by the MCF-7 cells and spheroids, confocal microscope (LSM 880, Zeiss) was used. Cells were treated with NCs for 4 h, before imaging was done. Further, flow cytometric evaluation was done, for which the cells were treated with NCs for 4 h. On excitation with 488 nm laser of FACS, red luminescence of the NPs uptaken by cells was detected in the FL3 channel.

5.2.10Sstudying the mode of cell death

The different apoptotic cell populations were quantified using PE (phycoerythrin) Annexin V and 7-AAD (7-aminoactinomycin D), following treatment with 4-PB and/or NC. After treatment, cells were stained with PE Annexin V and 7-AAD, following the

manufacturer's protocol (BD Biosciences). Further, the extent of apoptosis in the cells were analysed using flow cytometer (CytoFLEX, Beckman Coulter).

5.2.11 ROS generation

For determination of reactive oxygen species (ROS) generation, the MCF-7 cells were treated separately with 4-PB, NC and NC-4-PB for 4 h. Subsequently, the cells were stained with dichlorofluorescin diacetate (DCFDA) and the data were then acquired using CytoFLEX flow cytometer (Beckman Coulter).

5.2.12 Statistical analysis

Data points were expressed as the mean ± SD (SD = standard deviation) and experiments were performed at least thrice in triplicates. To assess the statistical significance of differences, the one- and two-way analysis of variance (ANOVA) and Tukey's post hoc test were used for pairwise comparisons. Data were analysed using Prism, version 6.01 (GraphPad Software Inc., San Diego, CA, USA). Statistically significant values (p-value) for unpaired two-tailed t-test were provided in the result section while for one- and two-way analysis of variance (ANOVA) the p-value corresponds to *p< 0.05, **p< 0.01, ***p< 0.001 and ****p< 0.0001.

5.3 Results and Discussion

5.3.1 Characterization NCs

The as-synthesized NCs was synthesized in two steps; first, AgNCs were synthesized by taking chitosan and lipoic acid as template. Lipoic acid and chitosan were stirred in presence of sodium borohydride for 2 h. Addition of $AgNO_3$ completed the reaction, marked by formation of pink luminescent, brownish colour AgNC. In the second step, when TPP was added to the chi-AgNC-lip, a bright luminescent round NC was formed by assembling nanoclusters. The formation of NC was confirmed by its characteristics surface plasmon resonance peak at 650 nm when excited at 450 nm in UV-Vis spectroscopy **(Fig. 5.2a)**. The formation of silver nanoparticles was ruled out as there was minimal absorbance at 334 nm and 432 nm was observed **(Fig. 5.2b)**, which was probably due to formation of extremely small nanoparticles. The reasonably high quantum yield (9.3%) provided an intense photoluminescence to AgNC-based composites, making this composite appropriate for theranostic applications.

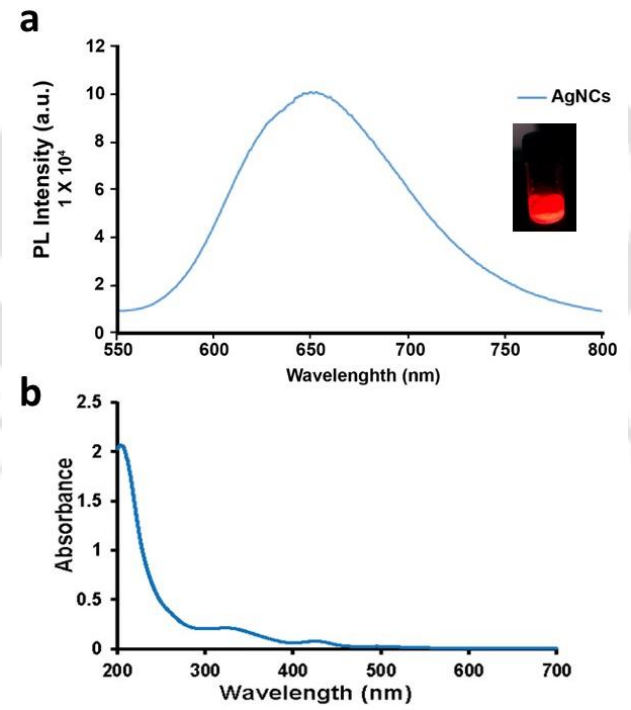

Figure 5.2. (a) Emission spectrum of chi-AgNCs-lip NC connotes red luminescence (650 nm), when excited with 450 nm wavelength of light. (B) UV-visible absorption spectrum of chi-AgNCs-lip NC. The minor peaks at 334 nm and 432 nm were possibly due to the formation of extremely small silver nanoparticles.

The formation of spherical NC was confirmed by TEM imaging **(Fig. 5.3a & b)**. DLS and TEM data showed that the size of the NC synthesised was about 210 ± 34.31 nm and after incubation with 4-PB the size was increased to 261 ± 45.26 nm **(Fig. 5.4)**. Zeta potential study showed the net surface charge on as-synthesised NC to be –3.2 mV **(Fig. 5.5)**.

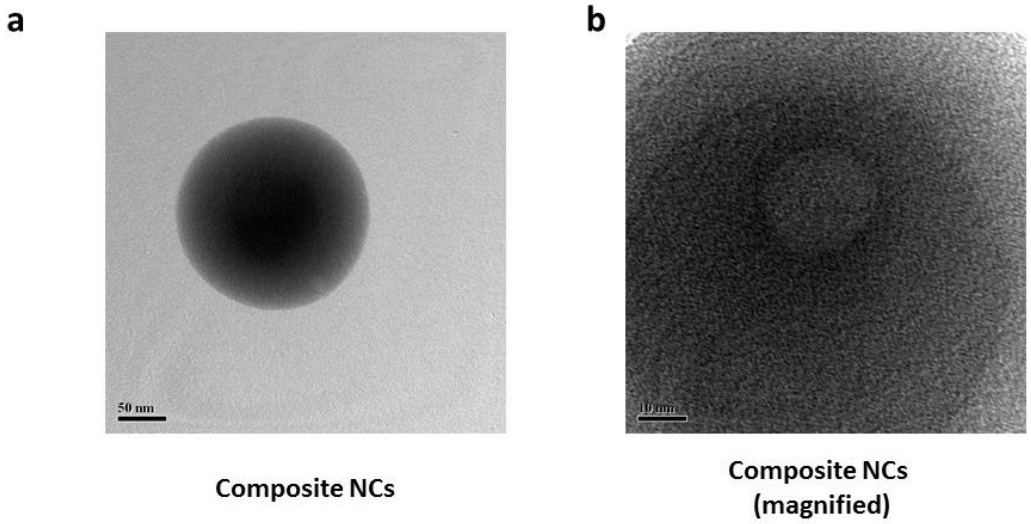

Figure 5.3. (a) TEM images prove conclusively, the formation of nearly uniform spherical NC of 210-230 nm in diameter. (b) Magnified NC, with distinct chi-AgNC-lip.

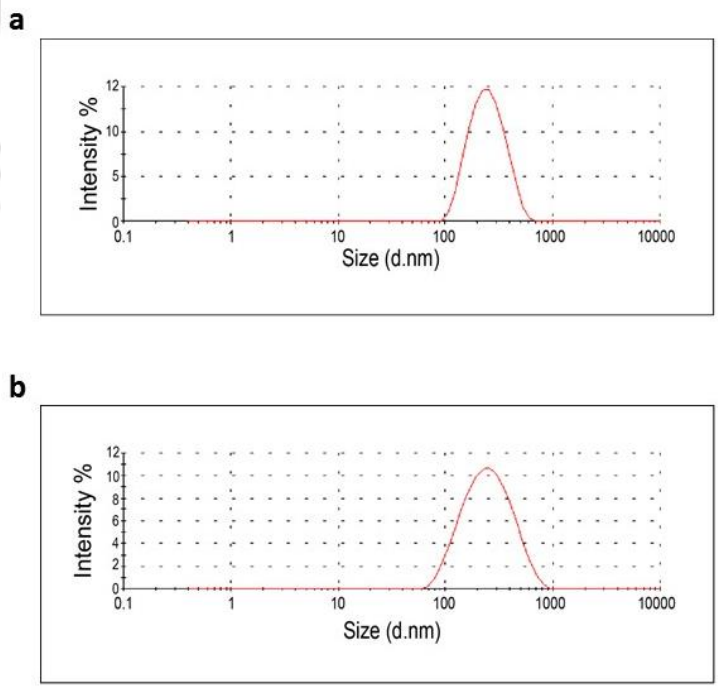

Figure 5.4. (a) DLS analysis of NC showed 210 ± 34.31 nm size and (b) 261 ± 45.26 nm size after binding with 4-PB.

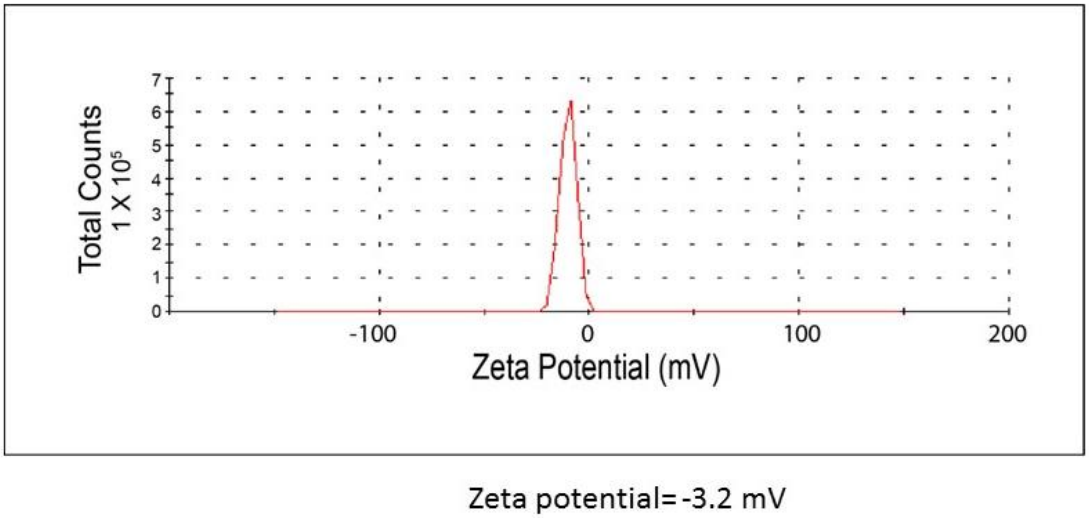

Figure 5.5. Zeta potential study of NC.

To immobilize the 4-PB on the surface of the composite NC, varying concentrations of the 4-PB were incubated with the fixed amount of NC for 1 h at 37°C, followed by centrifugation to remove the unbound NC. The NC bound 4-PB collected by centrifugation revealed that the luminescent intensity of the NC gradually decreased with the addition of 4-PB to 7mM after which it became almost saturated **(Fig. 5.6)**.

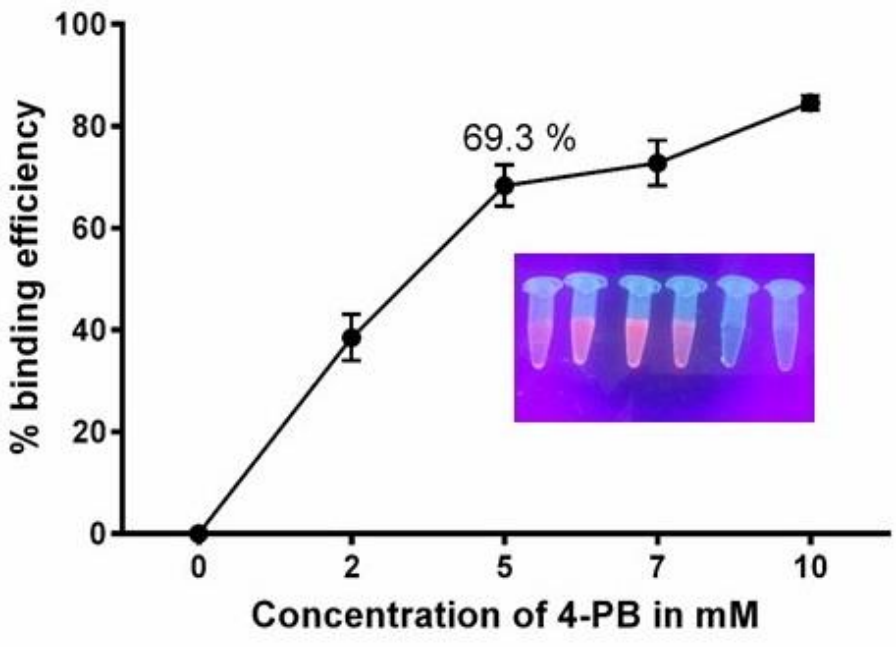

Figure 5.6. Binding efficiency of 4-PB with NC was calculated by adding varying concentration of 4-PB with fixed concentration of NC, maximum binding of 63% was obtained at 5-mM of 4-PB.

5.3.2 Therapeutic efficacy determined by cell viability assays

The 4-PB-NC was tested for its cell cytotoxicity and therapeutic efficiency on MCF-7 cells. The MTT based cell viability assay was performed to assess the increased activity of 4-PB when bound with NC **(Fig. 5.7)**. Various doses of 4-PB were used ranging from 1 mM to 10 mM in cell viability assay. The MCF-7 cells were treated with 4-PB, NC and 4-PB bound NC, here the dose of only NC was same as of required to bound 4-PB. The cell viability data clearly indicated the enhancement in the cell cytotoxicity of 4-PB when bound to NC. This might be because of additive effect of the cytotoxicity of 4-PB and NC alone. The presence of Ag in NC, rendered some amount of cell cytotoxicity.

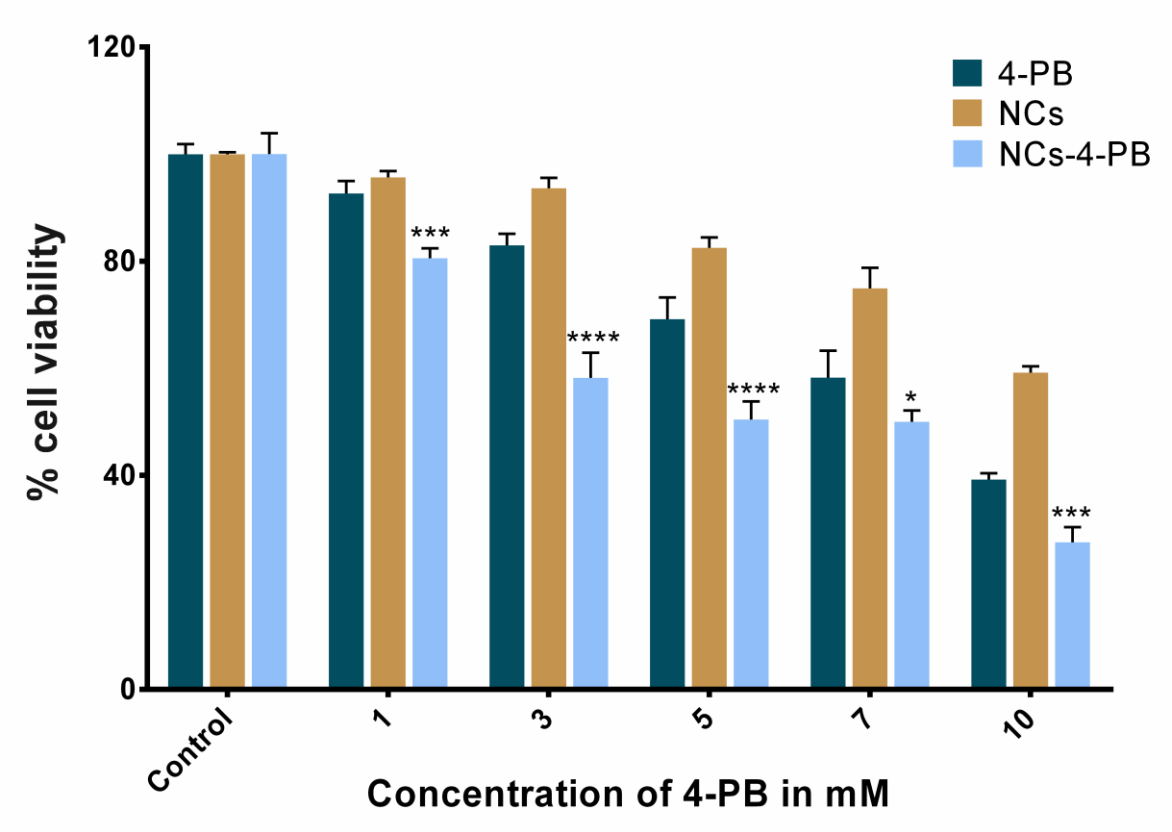

Figure 5.7. Cell viability assay (MTT assay) was performed for initial comparative analysis between 4-PB, NC and 4-PB-NC. The data showed a significant decrease in cell viability after treatment with 4-PB-NC compared to 4-PB alone. Statistically significant values were denoted by * ($p<0.05$), ** ($p<0.01$), *** ($p<0.001$) and **** ($p<0.0001$).

5.3.3 Cellular uptake of luminescent NC assessed by Confocal microscopy and Flow cytometry

AgNC embedded nanocarriers showed the cytotoxic effect due to their gradual uptake by MCF-7 cells, as divulged by simultaneous flow cytometric and confocal microscopy analysis. Images acquired using confocal microscope revealed that after 4 h of incubation the NC was almost completely uptaken **(Fig. 5. 8a)**. To find out the

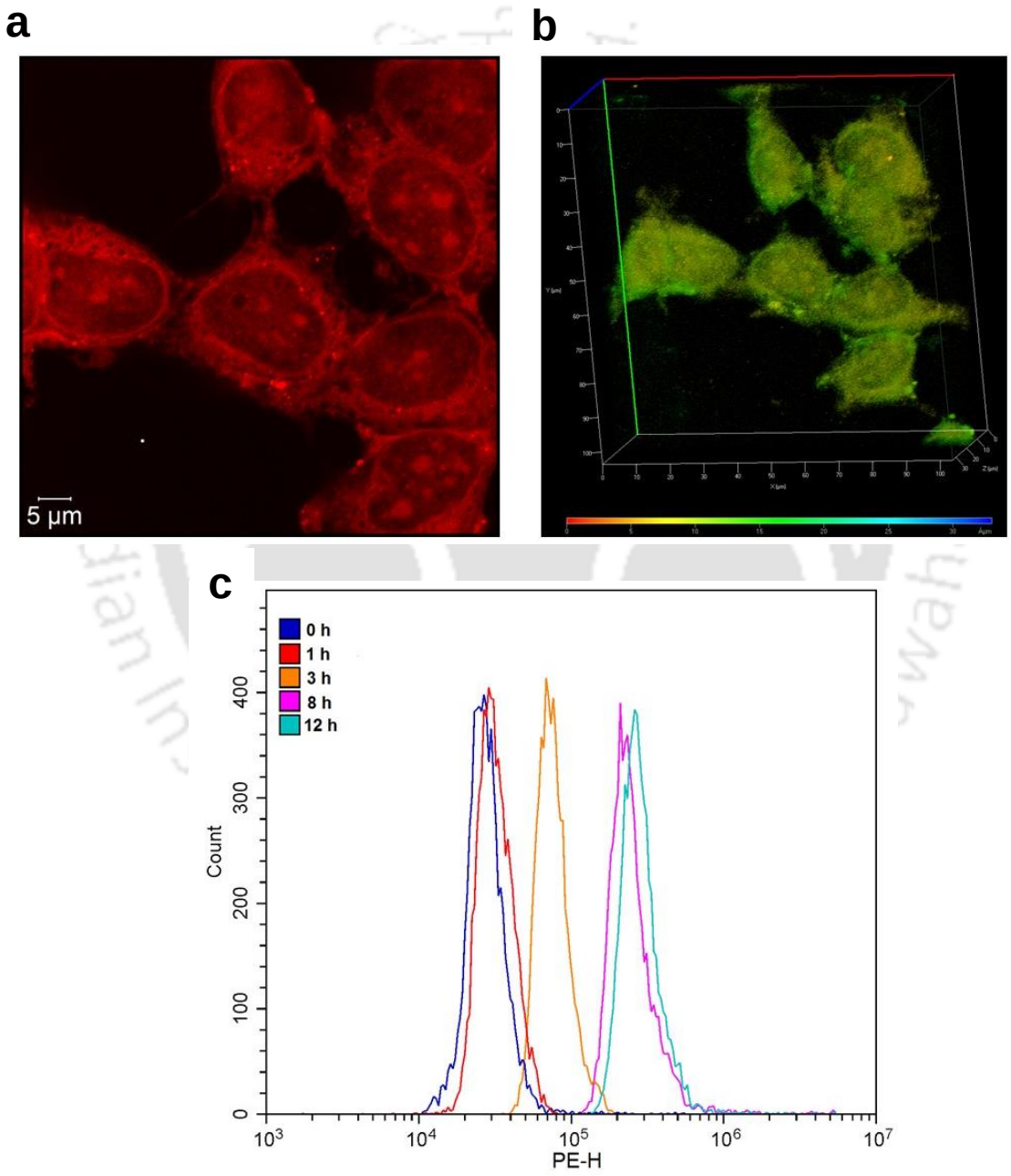

Figure 5.8. Cellular uptake of NC was analysed using (a) confocal microscope imaging, (b) z-stacking and (c) flow cytometry.

localisation of the NC, z-stacking was performed using confocal microscope **(Fig. 5.8b)**. It further showed that the NC was residing inside the cells not on the surface of the cells. The observation was concurrent with the FACS-based quantitative analysis **(Fig. 5.8c)**, which connote cellular uptake of NC over a period of several hours. Hence, the bright luminescence of these AgNCs makes them suitable for probing and imaging in biological systems.

5.3.4 Induction of apoptosis by composite

PE Annexin V and 7-AAD assay was used to differentiate the early apoptotic, late apoptotic and necrotic cells after 4-PB, NC and 4-PB-NC treatment **(Fig. 5.9)**. The percent of apoptotic population was considerably higher in NCs-4-PB treated cells (43.42 %), versus that of control (2.05 %), NCs (13.05 %) and 4-PB (25.95 %).

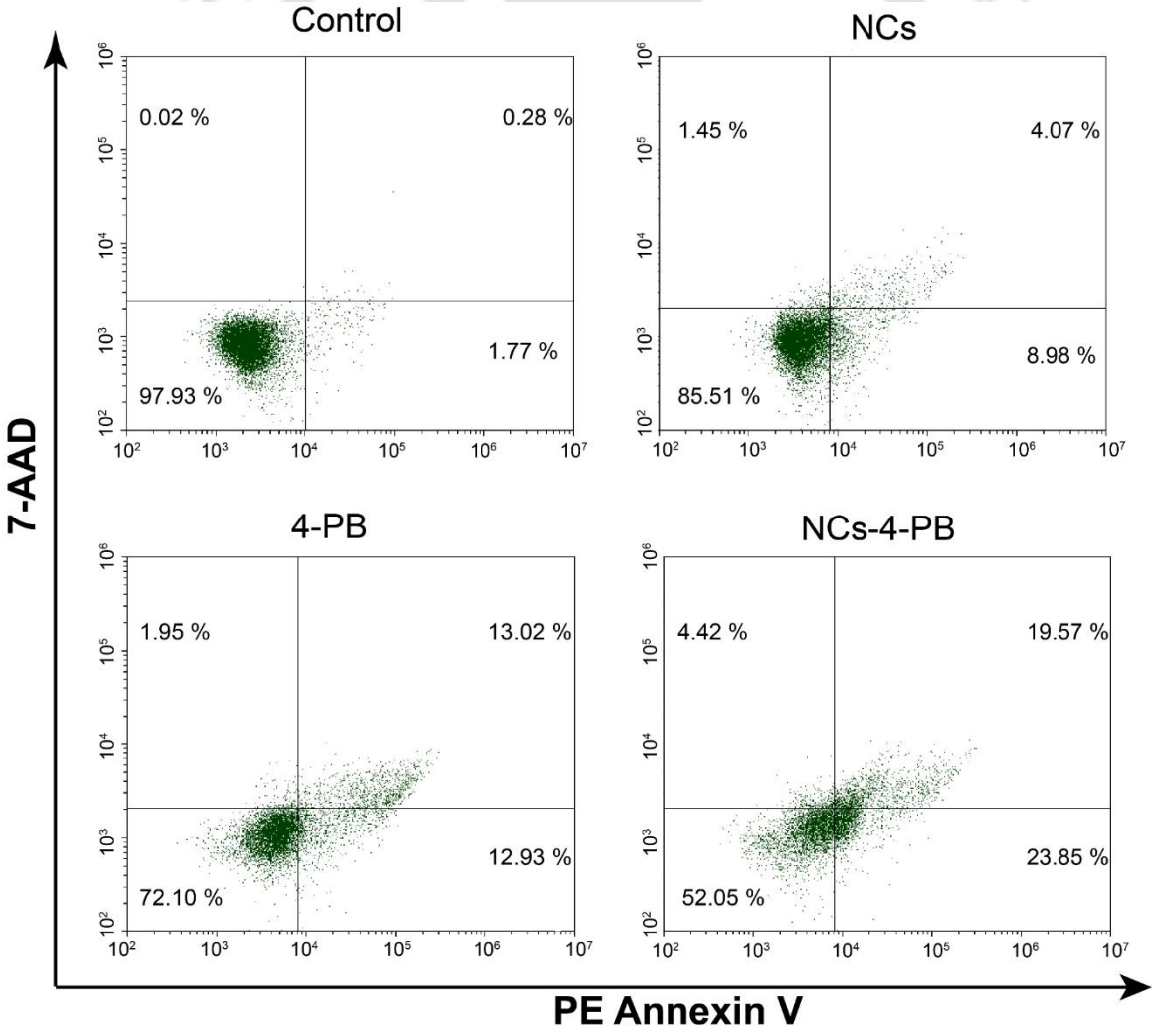

Figure 5.9. Cellular uptake of NC was analysed using (a) confocal microscope imaging, (b) z-stacking and (c) flow cytometry.

The presence of large population of apoptotic cells in NCs-4-PB treated cells as compared to 4-PB and NCs alone, provided a clear insight about the enhancement in the activity of 4-PB bound NCs. Further, it was previously known that the Ag generate ROS in the cells [9], so an investigation was made to assess ROS production after treatment. Flow cytometry based data confirmed the generation of ROS after treatment with NCs, 4-PB and NCs-4-PB **(Fig. 5.10)**. However, the accumulation of ROS was more prominent in the NCs-4-PB treated population.

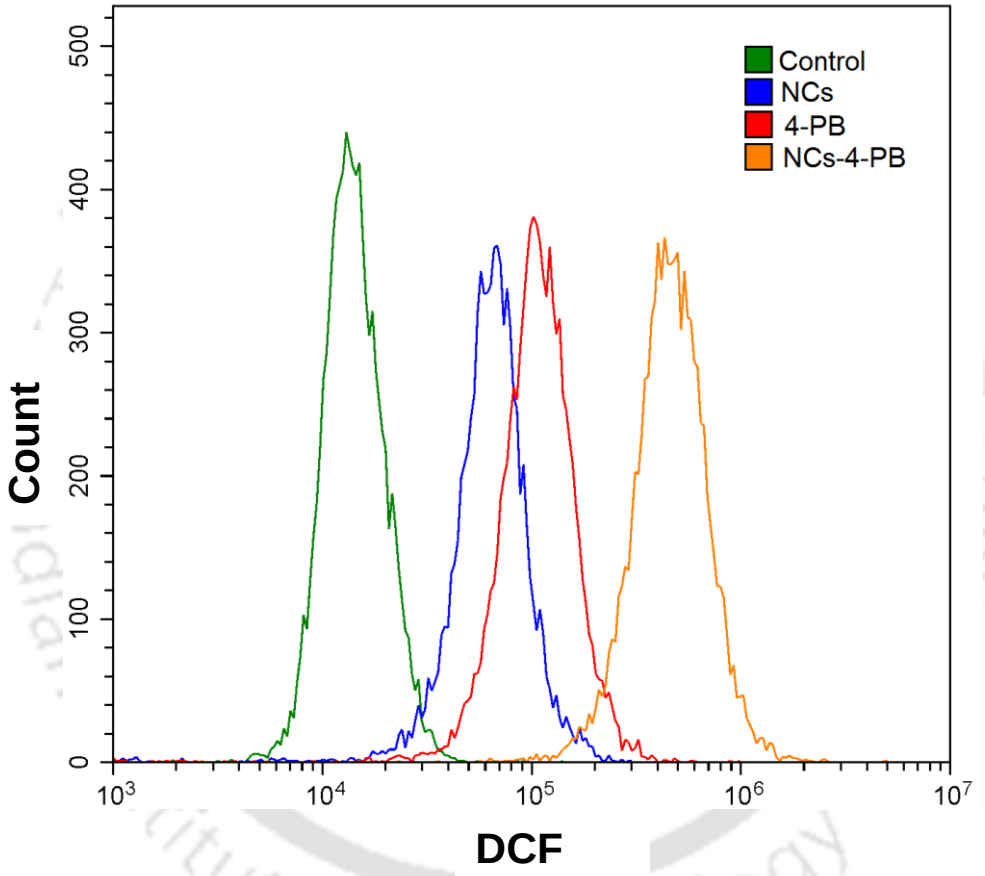

Figure 5.10. Flow cytometry based ROS production assay.

5.3.5 Assessment of the enhanced activity of NCs-4-PB on 3D spheroid model

3D spheroid provide an excellent model for various drug testing and screening. Spheroid mimics the actual tumour in terms of complexity, cell-cell interaction, hypoxia and other cellular microenvironments. Most of the cancer cells including MCF-7 cells are devoid of GJIC, thus in the tumour microenvironment the drugs cannot reach into the core of the tumour. Previously, it was reported that the 4-PB could restore Cx43 in cancer cells resulting in formation of functional GJIC.

In this study, 4-PB based NCs was used to assess the extending efficacy in MCF-7 cell based spheroid model. Initial alamar blue based cell viability revealed the potential impact of 4-PB on spheroids **(Fig. 5.11)**. A significant drop in cell viability of the spheroids was observed after treatment with NCs-4-PB compared to 4-PB and NCs alone.

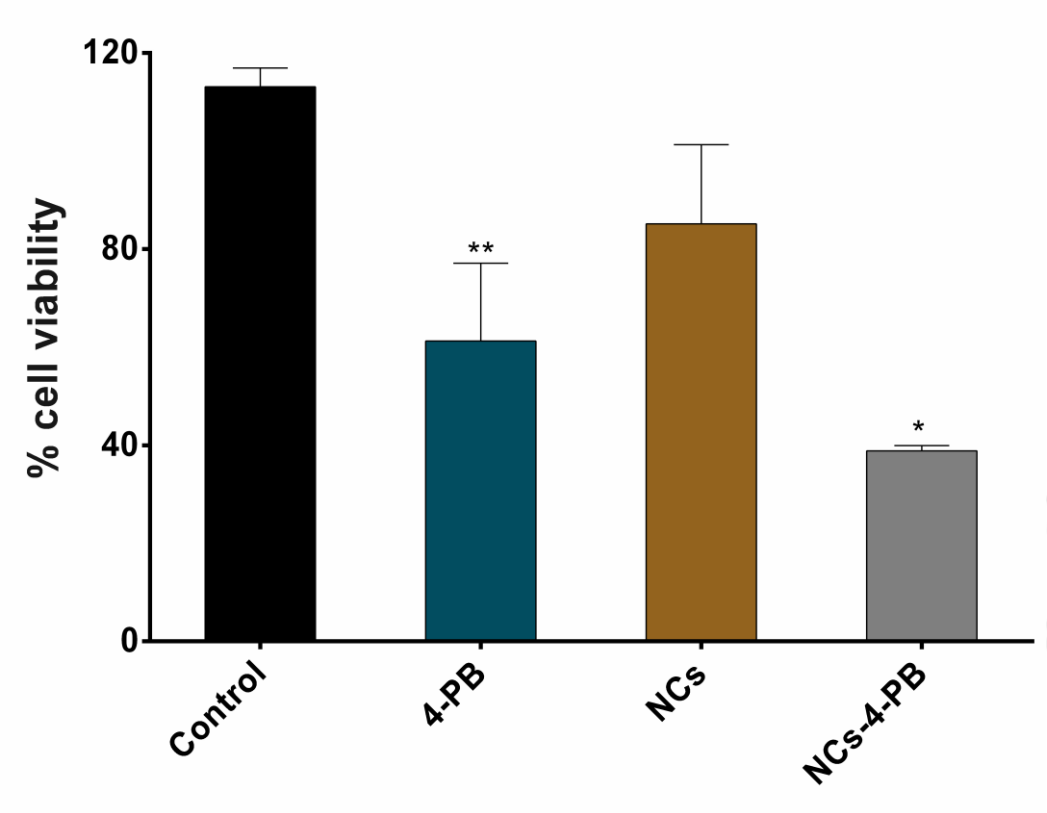

Figure 5.11. Alamar blue based cell viability assay of 4PB, NCs and NCs-4-PB treated spheroids.

The decrease in cell viability of the spheroids was due to uptake of 4-PB bound NCs. The confocal microscope image of the spheroids revealed the uptake of NCs after 4 h of incubation. The 3D image was generated after combining numerous images taken at different focal plane **(Fig. 5.12a & b)**.

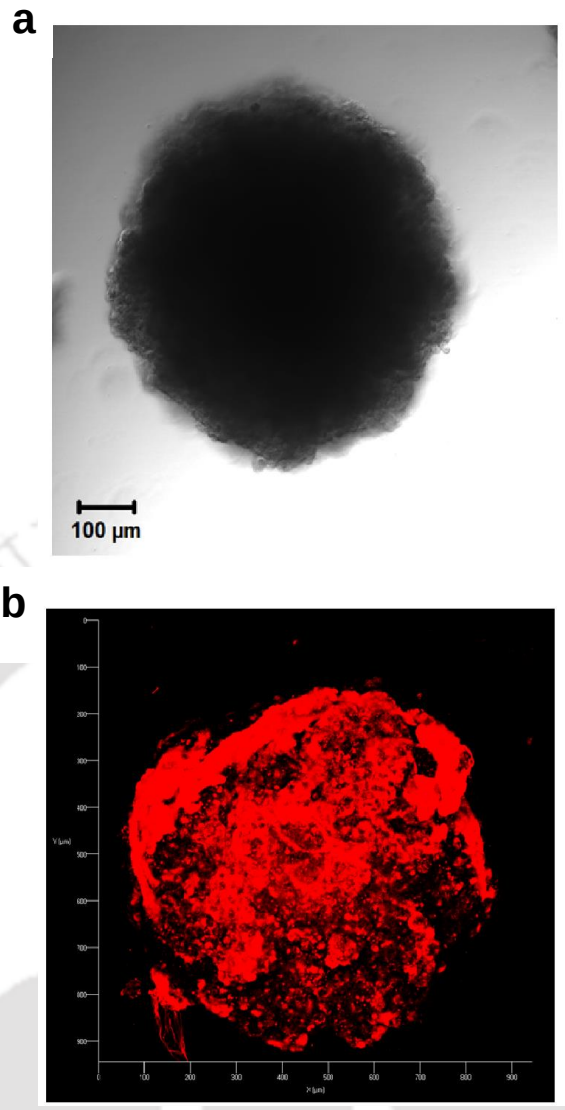

Figure 5.12. Images acquired with confocal microscope showed a phase contrast image of the spheroid (a) and the luminescence of NCs taken up by the spheroids (b).

To gain further insight into the mode of cell death, the treated cells were stained with fluorescent dyes namely calcein AM for live cell staining and DNA intercalating dye PI for membrane compromised or dead cells and observed under fluorescence confocal microscope. In **figure 5.13**, it was evident that untreated cells had uniformly stained green fluorescence indicating healthy viable cells. When 4-PB and NCs treated cells were labelled, it showed green, orange and red nuclei implying the presence of live, early and late apoptotic cells. However, by analyzing the cell population microscopically, it could be inferred that the NCs-4-PB treated cells in spheroid had much more apoptotic cells than 4-PB or NCs treated spheroid. Thus, calcein AM/PI staining results illustrated possible induction of apoptosis was more in NCs-4-PB treated spheroids.

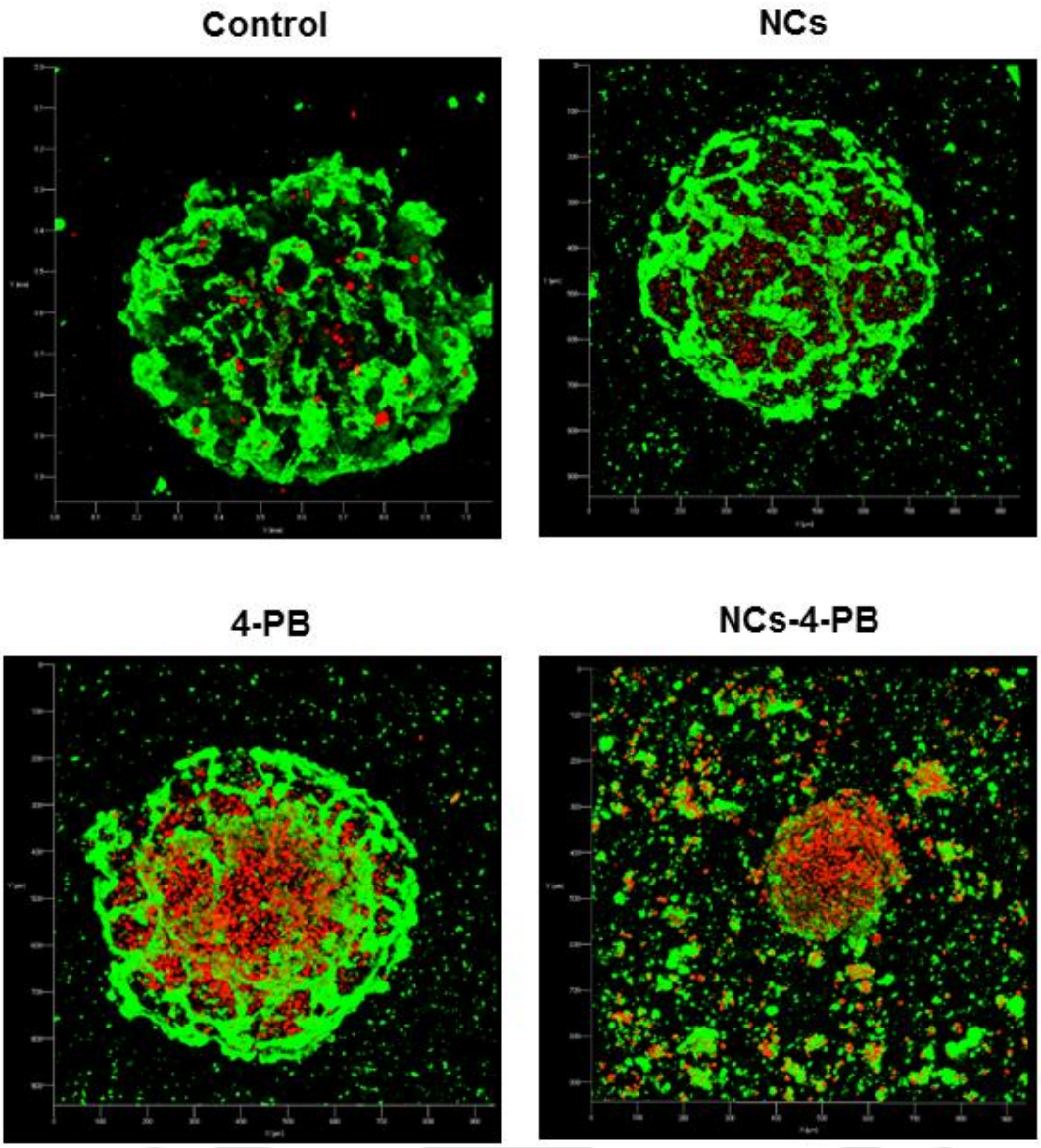

Figure 5.13. Calcein AM and PI based dual staining revealed the morphological evidence of the cell viability. Calcein AM stain live cells while PI stain dead cells.

5.4 Conclusion

In summary, the fabrication of a versatile novel 4-PB bound composite nanocarrier has been demonstrated. In this approach, AgNC embedded chitosan nanocarrier were utilized for analysis of binding, tracking, and sustained release of 4-PB from the nanocarrier. Inferences were drawn based on luminescence detection using fluorescence spectrometry, flow cytometry, and high-end confocal microscopy. The stability imparted by the nanocarrier to the 4-PB resulted in enhanced anti-tumour efficacy. Most importantly, this method implied improved cancer therapy without dose-dependent side effects of the drug, as the AgNC ensured the stability of the 4-PB in cancer cells. The efficacy of the 4-PB bound nanocarrier was also evaluated in spheroids based model. Time-dependent uptake of luminescent silver clusters was demonstrated by confocal microscopy and flow cytometry. The expression of Cx43 and establishment of GJIC (refer to chapter 3) enabled the NCs-4-PB to reach to the core of the spheroids to exhibit dispersive effect.

5.5 References

[1] T. Lammers, F. Kiessling, W.E. Hennink, G. Storm, Drug targeting to tumours: principles, pitfalls and (pre-) clinical progress, J Control Release 161(2) (2012) 175-187.

[2] Y.H. Bae, K. Park, Targeted drug delivery to tumours: myths, reality and possibility, J Control Release 153(3) (2011) 198.

[3] F. Danhier, E. Ansorena, J.M. Silva, R. Coco, A. Le Breton, V. Préat, PLGA-based nanoparticles: an overview of biomedical applications, J Control Release 161(2) (2012) 505-522.

[4] N. Vij, T. Min, R. Marasigan, C.N. Belcher, S. Mazur, H. Ding, K.-T. Yong, I. Roy, Development of PEGylated PLGA nanoparticle for controlled and sustained drug delivery in cystic fibrosis, J Nanobiotechnol 8(1) (2010) 22.

[5] H. Jiang, G. Xu, Y. Sun, W. Zheng, X. Zhu, B. Wang, X. Zhang, G. Wang, A "turn-on" silver nanocluster based fluorescent sensor for folate receptor detection and cancer cell imaging under visual analysis, Chem. Commun. 51(59) (2015) 11810-11813.

[6] B. Adhikari, A. Banerjee, Facile synthesis of water-soluble fluorescent silver nanoclusters and HgII sensing, Chem. Mater. 22(15) (2010) 4364-4371.

[7] F. Teale, Principles of Fluorescence Spectroscopy-Lakowicz, Jr, MACMILLAN MAGAZINES LTD PORTERS SOUTH, 4 CRINAN ST, LONDON, ENGLAND N1 9XW, 1984.

[8] J. Friedrich, C. Seidel, R. Ebner, L.A. Kunz-Schughart, Spheroid-based drug screen: considerations and practical approach, Nat. Protoc. 4(3) (2009) 309-324.

[9] C. Marambio-Jones, E.M. Hoek, A review of the antibacterial effects of silver nanomaterials and potential implications for human health and the environment, Journal of Nanoparticle Research 12(5) (2010) 1531-1551.

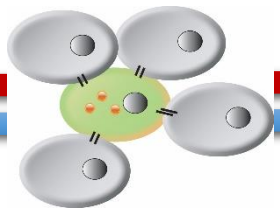

Conclusion and Future Outlook

Conclusion and Future Outlook

6.1 Summary of the present work

A final conclusion and future aspects of this thesis has been discussed in this section. The significance of this study, highlights of the work done as well as the aspect of the possible clinical implications of this research work have been explored herein.

The essence of overall thesis is the utilization of GJIC and the responsible Cx43 protein for therapeutic implications in cancer therapy. The expression of Cx43 and establishment of functional GJIC was achieved via two means; gene therapy as well as using HDACi. Cx43 gene was cloned from ACHN cell line into pEGFP-N1 mammalian expression vector, which further transfected into GJIC devoid MCF-7 cells. The expression of Cx43 in MCF-7 cells established a functional GJIC and showed its potency via GJ dependent as well as independent pathways. The first combination therapy was designed involving Cx43 gene therapy with plant based anti-malarial semi-synthetic drug, ART. Cx43 enhanced the activity of ART by regulating several anti-tumour proteins (GJ independent) and through establishment of functional GJIC, which further mediates the transfer of ROS and other stress signal generated by ART to neighbouring untreated cells (bystander effect). Through a well-orchestrated interplay between GJ dependent as well as GJ independent action of Cx43, a new perspective of the effective ART treatment was discovered in conjunction with Cx43 overexpression in MCF7 cells.

In the second approach, 4-PB, an HDACi, induced expression of Cx43 in MCF-7 cells, which was independent of gene therapy. The synergistic interaction of 4-PB with ART was studied extensively in *in vitro* as well as *in vivo* mice model. 4-PB attenuates the expression of DNA damage repair proteins, thus amplifying the DNA damage effect initiated by ROS production due to ART treatment. The outcome of this study could provide information about the potentiality of these two drug combinations as an effective and less toxic treatment for cancer. This study have presented a novel combination of the drugs, which are already in use for the treatment of other diseases, as probable anti-

cancer therapy. This drug combination holds an immense potential for further testing in the clinical trials.

Further, the Cx43 gene therapy system was combined with the CD mediated suicide gene therapy in which CD enzyme converts the prodrug, 5-FC into toxic metabolite, 5-FU. The previously redesigned CD mutant named F186W was screened for its heightened specificity, activity and efficacy in A549 cells. The results demonstrated that this mutant significantly enhanced the therapeutic efficacy of CD/5-FC mediated suicide gene therapy on A549 cells and has the potential to emerge as a substitute to wild type CD. Further, a co-transfected system was designed in which MCF-7 cells were stably transfected with both Cx43 as well as CD/F186W mutant. The expression of Cx43 protein in conjunction with the CD/F186W gene enhanced the activity of the suicide gene therapy mediated by CD and F186W mutant.

To enhanced the cytotoxic activity of 4-PB, an AgNCs based nanocarrier was synthesised and screened on MCF-7 cell based 3D spheroid model. Taking chitosan and lipoic acid as a base, Ag based nanoclusters was synthesized. Further, these AgNCs was converted into nanocarrier by adding TPP in the medium. 4-PB electrostatically attached with the NC, which further uptaken by the MCF-7 cells as well as by spheroids. Inducible expression of Cx43 and formation of GJIC in MCF-7 cells, thus in spheroids, led to the penetration of AgNC-4-PB into the core of the spheroids to exhibit dispersive effect. NC bound 4-PB showed significant enhancement in the cytotoxicity compared to 4-PB and NC alone. Binding with noble metal nanocarrier enhanced the efficacy of the 4-PB and enabled luminescence based binding, imaging, and uptake studies. The current novel theranostics approach holds immense potential in the field of *in vivo* cancer therapeutics.

This thesis emphasizes on the anti-cancer potential of the Cx43 protein in clinical translation, alone and in combination therapy. Future prospects include the study of the efficacy of this system in *in vivo* and clinical samples. Targeting the Cx43 signal cascade with the other potential anti-tumour proteins may serve to combat cancer if exploited clinically.

6.2 Future Outlook

- Mechanism behind the downregulation of Cx43 proteins in cancer cells need to be investigated
- Delineating the signalling cascade involved in downregulation of DDR proteins by 4-PB
- Recombinant F186W mutant protein purification and delivery into the cancer cells using nanocarrier
- Many cancer cells fail to form functional gap junctions with normal cells. The responsible pathway can be investigated. An approach can be made to overcome these barriers
- Major differences in the ability of different connexin family members to modify growth control can be studied

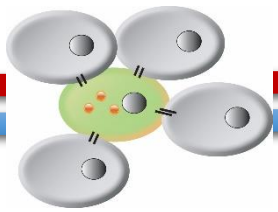

Appendix

Buffer Compositions

Buffers	Composition
4X protein loading dye (for 10 mL)	2.0 ml 1 M Tris-HCl (pH 6.8), 0.8 g SDS, 4.0 ml 100% glycerol, 0.4 ml 14.7 M β-mercaptoethanol, 8 mg bromophenol blue in water
6X DNA loading dye	0.25 (%)(w/v) bromophenol blue, 0.25% (w/v) xylene cyanol FF, 30% (v/v) glycerol in water
Alkaline lysis solution for plasmid isolation I	50 mM glucose, 25 mM Tris-Cl (pH-8.0), EDTA (10 mM)
Alkaline lysis solution II	0.2 N NaOH, (freshly diluted from 10 N stock), 1% (w/v) SDS
Alkaline lysis solution III	5 M potassium acetate (60 mL), glacial acetic acid (11.5 mL), water (28.5 mL)
Cleaning buffer 1 for column regeneration (pH-8.5)	0.1 M boric acid, 0.5 M NaCl, adjust the pH 8.5 with sodium hydroxide
Cleaning buffer 2 for column regeneration (pH-4.5)	0.1 M sodium acetate, 0.5 M NaCl, adjust the pH 4.5 with acetic acid
Lysis buffer for protein purification	10 mM PBS (pH-7.4), 1 mM EDTA, 1 mM PMSF, 0.32% N-lauroylsarcosine
Protein elution buffer	50 mM Tris, pH 9.5 and 15 mM L-reduced glutathione
Blocking buffer	3%-5% (w/v) BSA in PBST/TBST
Phosphate buffered saline	137 mM NaCl, 2.68 mM KCl, 7.98 mM Na_2HPO_4, 1.4 mM KH_2PO_4, pH-7.4
Polyacrylamide solution (30%)	29.2% (w/w) acrylamide, 0.8% (w/w) N,N'-methylenebisacrylamide
Tris Buffered Saline Tween-20	Tris-HCl (50 mM), NaCl (150 mM), Tween-20 (0.1% v/v) pH-7.5
Tris-acetate EDTA (TAE) 50X (100 mL)	24.2 g Tris base, 5.71 mL of glacial acetic acid, 10 mL of 0.5 M EDTA (pH-8.0)
Tris-EDTA	10 mM Tris-HCl (pH-8.0), 1 mM Na_2EDTA
TSS buffer for transformation	10% (w/v) PEG 8000, 0.6% (w/v) $MgCl_2.6H_2O$, 5% (v/v) DMSO in LB

List of Publications

1. **Asif Raza**, V. Kohila, Siddhartha Sankar Ghosh (2015), Redesigned *E.coli* cytosine deaminase: a new facet of suicide gene therapy, ***The Journal of Gene Medicine*** DOI: 10.1002/jgm.283 [Wiley publishing group]

   Featured in news article: NewsRX, Cancer Gene Therapy Week, Aug 24 2015

2. **Asif Raza**, Archita Ghoshal, S Chockalingam and Siddhartha Sankar Ghosh (2017). Connexin-43 enhances tumor suppressing activity of artesunate via gap junction-dependent as well as independent pathways in human breast cancer cells, **Scientific Reports** DOI: 10.1038/s41598-017-08058-y (Nature Publishing Group)
3. **Asif Raza**, Raghuram Kandimalla, Sanjeeb Kalita, Siddhartha Sankar Ghosh (2017). 4-phenylbutyrate Manifestate Synergistic Interaction with Artesunate by Suppressing DNA Repair Activity, *Manuscript Communicated*
4. **Asif Raza** and Siddhartha Sankar Ghosh (2017). Expression of Connexin 43 potentiated the cytosine deaminase mutant activity in MCF-7 cells (2017), *Manuscript Communicated*
5. **Asif Raza,** Upashi Goswami, Rajib Shome and Siddhartha Sankar Ghosh (2017). Silver nanocluster based nanocarrier enhances the activity of 4-phenylbutyrate synergistically, *Manuscript Under Preparation*

Collaborative Work:

6. Archita Ghoshal, Upashi Goswami, **Asif Raza**, Arun Chattopadhyay, and Siddhartha Sankar Ghosh (2016). Recombinant sFRP4 bound Chitosan-Alginate Composite Nanoparticles Embedded with Silver Nanoclusters for Wnt/ β-catenin targeting in Cancer Theranostics, RSC Advances, Vol 6, 85763 - 85772.
7. Upashi Goswami, Anushree Dutta, **Asif Raza**, Raghuram Kandimalla, Sanjeeb Kalita, Siddhartha Sankar Ghosh and Arun Chattopadhyay (2017). Transferrin-Copper Nanocluster-Doxorubicin Nanoparticles as Theranostic Cancer Nanodrug for Bioimaging through FRET, Targeted delivery and Therapy, Manuscript Communicated

8. Gudala Satish, Archi Sharma, Srinivasarao Ambati, **Asif Raza**, Janapala Venkateswara Rao and Santhosh Penta (2017). Design and efficient one pot synthesis of novel tumour targeted pyrimidinyl-thiazole derivatives from Dabrafenib moiety, Manuscript Communicated
9. Bandhan Chatterjee, **Asif Raza**, Arun Chattopadhyay and Siddhartha Sankar Ghosh, (2017). Single unit theranostics: drug templated lumniscent gold nanoclusters for cancer theranostics, Manuscript Under Preparation

Conferences and Workshpos:

10. Selected for attending workshop on **EMBO Practical Course: Current Methods in Cell Biology** from 11 to 19 September 2017 taking place at **EMBL Heidelberg, Germany**.
11. Participated in the Indo-Japan Workshop on Translational Agriculture, **IIT Guwahati**, India (2017)
12. Presented poster at the International Conference on Stem Cells and Cancer, **Goa**, India (2016)
13. Presented poster in the Research Conclave, Indian Institute of Technology Guwahati, **Guwahati**, India (2016)
14. Presented poster at the Global Cancer Summit, **Bangalore**, India (2015)
15. Presented poster at the International Conference on Stem Cells and Cancer, **New Delhi**, India (2014)
16. Participated in the Workshop on Advanced Techniques in Cell and Molecular Biology, **IIT Guwahati**, India (2014)
17. Participated in the Workshop on Analysis of Biological Networks, **IIT Guwahati**, India (2012)

Permissions

SPRINGER LICENSE
TERMS AND CONDITIONS

Aug 25, 2017

This Agreement between Md Asif Raza ("You") and Springer ("Springer") consists of your license details and the terms and conditions provided by Springer and Copyright Clearance Center.

License Number	4175790631201
License date	Aug 25, 2017
Licensed Content Publisher	Springer
Licensed Content Publication	Journal of Mammary Gland Biology and Neoplasia
Licensed Content Title	Developmental Regulation of Gap Junctions and Their Role in Mammary Epithelial Cell Differentiation
Licensed Content Author	Marwan E. El-Sabban
Licensed Content Date	Jan 1, 2003
Licensed Content Volume	8
Licensed Content Issue	4
Type of Use	Thesis/Dissertation
Portion	Figures/tables/illustrations
Number of figures/tables /illustrations	1
Author of this Springer article	No
Order reference number	
Original figure numbers	Figure 1
Title of your thesis / dissertation	Connexin-43 Mediated Communication in Cancer Gene Therapy
Expected completion date	Oct 2017
Estimated size(pages)	150
Requestor Location	Md Asif Raza N Block, Ground floor, Dept of BSBE, IIT Guwahati Guwahati, other 781039 India Attn:
Billing Type	Invoice
Billing Address	Md Asif Raza N Block, Ground floor, Dept of BSBE, IIT Guwahati Guwahati, India 781039 Attn: Md Asif Raza
Total	0.00 USD
Terms and Conditions	

*Thesis cover page

NATURE PUBLISHING GROUP LICENSE TERMS AND CONDITIONS

Aug 27, 2017

This Agreement between Md Asif Raza ("You") and Nature Publishing Group ("Nature Publishing Group") consists of your license details and the terms and conditions provided by Nature Publishing Group and Copyright Clearance Center.

License Number	4157661240179
License date	Jul 28, 2017
Licensed Content Publisher	Nature Publishing Group
Licensed Content Publication	Nature Reviews Cancer
Licensed Content Title	Gap junctions and cancer: communicating for 50 years
Licensed Content Author	Trond Aasen, Marc Mesnil, Christian C. Naus, Paul D. Lampe, Dale W. Laird
Licensed Content Date	Oct 21, 2016
Licensed Content Volume	16
Licensed Content Issue	12
Type of Use	reuse in a dissertation / thesis
Requestor type	academic/educational
Format	print and electronic
Portion	figures/tables/illustrations
Number of figures/tables /illustrations	3
High-res required	no
Figures	Figure 1 and Figure 2
Author of this NPG article	no
Your reference number	
Title of your thesis / dissertation	Connexin-43 Mediated Communication in Cancer Gene Therapy
Expected completion date	Oct 2017
Estimated size (number of pages)	150
Requestor Location	Md Asif Raza N Block, Ground floor, Dept of BSBE, IIT Guwahati Guwahati, other 781039 India Attn:
Billing Type	Invoice
Billing Address	Md Asif Raza N Block, Ground floor, Dept of BSBE, IIT Guwahati Guwahati, India 781039 Attn: Md Asif Raza
Total	**0.00 USD**
Terms and Conditions	

Terms and Conditions for Permissions

Nature Publishing Group hereby grants you a non-exclusive license to reproduce this material for this purpose, and for no other use,subject to the conditions below:

OXFORD UNIVERSITY PRESS LICENSE TERMS AND CONDITIONS

Aug 27, 2017

This Agreement between Md Asif Raza ("You") and Oxford University Press ("Oxford University Press") consists of your license details and the terms and conditions provided by Oxford University Press and Copyright Clearance Center.

License Number	4158731220531
License date	Jul 30, 2017
Licensed Content Publisher	Oxford University Press
Licensed Content Publication	Cardiovascular Research
Licensed Content Title	Gap junctions and the connexin protein family
Licensed Content Author	Söhl, Goran; Willecke, Klaus
Licensed Content Date	May 1, 2004
Type of Use	Thesis/Dissertation
Institution name	
Title of your work	Connexin-43 Mediated Communication in Cancer Gene Therapy
Publisher of your work	n/a
Expected publication date	Oct 2017
Permissions cost	0.00 USD
Value added tax	0.00 USD
Total	**0.00 USD**
Requestor Location	Md Asif Raza N Block, Ground floor, Dept of BSBE, IIT Guwahati Guwahati, other 781039 India Attn:
Publisher Tax ID	GB125506730
Billing Type	Invoice
Billing Address	Md Asif Raza N Block, Ground floor, Dept of BSBE, IIT Guwahati Guwahati, India 781039 Attn: Md Asif Raza
Total	**0.00 USD**
Terms and Conditions	

STANDARD TERMS AND CONDITIONS FOR REPRODUCTION OF MATERIAL FROM AN OXFORD UNIVERSITY PRESS JOURNAL

1. Use of the material is restricted to the type of use specified in your order details.
2. This permission covers the use of the material in the English language in the following territory: world. If you have requested additional permission to translate this material, the terms and conditions of this reuse will be set out in clause 12.
3. This permission is limited to the particular use authorized in (1) above and does not allow you to sanction its use elsewhere in any other format other than specified above, nor does it apply to quotations, images, artistic works etc that have been reproduced from other sources which may be part of the material to be used.
4. No alteration, omission or addition is made to the material without our written consent. Permission must be re-cleared with Oxford University Press if/when you decide to reprint.
5. The following credit line appears wherever the material is used: author, title, journal, year, volume, issue number, pagination, by permission of Oxford University Press or the sponsoring society if the journal is a society journal. Where a

SPRINGER LICENSE TERMS AND CONDITIONS

Aug 27, 2017

This Agreement between Md Asif Raza ("You") and Springer ("Springer") consists of your license details and the terms and conditions provided by Springer and Copyright Clearance Center.

License Number	4158730982844
License date	Jul 30, 2017
Licensed Content Publisher	Springer
Licensed Content Publication	Springer eBook
Licensed Content Title	The Family of Connexin Genes
Licensed Content Author	Eric C. Beyer
Licensed Content Date	Jan 1, 2009
Type of Use	Thesis/Dissertation
Portion	Figures/tables/illustrations
Number of figures/tables /illustrations	2
Author of this Springer article	No
Order reference number	
Original figure numbers	Table 1.1
Title of your thesis / dissertation	Connexin-43 Mediated Communication in Cancer Gene Therapy
Expected completion date	Oct 2017
Estimated size(pages)	150
Requestor Location	Md Asif Raza N Block, Ground floor, Dept of BSBE, IIT Guwahati Guwahati, other 781039 India Attn:
Billing Type	Invoice
Billing Address	Md Asif Raza N Block, Ground floor, Dept of BSBE, IIT Guwahati Guwahati, India 781039 Attn: Md Asif Raza
Total	**0.00 USD**
Terms and Conditions	

Introduction

The publisher for this copyrighted material is Springer. By clicking "accept" in connection with completing this licensing transaction, you agree that the following terms and conditions apply to this transaction (along with the Billing and Payment terms and conditions established by Copyright Clearance Center, Inc. ("CCC"), at the time that you opened your Rightslink account and that are available at any time at http://myaccount.copyright.com).

Limited License

With reference to your request to reuse material on which Springer controls the copyright, permission is granted for the use indicated in your enquiry under the following conditions:

- Licenses are for one-time use only with a maximum distribution equal to the number stated in your request.